Title

Physical Processes Driving Environmental Gradients on Coral Reef Ecosystems

Permalink

https://escholarship.org/uc/item/7802865k

Author

Reid, Emma Catherine

Publication Date

2021

Peer reviewed|Thesis/dissertation

UNIVERSITY OF CALIFORNIA,
IRVINE

Physical Processes Driving Environmental Gradients on Coral Reef Ecosystems

DISSERTATION

submitted in partial satisfaction of the requirements
for the degree of

DOCTOR OF PHILOSOPHY

in Civil and Environmental Engineering

by

Emma Catherine Reid

Dissertation Committee:
Associate Professor Kristen Davis, Chair
Professor Brett Sanders
Associate Professor Ryan Walter

2021

DEDICATION

To my family and friends, who have shared with me a love for the ocean.

TABLE OF CONTENTS

LIST OF FIGURES

LIST OF TABLES

ACKNOWLEDGMENTS

CURRICULUM VITAE

Emma Catherine Reid

EDUCATION

Doctor of Philosophy in Civil and Environmental Engineering   **2021**
University of California, Irvine   *Irvine, California*

Master of Science in Environmental Engineering   **2014**
University of California, Irvine   *Irvine, California*

Bachelor of Applied Science, Civil Engineering   **2007**
Queen's University   *Kingston, Ontario*

REFEREED JOURNAL PUBLICATIONS

1. **Reid, Emma C.** and Lentz, Steven J. and DeCarlo, Thomas and Cohen, Anne and Davis, Kristen, **Physical processes determine spatial structure in water temperature and residence time on a wide reef flat**, *Journal of Geophysical Research: Oceans, 2020*

2. Davis, Kristen, Arthur, Robert, **Reid, Emma C.**, Rogers, Justin, Fringer, Oliver, DeCarlo, Thomas and Cohen, Anne **Fate of internal waves on a shallow shelf**, *Journal of Geophysical Research: Oceans, 2020*

3. Sinnett, Gregory, Davis, Kristen, Lucas, Andrew, Giddings, Sarah, **Reid, Emma C.**, Harvey, Madeleine and Stokes, Ian, **Distributed Temperature Sensing for Oceanographic Applications**, *Journal of Atmospheric and Oceanic Technology, 2020*

4. Kealoha, Andrea, Shamberger, Kathryn, **Reid, Emma C.**, Davis, Kristen, Lentz, Steven, Brainard, Russell, Oliver, Thomas, Rappé, Michael, Roark, Brendan and Rii, Yoshimi, **Heterotrophy of oceanic particulate organic matter elevates net ecosystem calcification**, *Geophysical Research Letters, 2019*

5. **Reid, Emma C.**, DeCarlo, Thomas, Cohen, Anne, Wong, George, Lentz, Steven J., Safaie, Aryan, Hall, Austin, Davis, Kristen, **Internal waves influence the thermal and nutrient environment on a shallow coral reef**, *Limnology and Oceanography, 2019*

6. Walter, Ryan, **Reid, Emma C.**, Davis, Kristen, Armenta, Kevin, Merhoff, Kevin and Nidzieko, Nicholas, **Local diurnal wind-driven variability and upwelling in a small coastal embayment**, *Journal of Geophysical Research: Oceans, 2017*

CONFERENCE PRESENTATIONS

1. E. Reid, K. Davis, S. Lentz, "Dynamics of flow on a wide reef flat at Dongsha Atoll." Poster Presentation at *2020 Ocean Sciences Meeting.*

2. E. Reid, K. Davis, T. DeCarlo, A. Hall, A. Safaie, G. Lohmann, A. Cohen and G. Wong. "Internal wave-driven cooling and nutrient flux on a shallow coral reef." Oral presentation at *2018 Ocean Sciences Meeting.*

3. E. Reid, K. Davis, T. DeCarlo, A. Hall, G. Lohmann, A. Cohen and G. Wong. "Internal wave-driven cooling and nutrient flux on a shallow coral reef." Poster presentation at *2017 Gordon Research Conference – Coastal Ocean Dynamics.*

4. E. Reid, K. Davis, T. DeCarlo, A. Hall, G. Lohmann, A. Cohen and G. Wong. "Using Distributed Temperature Sensing to quantify the influence of internal waves on heat flux and temperature variability on a coral reef." Poster presentation at *2016 Ocean Sciences Meeting.*

5. E. Reid, K. Davis, T. DeCarlo, A. Hall, G. Lohmann, A. Cohen and G. Wong. (2015) "Intrusion of subthermocline water onto a shallow reef system." Oral presentation at *2015 Taiwan-US Joint Workshop. The role of oceanographic processes on the response of tropical coral reef ecosystems to ocean acidification & ocean warming.*

AWARDS

UCI Oceans Graduate Fellow	2017
Henri Samueli Endowed Fellowship	2017–2018

TEACHING EXPERIENCE

Teaching Assistant	**2014-2020**
University of California, Irvine	*Irvine, California*
Water Resources Engineering (CEE171)	*Winter 2014*
Computational Problem Solving (CEE21)	*Spring 2016–2020*

ABSTRACT OF THE DISSERTATION

Physical Processes Driving Environmental Gradients on Coral Reef Ecosystems

By

Emma Catherine Reid

Doctor of Philosophy in Civil and Environmental Engineering

University of California, Irvine, 2021

Associate Professor Kristen Davis, Chair

Coral reefs worldwide are being threatened by increasing seawater temperatures, ocean acidification, overfishing, pollution, and increased intensity of storms. Small scale spatial (<1 km) variability in temperature has been observed on coral reefs; however, it currently cannot be measured by remote sensing products. Furthermore, small scale temporal (<1 cycle/day) variability has been shown to be significant for coral bleaching resilience. Here, I aim to further our understanding of the physical processes which drive the spatial and temporal variability in environmental parameters on reef ecosystems.

First, I examine the physical processes driving flow on the east reef flat at Dongsha Atoll, in the northern South China Sea. There are observable thermal microclimates on the shallow and wide reef flat, which distinguishes the reef from open ocean temperatures. A simple analytical model of flow reveals that tides and surface waves are driving flow here, and the influence is variable in time and space. The wide reef flat at Dongsha Atoll leads gradients in the residence time and source of water (offshore vs. lagoon), and an asymmetry in the tidal excursion of water on the reef flat.

Next, I investigate the influence of the internal waves on the thermal and nutrient environment on the east reef flat at Dongsha Atoll. A heat budget was created to estimate the

temperature on the reef without the internal wave influence, and instantaneous temperatures on the reef can be up to $2.0°C \pm 0.2°C$ warmer. Also, internal waves increase the instantaneous flux of nutrients onshore by four-fold, which can have significantly influence biogeochemistry on the reef.

Finally, high spatial and temporal resolution temperature measurements were collected from three coral reefs with different morphologies, and used to determine the physical processes driving reef scale variability in water temperature. Distinctive thermal environments were observed, including reef-scale gradients in mean temperature and daily temperature range (DTR), which distinguish the shallow reefs from offshore. Daily temperature range has been shown to be the most influential metric in predicting bleaching prevalence on reefs, and studies have shown it can be predicted from average water depth. By using a heat budget, and including advection in the estimate of temperature, we are able improve predictions of DTR with minimal *in-situ* measurements.

Chapter 1

Introduction

1.1 Motivation

Coral reefs are one of the most biologically diverse ecosystems on our planet, and provide essential coastal protection, nutrition and economic opportunity. Unfortunately, the decline of coral reefs has been substantial in the past 50 years, due to rising seawater temperatures, ocean acidification, overfishing and pollution and increased intensity of storms (Hoegh-Guldberg, 1999; Hughes et al., 2003; Hoegh-Guldberg et al., 2007; Donner, 2009; Van Hooidonk et al., 2016). A recent global coral bleaching event lasted for three years from 2014 to 2017, and was the most destructive event on record, with 75% of global reefs experiencing bleaching-level heat stress (Alert 1 level), and 30% of reefs experiencing mortality-level stress (see Figure 1.1, Eakin et al., 2018; Liu et al., 2018). Understanding the physical processes which may allow corals to prosper, or contribute to their decline, will be critical for management decisions and protection in a changing climate.

Coral bleaching, when the coral host expels the dinoflagellate algae, is driven primarily
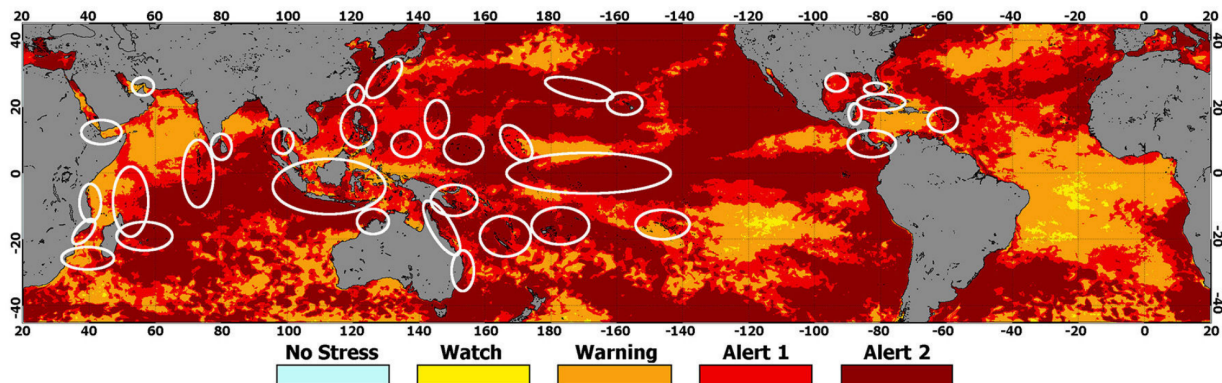
Figure 1.1: Maximum Bleaching Alert Area 2014-2017
Maximum composite of CRW's daily global 5 km satellite Bleaching Alert Area (Version 3) for June 2014-May 2017. Major bleaching has been reported to CRW by resource managers, scientists, and the public in the coral reef regions outlined by ellipses (Liu et al., 2018).

by elevated seawater temperatures (Hoegh-Guldberg and Smith, 1989; Glynn, 1991; Hughes et al., 2017), but can also be driven by changes in light (Hoegh-Guldberg and Smith, 1989; Lesser et al., 1990), and salinity (Goreau, 1964; Coles and Jokiel, 1992). When a coral bleaches, it is more susceptible to disease, decreased growth rates, and eventual mortality (Hoegh-Guldberg, 1999; Cantin and Lough, 2014).

Currently, thermal stress on corals, and coral bleaching events are predicted by remotely sensed sea surface temperatures (SSTs), which exceed locally defined threshold temperatures (Goreau and Hayes, 1994). These events can be tracked in real-time from satellite data, however, long-term prediction can be difficult. The National Oceanic and Atmospheric Administration's Coral Reef Watch (CRW) uses remotely sensed, modelled, and *in-situ* data to predict coral bleaching, disease and mortality (Liu and Hsu, 2004). Spatial variability in temperature on a reef-scale (<750m) may lead to complex patterns of bleaching and recovery, which are not currently available from global satellite products.

Long-term conservation of coral ecosystems will require identification of resilient corals or reefs and the physical mechanisms which drive this resilience (Oppen et al., 2017). Re-

cent studies have shown substantial variation, over small spatial and temporal scales, of the physiological response of coral colonies and reefs to environmental stressors (Riegl and Piller, 2003; Pandolfi et al., 2011; Oliver and Palumbi, 2011; van Woesik et al., 2011, 2012; DeCarlo et al., 2017a). Seawater temperature and thermal tolerance of corals has been shown to vary significantly across a reef (e.g. Pineda et al., 2013; Palumbi et al., 2014; Safaie et al., 2018), and some studies have shown diverse and thriving coral communities in acidic environments (e.g. Shamberger et al., 2014; Barkley et al., 2015). Furthermore, corals which live in regions of natural thermal variability, may have higher temperature tolerance (McClanahan et al., 2005; Safaie et al., 2018). In a changing climate, these coral organisms and reefs that have been shown to be resilient and/or adaptable, may persist despite stressors (Pandolfi et al., 2011; Spalding and Brown, 2015). Factors which may contribute to environmental variability, and subsequently the variation in response of corals, at small spatial scales include flow conditions (McClanahan et al., 2005), exposure to solar radiation (Lesser and Farrell, 2004), and other physical mechanisms such as internal waves (Wolanski and Pickard, 1983; Wolanski and Delesalle, 1995; Leichter et al., 1996; Green et al., 2018).

Thermal and chemical environments on coral reefs are shaped by the circulation processes acting on the system. Dynamical scales on coral reefs can range from millimeters to kilometers, and the geometry of coral reefs leads to complex flows (Monismith, 2007; Lowe and Falter, 2015). Hydrodynamic processes which drive flow in coastal regions, and specifically on coral reefs, include tidal, wave and wind driven flow (Lowe and Falter, 2015). Ocean currents and internal waves may also be important on deeper coral reefs (Davis et al., 2008; Lowe and Falter, 2015; Schramek et al., 2018; Davis et al., 2020). Understanding the flow dynamics on coral reefs can inform what is driving changes in residence time of water and variability of environmental properties, and can explain why some corals may thrive under different conditions.

1.2 Research Questions and Objectives

This dissertation describes the physical mechanisms that are driving flow and variability at Dongsha Atoll, in the South China Sea, Kaneohe Bay, on Oahu, Hawaii, and Ofu-Olosega, in American Samoa. The physical mechanisms driving flow on the east reef flat at Dongsha Atoll are explored in depth, as well as the influence of internal waves. The following questions are addressed:

1. What are the physical processes controlling the residence time of water, and creating reef-scale (<1km) environmental gradients on coral reef ecosystems?

Objectives:

- Analysis of *in-situ* observations of circulation, reef-scale gradients in physical parameters (e.g. temperature, flow), and atmospheric forcing on Dongsha Atoll in the South China Sea will be used to quantify the residence time of water on the reef flat under different flow and atmospheric forcing conditions.

- Using an analytical model of flow on the reef flat, I can attribute the portion of flow that is due to tidal, wind and wave (surface gravity and internal wave) processes.

2. How do internal waves shape the physical and chemical environment on coral reefs?

Objectives:

- I will quantify the impact of internal waves at Dongsha Atoll using spatially-continuous temperature measurements from a Distributed Temperature Sensing instrument (DTS), a new instrument in the field of physical oceanography.

- From observations of flow and high resolution temperature, I will create a heat budget for the reef flat, quantifying the impact of internal waves on heat fluxes onto the reef.

- Using offshore measurements of nutrient concentrations, I will create a temperature/nutrient relationship to determine the flux of nutrients coming onshore due to internal waves.

3. What are the physical processes which are shaping reef-scale (<1km) gradients in temperature, and can important temperature metrics, such as daily temperature range, be predicted from larger scale, globally available data sources, paired with a dynamical understanding of reef-scale circulation and heat fluxes?

Objectives:

- Using spatially continuous temperature data from Dongsha Atoll, Kaneohe Bay and Ofu-Olosega, I will quantify spatial patterns in temperature variability.

- Using the dynamical understanding of flow on coral reefs obtained in the work addressing Question 1, I will predict reef-scale spatial variability in daily temperature range using globally available data products such as sea surface temperature (SST), surface wave parameters, bathymetry and atmospheric forcing (wind stress and solar forcing).

1.3 Overview of Work

This data included in this dissertation is from deployments completed at three coral reefs. The first study was completed at Dongsha Atoll, a coral reef in the northern South China Sea, in June 2014. The goal of the deployment was to characterize the benthic thermal environment and physical processes which drive flow across the wide east reef flat and fore-reef slope. The observations presented in this dissertation were part of a larger study of the coral

ecology, reef-scale circulation, and internal wave dynamics at Dongsha Atoll (DeCarlo et al., 2017a,b; Reid et al., 2019; Davis et al., 2020; Reid et al., 2020). The site was chosen due to the large internal waves which shoal here, and bring cold, nutrient rich water onto the shallow reef flat.

The second study was completed at Kaneohe Bay, Hawaii, in January 2017. The observations presented here were part of a larger study of coral ecology and reef-scale circulation (Kealoha et al., 2019). The goal of the deployment was to characterize the benthic thermal environment on the reef flat and offshore, and to understand the physical processes driving environmental variability.

The final study was completed at Ofu-Olesega, in American Samoa, in March 2017. The observations presented here were part of a larger study of reef-scale circulation (Rogers et al., 2018). The goal of the deployment was to characterize the benthic thermal environment in the back reef pools and on the fore-reef slope, and to understand the physical processes which drive variability.

1.4 Outline of Dissertation

This dissertation is divided into six chapters. Chapter 1 outlines the motivation for the research, as well as the questions that will be answered in the dissertation. An outline of the work completed is included here. In Chapter 2, I review relevant literature on the physical processes which drive flow and temperature variability on coral reefs, as well as some background specific to the three deployment sites included in this dissertation. Literature review specific to Chapter 3-5 is included in those chapters. Chapter 3 presents results of the high resolution temperature measurements and circulation measurements taken at Dongsha

Atoll. The physical mechanisms that drive temperature variability on the east reef flat is discussed. Chapter 3 was published as a peer-reviewed article in the *Journal of Geophysical Research - Oceans* (2020, doi: 10.1029/2020JC016543). Chapter 4 examines the influence of internal waves on the thermal and nutrient environment on the east reef flat at Dongsha Atoll. Chapter 4 was published as a peer-reviewed article in *Limnology and Oceanography* (2019, doi: 10.1002/lno.11162). Chapter 5 presents results of the deployments at Dongsha Atoll, Kaneohe Bay and Ofu-Olosega, and characterizes the benthic thermal environments and the physical mechanisms which drive variability at these sites. Chapter 6 summarizes the research presented in the dissertation, and outlines areas for future research.

Chapter 2

Literature Review

2.1 Site Descriptions

2.1.1 Dongsha Atoll, Taiwan

Dongsha Atoll is a coral atoll located in the northern South China Sea (Figure 2.1c). The atoll is 28km in diameter, with an area of approximately 600km^2 (Dai, 2004). The observations included in this dissertation are focused on the east reef flat of the atoll. The reef flat here is anomalously wide ($\sim$ 3km), compared to other reefs in literature (Falter et al., 2013; Goldberg, 2016), which may contribute to some of the unique patterns of variability here.

This site was chosen due to the large internal waves which shoal on the forereef slope here. Internal waves are generated in the Luzon Strait and travel westward towards the atoll as waves of depression. They transform into waves of elevation as the shoal in depths <200m (Fu et al., 2012). The waves become highly non-linear in in depths <30m, and mix cold, nutrient rich water into shallow depths (Leichter et al., 2003; Wang et al., 2007; Moore et al.,
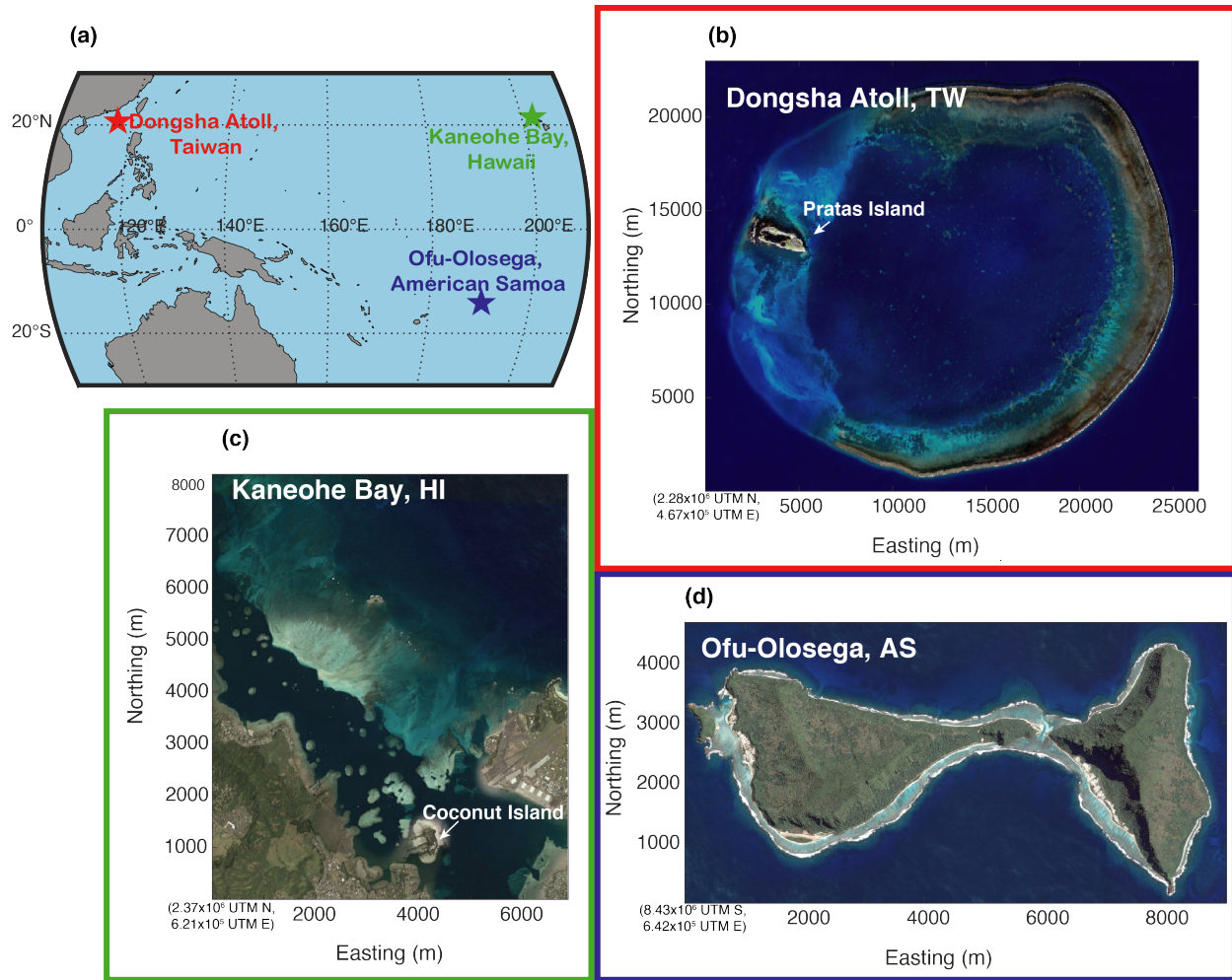
Figure 2.1: The study sites.
(a) Map showing the location of the three sites. **(b)** Satellite image of Dongsha Atoll from the Taiwan National Space Organization. **(b)** Satellite image of Kaneohe Bay from Google Earth, Maxar Technologies. **(d)** Satellite image of Ofu-Olosega from Google Earth, CNES/Airbus.

2016).

Furthermore, the reef at Dongsha Atoll has been shown to have the highest net ecosystem calcification rates recorded to date (DeCarlo et al., 2017b), making it an interested study site. There has also been observed variability in bleaching response of corals between the forereef slope and lagoon, likely due to the influence of internal waves (Dai, 2004; DeCarlo et al., 2017a; Tkachenko and Soong, 2017).

2.1.2 Kaneohe Bay, Hawaii

Kaneohe Bay is a semi-enclosed embayment, bounded by a barrier reef, on the eastern side of the island of Oahu, Hawaii (Figure 2.1c). The bay has many patch reefs and two large channels at the north and south. The barrier reef is approximately 6km long and 2km wide. Surface wave forcing is the primary mechanism driving flow over the reef at Kaneohe Bay (Lowe et al., 2005, 2009a,b). Guadayol et al. (2014) studied water temperature variability on the fringing reef off of Coconut Island (Figure 2.1c), and found that total variance of temperature, pH and oxygen decreased in an offshore direction with increased depth. Diurnal variability was found to be more significant in shallow regions, and decreased offshore.

2.1.3 Ofu-Olosega, American Samoa

Ofu-Olosega (Figure 2.1d) is a pair of islands located in American Samoa. The islands are surrounded by fringing reefs. Tidal modulation of breaking waves on the reef crest is the primary mechanism driving flow here (Koweek et al., 2015). Studies have shown that the back-reef lagoons on Ofu have significant small-scale heterogeneity in temperature, water chemistry (pH, dissolved O2), and flow (Craig et al., 2001; Smith et al., 2008; Monismith, 2014). Biodiversity is high in the coral reef ecosystem at Ofu (Craig et al., 2001), and the

back-reef lagoons (called pools) have been observed to have recognizably different thermal variability (Oliver and Palumbi, 2011). Smaller pools have shown to have higher diurnal variability, and extreme temperatures than the larger pools, despite having similar mean temperatures. Also, there has been observed variation in bleaching response of the corals in the back-reef pools at Ofu, and corals in the high variability pools have demonstrated a higher tolerance for extreme temperatures (Barshis et al., 2010; Oliver and Palumbi, 2011; Barshis et al., 2013; Bay and Palumbi, 2014; Palumbi et al., 2014).

2.2 Physical processes driving flow on coral reefs

The processes which drive flow on and shape the environment of coral reefs range from large scale processes such as tides, down to small scale processes such as flow through a coral canopy (Figure 2.2) (Lowe and Falter, 2015). Intermediate scale processes, such as upwelling or internal waves, can also have an impact on coral communities and structure. Circulation on reefs, and the subsequent residence time of water on the reef, impacts the biology and chemistry of coral reefs (Monismith et al., 2010; Cuet et al., 2011; Davis et al., 2011; Hearn, 2011; Falter et al., 2013). Understanding this circulation is crucial for understanding what is governing residence time, and consequently distribution and growth of corals. Radiation stresses cause a set-up of sea surface height when offshore surface waves break on the reef crest. This creates a pressure gradient, which drives flow across a coral reef. This mechanism of flow dominates on most coral reef systems, and for this reason, many studies have focused on understanding this forcing (Symonds et al., 1995; Kraines et al., 1998; Hearn, 1999; Gourlay and Colleter, 2005; Lowe et al., 2005, 2009a,b; Hench et al., 2008; Taebi et al., 2011). Observational studies have shown that there is a linear relationship between cross-shore currents and offshore wave height (Hearn, 1999; Lowe et al., 2009b).
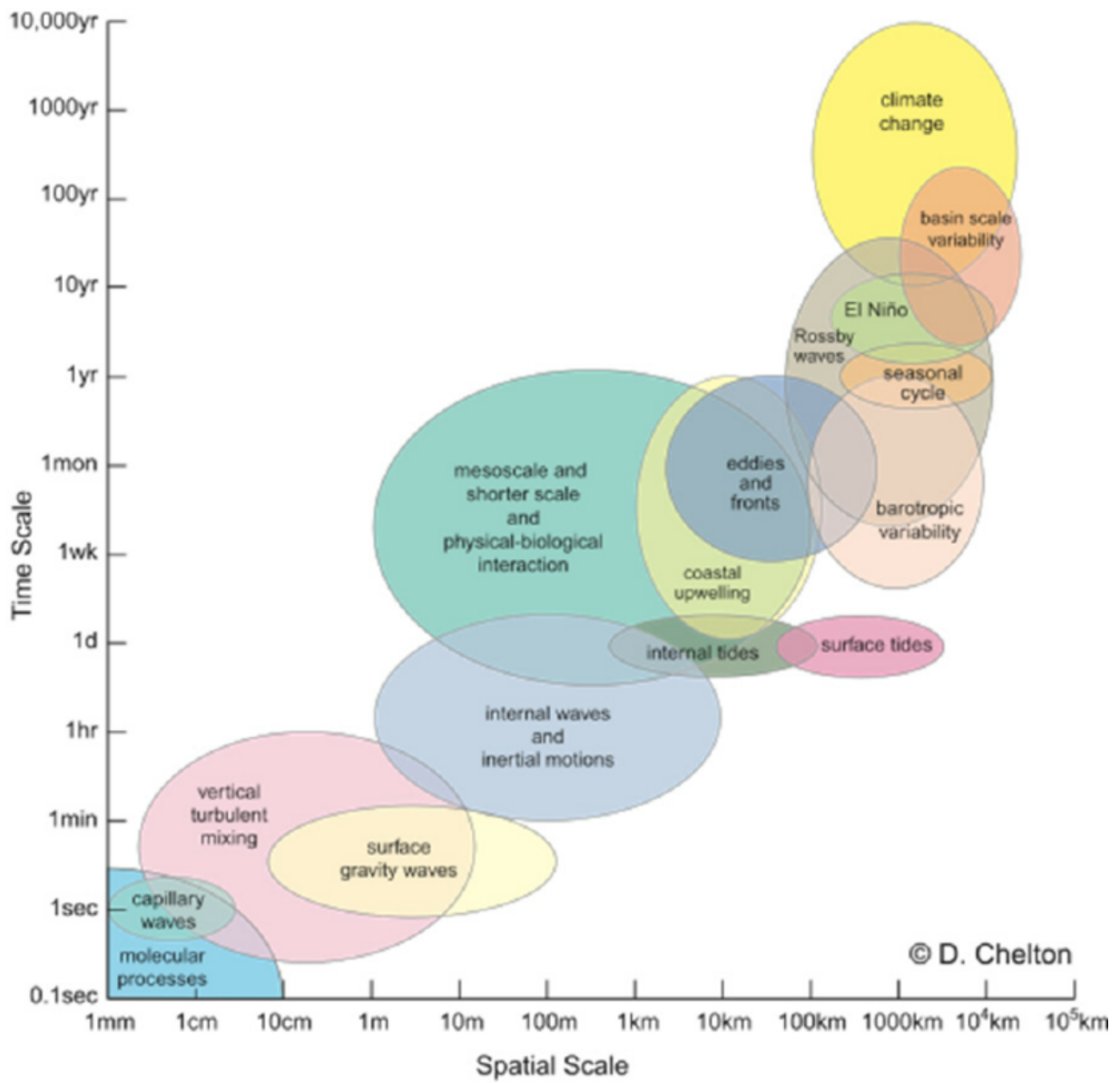
Figure 2.2: Time and space scales of ocean variability
(courtesy D. Chelton, Oregon State University)
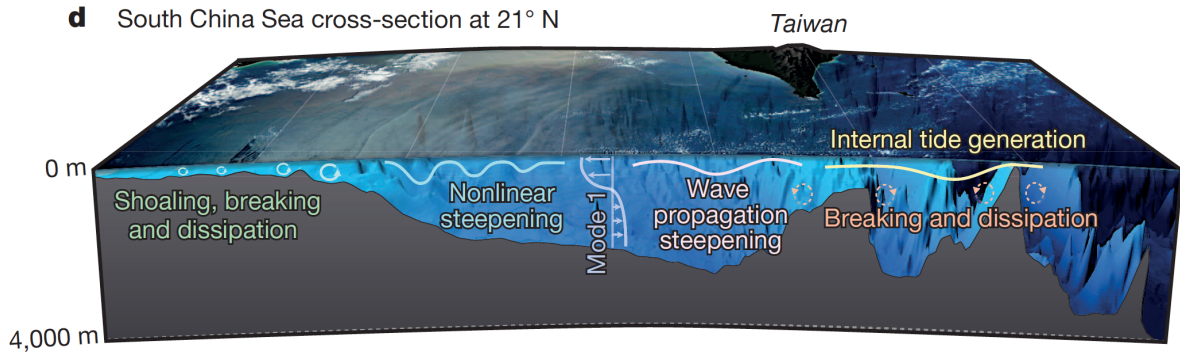
Figure 2.3: Internal waves in the South China Sea
(Alford et al., 2015)

Wind-driven flow has been found to be a relatively minor compared to wave- and tidally-driven circulation on reef flats (Taebi et al., 2011; Hench et al., 2008; Rogers et al., 2016). However, in some deep lagoons, wind forcing plays a larger role in driving flow (Lowe et al., 2009a; Lentz et al., 2017). Both wind and wave driven flow are highly dependent on drag coefficients, which vary with water depth (Lentz et al., 2017).

Another dominant process driving flow on coral reefs is tidal forcing (Taebi et al., 2011; Rogers et al., 2016), especially when tidal ranges <3m (Lowe and Falter, 2015). However, not all coral reefs experience significant tidal forcing (Hench et al., 2008). How and where waves break on reefs with wave-driven circulation can be modulated by tides (Taebi et al., 2011; Becker et al., 2014). Spatial variability in tidal forcing may also exist on some reefs; flow may be modulated by tides in the lagoon or channels, but not on the reef flat (Lowe et al., 2009b).

2.3 Internal waves

A physical process which is present in lakes and oceans worldwide are internal waves (IW), which have significant physical and biological impacts on coastal ecosystems. Shoaling IWs

can transport cold and nutrient rich water into shallow coastal regions (Lucas et al., 2011; Noble et al., 2009; Leichter et al., 1996). This delivery of subthermocline water from IWs can significantly impact coral communities. Quantifying their impact on a shallow coral reef will help us to understand which reefs will be more resilient to climate change.

Internal waves are gravity waves generated within a stratified water column; they can propagate along density gradients throughout the ocean (Garrett and Munk, 1979; Helfrich and Melville, 2006; Nash et al., 2012). Interfacial internal waves, like surface waves, are generated by a perturbation on an interface, which when restored by gravity generates a wave on that interface (Garrett and Munk, 1979). One mechanism of generation is between the interaction of the barotropic tide with topographic features in the ocean that causes a perturbation on a density interface (Garrett and Munk, 1979; Nash et al., 2012). Buoyancy restores the perturbation, and consequently generates a propagating wave, which can travel long distances ($\sim$ 100-500km) (Ramp et al., 2004, 2010; Shroyer et al., 2010; Inall et al., 2011). Internal waves drive mixing when they break on coastal shelves which can be important for coastal ecology (Wolanski and Pickard, 1983; Helfrich, 1992; Walter et al., 2014). Some of the largest internal waves observed (with amplitudes of 100-150m) are generated in the Luzon Strait (see Figure 2.3, Alford et al., 2015), and travel westward in the northern South China Sea towards Dongsha Atoll (Hsu and Liu, 2000; Alford et al., 2015).

Internal waves have been studied extensively by physical oceanographers in deep waters (>30m), but more recently, studies have also highlighted their influence in the nearshore environment (Walter et al., 2012; Sinnett and Feddersen, 2014; Walter et al., 2014; Davis et al., 2020). For example, large IWs shoaling on Dongsha Atoll, in the northern South China Sea, inject colder water to the shallow reef (Wang et al., 2007; Fu et al., 2012; Alford et al., 2015; DeCarlo et al., 2015). The upwelling of this colder water has been shown to protect reefs from bleaching caused by high temperatures (Riegl and Piller, 2003). During the 1997-1998

El Niño event, corals on the reef slope at Dongsha Atoll that receive IWs remained healthy, whereas the corals in the protected lagoon were severely damaged (Dai, 2004). Similarly, a study in the Andaman Sea showed that in sheltered regions (i.e. regions that would not be affected by IWs) corals showed higher mortality post-bleaching compared to unsheltered regions (Wall et al., 2015). Furthermore, Riegl and Piller (2003) suggested that corals that live in medium-depth regions which experience upwelling may provide regeneration potential for shallow regions that experience bleaching and mortality.

Subthermocline water that is injected onto coral reefs from shoaling IWs can also be nutrient rich (Leichter et al., 1998; Monismith et al., 2010; Lucas et al., 2011; Jantzen et al., 2013). Studies have shown that IWs delivering nutrient rich water to reefs can promote algae growth over corals (Leichter et al., 2003; Jantzen et al., 2013). Some researchers suggest an addition mechanism for IWs to influence reef communities is by providing a source of food for corals (DeCarlo et al., 2015). With increased levels of atmospheric CO2, ocean acidification continues to threaten coral reefs as decreased availability of carbonate ions hinders calcification and skeletal growth (Hoegh-Guldberg et al., 2007). However, studies have shown that increased heterotrophic feeding or inorganic nutrient availability boosts the energy of corals, which allows them to continue calcifying in low pH seawater (Cohen and Holcomb, 2009; Holcomb et al., 2010). Enhanced growth rates of suspension feeding corals has been observed where IWs are present (Leichter et al., 1998). Quantifying the impact of IWs on the nutrient budget will help us to understand coral resilience and growth.

2.4   Environmental variability at reef-scales

Since patterns of reef-scale temperature variability (<750m) cannot be measured by current satellite products, many studies have focused on *in-situ* observations of temperature variabil-

ity across a reef (Leichter et al., 2006; van Woesik et al., 2012; Pineda et al., 2013; Guadayol et al., 2014; DeCarlo et al., 2017a). It has been shown that corals can adapt or acclimate to withstand thermal stress when located in areas of large temperature fluctuations (Oliver and Palumbi, 2011; Rogers et al., 2016; Castillo et al., 2012). There is a clear correspondence between high frequency time scales and small spatial scales of physical processes (Figure 2.2). We also know that high frequency temperature variability is important to coral communities (Safaie et al., 2018), and on a reef-scale (<1km), it is the high frequency variability that defines different thermal environments (Davis et al., 2011). Connecting the physical processes which drive this high frequency variability on a reef-scale is vital to understanding spatial variability in bleaching response.

Different regions of the reef may experience very distinctive thermal environments, and consequently have different percentages of coral cover. These thermal environments are controlled by the physical processes that the region is subject to. A study by Rogers et al. (2016) in Palmyra showed that regions with high coral cover (>50%) had highly variable temperature distributions. These regions had lower average weekly temperatures, and low coral cover was associated with high weekly temperatures, although they both experienced similar diurnal temperature ranges.

Evidence of spatial variability in coral resilience on reefs has prompted studies with high spatial resolution temperature measurements to identify thermal microclimates. In a study of environmental variability on a reef in Kaneohe Bay, Hawaii, Guadayol et al. (2014) found that total variance of temperature, pH and oxygen decreased in an offshore direction. Also, variability was decomposed to look at the contribution of different frequency ranges, and Guadayol et al. (2014) found that the contribution of daily frequencies decreased in an offshore direction, compared to weekly frequencies which increased in an offshore direction. These patterns were attributed to increased depth offshore; in shallower regions, atmospheric

forcing can lead to high-frequency responses in physical and biological parameters (Pineda et al., 2013; Guadayol et al., 2014). Also, limited cross-shore flow and mixing between the reef slope and flat contributed to these patterns of variability in Kaneohe Bay (Guadayol et al., 2014).

Controlling factors such as residence time contribute to spatial variability in temperature. Flow across a reef, driven by tide, winds, and waves, can contribute to the patterns in temperature observed. A study by Schoepf et al. (2015), in the Kimberley region in northwest Australia, looked at large tidal ranges (up to 10m) and the impact to spatial temperature variability on a reef-scale. Increased thermal tolerance was observed in corals located in the more variable intertidal region than subtidal region, under the same levels of heat stress.

Wind driven flow is typically not a driving force on coral reefs (Hench et al., 2008; Taebi et al., 2011; Rogers et al., 2016), however a recent study from 2016 at Dongsha Atoll found that periods of low wind stress can lead to high temperature variability and subsequent bleaching of corals (DeCarlo et al., 2017a). This study found that during a period of low wind, temperatures on the reef flat were $6°C$ above normal summertime levels, and mass bleaching occurred.

Wave stress not only contributes flow across the reef, and the resulting temperature regime, but also to physical damage to coral structures. In the Red Sea, wave-protected regions on the back of the reef flat experienced high mean temperatures, and wave-exposed regions near the reef crest had lower mean temperatures Davis et al. (2011); Pineda et al. (2013). In Palmyra, regions with high wave stress were associate with low coral cover (Rogers et al., 2016).

Although variability due to surface forcing, tide, wind, and wave driven currents is impor-

tant in shallow regions, deep regions also experience high variability in not only temperature, but also salinity, nutrients and other ecologically relevant parameters. Variability can increase with depth, especially in regions that experience IWs. A study done by Leichter and Genovese (2006), concluded that IWs are a mechanism of variability at deep sites. This variability due to IWs may not be present on all coral reefs, although it is present on many Jackson and Apel (2004); however, it is an important factor to consider as it can create strong spatial gradients.

Chapter 3

Physical processes determine spatial structure in water temperature and residence time on a wide reef flat

3.1 Introduction

Coral reefs are increasingly threatened by rising seawater temperatures, and the collapse of reefs on a global scale has been predicted to occur in the near future (Hoegh-Guldberg et al., 2007; Donner, 2009; Van Hooidonk et al., 2016). Understanding the variation in environmental conditions over small spatial and temporal scales has become increasingly important when considering the variation in the physiological responses of coral colonies within a reef

to stressors (Riegl and Piller, 2003; McClanahan et al., 2005; Oliver and Palumbi, 2011; Pandolfi et al., 2011; van Woesik et al., 2012; Guadayol et al., 2014; DeCarlo et al., 2017a). Since patterns of spatial variability on a reef-scale (<750 m) are not available globally with current satellite products, many studies have focused on *in-situ* observations of temperature variability across a reef (Leichter et al., 2006; van Woesik et al., 2012; Pineda et al., 2013; Guadayol et al., 2014; DeCarlo et al., 2017a). Recent evidence suggests that resilience to thermal stress may be influenced by a coral's thermal history, particularly at diurnal and semidiurnal time scales (Oliver and Palumbi, 2011; Castillo et al., 2012; Guadayol et al., 2014; Rogers et al., 2016; DeCarlo et al., 2017a; Safaie et al., 2018). The shallow depths of reef structures lead to high spatial and temporal variability in the physical environment (e.g. temperature, flow), distinguishing the reef environment from the surrounding open ocean. It is this variability that influences coral community structure and may promote resilience to thermal stress (Safaie et al., 2018), and likely other stressors (e.g. acidification, Shamberger et al., 2014; Barkley et al., 2015). Understanding the physical mechanisms underpinning this variability is important for not only recognizing resilience potential, but also predicting how reef conditions will be modified by a changing climate.

Thermal and chemical environments on coral reefs are shaped by circulation. The processes that drive flow on coral reefs range from large spatial scales, such as tides, down to small spatial scales, such as turbulence within a coral canopy (Monismith, 2007; Lowe and Falter, 2015). The major physical processes driving circulation on most shallow coral reef systems are tides, waves and wind, and the contribution of each mechanism can vary (Lowe and Falter, 2015). For deeper reefs, ocean currents and internal waves can be important, too (Davis et al., 2008; Lowe and Falter, 2015; Schramek et al., 2018; Davis et al., 2020).

As surface waves break on coral reef crests, radiation stresses cause a setup of the sea surface height at the reef crest. A pressure gradient is developed that forces flow across the

reef. Surface gravity waves dominate circulation on many shallow coral reef systems, and for this reason, many studies have focused on understanding this forcing (Symonds et al., 1995; Kraines et al., 1998; Hearn, 1999; Gourlay and Colleter, 2005; Lowe et al., 2005; Hench et al., 2008; Lowe et al., 2009a,b; Taebi et al., 2011).

The role of wind and tidal forcing varies across coral reefs globally. Wind-driven flow has been found to be relatively minor compared to wave- and tidally-driven circulation on many reef flats (Hench et al., 2008; Taebi et al., 2011; Rogers et al., 2016). While some reefs do not experience significant tides (Hench et al., 2008), tidal forcing can be a dominant process driving flow on other reefs (Taebi et al., 2011; Rogers et al., 2016), especially when tidal ranges >3 m (Lowe and Falter, 2015). Tides can also modulate where waves break (Taebi et al., 2011; Becker et al., 2014). In some cases, tides control flow in areas such as the lagoon or channels, but not on the reef flat (Lowe et al., 2009b).

Dongsha Atoll is a vibrant coral reef and Taiwanese National Park located in the northern South China Sea (SCS) (Figure 3.1a,b). Previous work has shown that cold and nutrient-rich water is regularly injected onto the shallow east reef flat, from large shoaling internal waves (Wang et al., 2007; Fu et al., 2012; Reid et al., 2019; Davis et al., 2020). Here, we examine the processes that drive flow on the east reef flat of Dongsha Atoll and characterize the resulting benthic thermal environments using a Distributed Temperature Sensing (DTS) system, which resolves spatially-continuous temperature measurements along a fiber optic cable (Selker et al., 2006; Tyler et al., 2009; Hausner et al., 2011; Reid et al., 2019; Sinnett et al., 2020).

3.2 Materials and Methods

3.2.1 Site description

Dongsha Atoll is 28 km in diameter and has an area of approximately 600 km^2 (Dai, 2004). The east reef flat, which is the focus of this paper (Figure 3.1c), is roughly 3 km wide, and water depth at mean sea level ranges from 0.3 to 4.0 m (Shih et al., 2011), with shallower depths towards the reef crest. The tidal range on the reef flat is approximately 0.9 m. The forereef has a 4% slope down to 25 m depth, beyond which it steepens to 15% to 50 m depth, after which it flattens slightly to 7% to 300 m depth. A survey of the benthic composition of the reef flat shows the region is dominated by fleshy algae, sea grass and live coral (DeCarlo et al., 2017b). The reef slope has a spur and groove formation, which is primarily soft corals.

General ocean circulation in the northern SCS during the summer is controlled by monsoon winds (Hu et al., 2000). Wind from the southwest drives surface currents generally to the northeast (Morton and Blackmore, 2001). Internal waves generated in the Luzon Strait (between Taiwan and the Philippines) travel westward towards Dongsha Atoll, where they become highly nonlinear bores and boluses in shallow waters (<30 m), and transport subthermocline (cold and nutrient rich) water into the nearshore region (Fu et al., 2012; Alford et al., 2015; Davis et al., 2020). Internal waves and locally generated internal tides change the stratification offshore, and can modify sea level at the reef crest, which may contribute to driving flow across the reef (see Section 3.4.1). This water is subsequently transported onto the shallow reef flat by tides, wind and surface waves, where it alters the thermal and chemical environment (Reid et al., 2019).
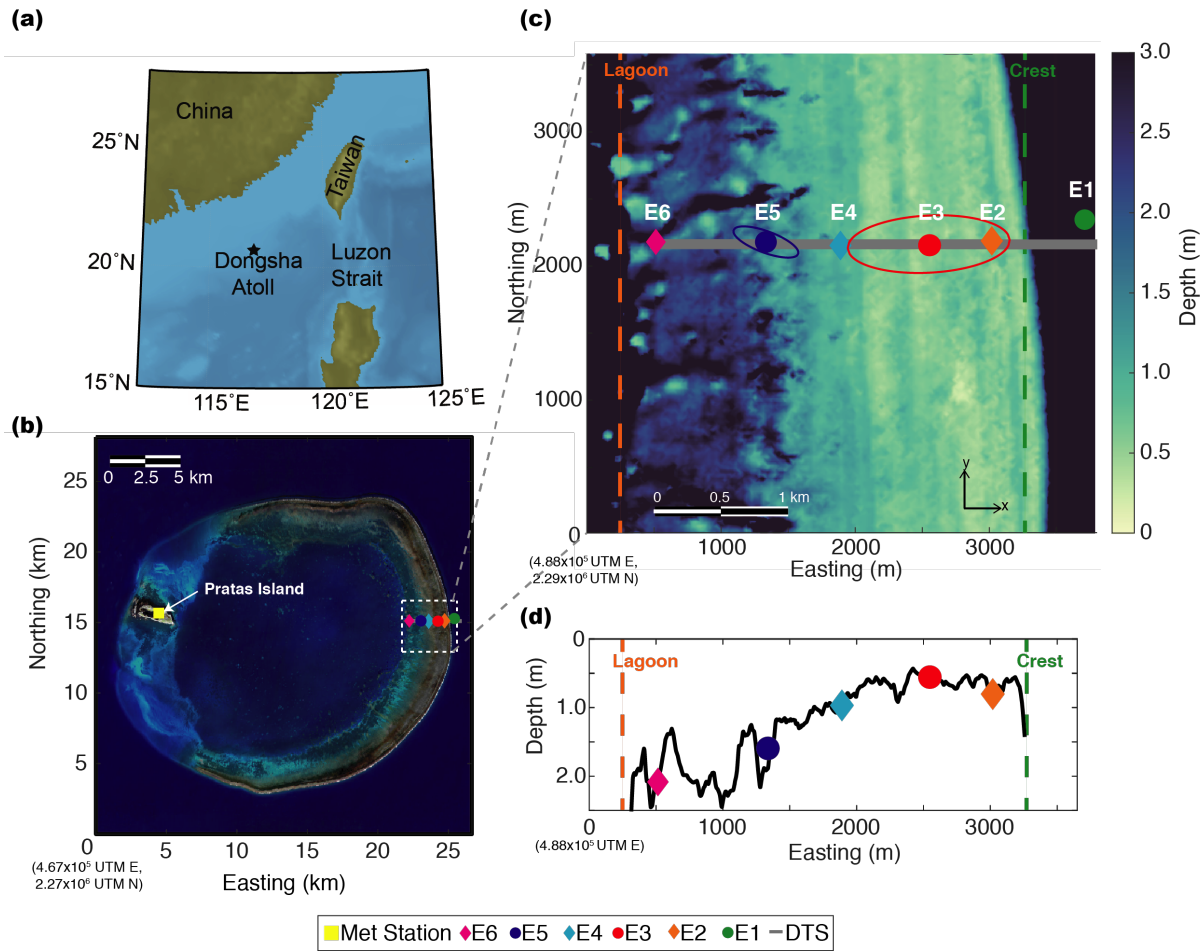
Figure 3.1: Oceanographic setting of Dongsha Atoll

(a) Location of Dongsha Atoll within the northern South China Sea and **(b)** Satellite image of Dongsha Atoll from the Taiwan National Space Organization. White box indicates region covered by (c). The meteorological station located on Pratas Island is shown with a yellow square marker. **(c)** East reef flat of Dongsha Atoll, where moorings E1 to E6 are shown. Bathymetry from LIDAR data is shown (Shih et al., 2011). The locations of Seagauge pressure sensors are shown with diamonds (E2, E4 and E6), and Aquadopp current meters (E3 and E5) and AWAC current meter (E1) are shown with circles. The location of the DTS cable is shown as a gray line. Ellipses of the principal axes of the depth-averaged currents at E3 and E5 are shown at their respective locations on the reef. The reef flat boundaries, used in particle tracking (Section 3.2.4), are shown with orange (lagoon) and green (reef crest) dashed lines. **(d)** Cross section of the LIDAR bathymetry of the reef flat where the DTS was located, and moorings E2 to E6.

3.2.2 Experiment

The observations presented here are part of a larger study of coral ecology, reef-scale circulation, and internal wave dynamics at Dongsha Atoll (see DeCarlo et al., 2017a,b; Reid et al., 2019; Davis et al., 2020). In this study we focus on measurements of currents, pressure, and water temperature taken on the reef flat on the east side of the atoll and meteorological conditions measured on Pratas Island (Figure 3.1b,c), collected from 04 to 17 June 2014. This study took place during the summer monsoon season in the SCS.

Two 2-MHz Nortek AquaDopp Profilers (ADPs) were placed on the reef flat at E3 and E5 (Figure 3.1c) to measure currents and pressure at 4-minute intervals. The depth at E3 and E5 was on average 0.4 m and 1.5 m, respectively. At times, water depth at E3 was too shallow for the AquaDopp to accurately measure currents. Gaps in velocity data were interpolated if the gap was less than 6 hours. When water depth was less than 0.25 m, velocity data is not shown or used in this study.

An upward-looking Acoustic Wave and Current Profiler (AWAC, Nortek AS) was deployed at 18.1 m depth at E1 on the forereef (Figure 3.1b,c), and recorded current measurements at 1-minute intervals and measured surface wave statistics in 20-minute bursts every three hours. Current measurements from E1 were not used in this study; however, for reference they can be found in Figure 2 of Reid et al. (2019).

Three Seabird Electronics Seagauges (SBE-26) were placed on the reef flat at E2, E4 and E6 (Figure 3.1c) to measure pressure at 10-minute intervals. Water depths at E2, E4 and E6 were on average 0.6 m, 0.9 m and 2.0 m, respectively.

The meteorological data used in this study were measured from the weather station lo-

cated on Pratas Island (Figure 3.1b). The station carries sensor suites for measuring wind speed and direction.

Raman spectra fiber-optic Distributed Temperature Sensing (DTS) technology was deployed at Dongsha Atoll from 04 to 11 June 2014 to measure near bed water temperatures across the east reef flat and forereef slope over a 4-km distance. A Sentinel Oryx DTS interrogator collected continuous independent temperature measurements every two meters along a Kaiphone (flexible white, 6 mm, steel-reinforced) fiber optic cable at a sample frequency of one temperature trace per minute.

The fiber optic cable was deployed on the bottom in the cross-shelf direction on the east reef flat starting near the lagoon and going east across the reef flat and down the reef slope to a depth of approximately 50 m (Figure 3.1b). For the purposes of this study, we will focus on the temperature measurements taken from a 3-km section of the cable deployed on the reef flat. The DTS measurements started on 04 June 2014, and continued until the machine lost power due to Tropical Storm Hagibis on 12 June 2014. Details of deployment and calibration are found in Reid et al. (2019). The average bias and root-mean-square difference between the validation loggers (SBE-56s) and the DTS was 0.07 ± 0.01 °C and 0.20 ± 0.02 °C, respectively.

Spectral analysis of DTS temperature data across the reef flat was completed using the multitaper method (Thomson, 1982; Lilly, 2019). The 95% confidence interval is found from the χ_k^2 distribution with the 6 degrees of freedom given by orthogonal Slepian tapers (Thomson, 1982).

Tidal velocities offshore of the reef crest (near E1) were estimated using the Oregon State Tidal Inversion Software (Egbert and Erofeeva, 2002) and the TMD toolbox (Padman and Erofeeva, 2004).

3.2.3 Estimating Tide, Wave and Wind-Driven Flow

An analysis of the currents on the Dongsha reef flat at E3 and E5 was performed to determine the physical processes that govern flow, following Lentz et al. (2016). Assuming steady state flow and neglecting alongshore variations (i.e. that along-reef variations in bathymetry are negligible and waves break uniformly along the length of the reef) continuity in depth-averaged flow implies that cross-reef transport, $q_0(t)$, does not vary across the reef (Lentz et al., 2016).

$$U(\eta + \eta_0 + h) = U(\eta + D) = q_0 \tag{3.1}$$

where $U(x,t)$ is the depth-averaged cross-reef current including the Stokes velocity due to waves, $\eta(x,t)$ is the sea level variation over the scale of the reef due to wave forcing (wave setup), η_0 is the sea level variation on spatial scales that are large compared to the reef, which include tides, wind forcing and seasonal buoyancy forcing, $h(x)$ is the water depth relative to mean sea level when currents are weak, and $D(x,t) = \eta_0(t) + h(x)$. Based on our observations, we know that $\eta << D$, so that $\eta + D \approx D$, as variations in η are typically centimeters and D is about 1 m.

The steady, depth-averaged cross-reef momentum balance becomes:

$$\frac{\partial (U^2 D)}{\partial x} = -gD\frac{\partial \eta}{\partial x} - \frac{1}{\rho}\frac{\partial S_{xx}}{\partial x} + \frac{\tau^{sx}}{\rho} - \frac{\tau^{bx}}{\rho} \tag{3.2}$$

where $g = 9.81\ m\,s^{-2}$ is gravitational acceleration, S_{xx} is the cross-reef component of the wave-radiation stress tensor, in $kg\,s^{-2}$, ρ is the density of seawater, in $kg\,m^3$, τ^{sx} is the wind stress and τ^{bx} is the bottom stress, in Pa (Mei, 1989; Lowe et al., 2009b). The wave-radiation

stress tensor, S_{xx} is estimated as follows:

$$S_{xx} = \frac{\rho g H_s^2}{16} \left\{ (\cos^2(\theta_w) + 1)\frac{c_g}{c} - \frac{1}{2} \right\} \tag{3.3}$$

where H_s is significant wave height, in m, measured at E2, E4 and E6, and θ_w is wave direction, c_g is group velocity, and c is phase velocity (Longuet-Higgins and Stewart, 1962, 1964).

Bottom stress is estimated as:

$$\tau^{bx} = \rho C_{da} U |U| = \rho C_{da} \frac{q_0 |q_0|}{D^2} \tag{3.4}$$

where $C_{da}(x,t)$ is a bulk drag coefficient for the depth-averaged current (Rosman and Hench, 2011). The depth-dependence of drag has been shown to be important on coral reefs (Lentz et al., 2017) and is estimated as follows:

$$C_{da} = \kappa^2 \left\{ log\left(\frac{D}{z_0}\right) + (\Pi - 1) \right\}^{-2} \tag{3.5}$$

where $\kappa = 0.4$ is the von Karman constant, z_0 is the hydrodynamic roughness, and Π is Cole's wake strength, which is taken as 0.2. Hydrodynamic roughness, z_0, was estimated for the Dongsha Atoll reef flat in a previous study by Lentz et al. (2017), as 3.2 cm for E3 and 1.4 cm for E5 (Figure 3.1c).

Dividing Equation 3.2 by D and using Equation 3.1 yields:

$$-\frac{q_0^2}{D^3}\frac{\partial D}{\partial x} = -g\frac{\partial \eta}{\partial x} - \frac{1}{\rho D}\frac{\partial S_{xx}}{\partial x} + \frac{\tau^{sx}}{\rho D} - C_{da}\frac{q_0 q_0}{D^3} \tag{3.6}$$

Integrating Equation 3.6 from x_1 to x_2 to estimate the sea level difference $\Delta\eta = \eta(x_2) - \eta(x_1)$:

$$g\Delta\eta = -q_0|q_0| \left(\int_{x_1}^{x_2} C_{da} D^{-3} \mathrm{d}x + \frac{1}{2} sgn(q_0) D^{-2} \Big|_{x_1}^{x_2} \right) + \int_{x_1}^{x_2} \left(-\frac{1}{\rho D} \frac{\partial S_{xx}}{\partial x} + \frac{\tau^{sx}}{\rho D} \right) \mathrm{d}x \quad (3.7)$$

Solving for q_0 yields:

$$q_0|q_0| = \left(\int_{x_1}^{x_2} \left(-\frac{1}{\rho D} \frac{\partial S_{xx}}{\partial x} + \frac{\tau^{sx}}{\rho D} \right) \mathrm{d}x - g\Delta\eta \right) \Big/ \left(\int_{x_1}^{x_2} C_{da} D^{-3} \mathrm{d}x + \frac{1}{2} sgn(q_0) D^{-2} \Big|_{x_1}^{x_2} \right) \quad (3.8)$$

Similar to Lentz et al. (2016), Equation 3.8 can be simplified by recognizing that the bathymetric slope on the reef flat is very small (i.e. the magnitude of dD/dx is negligible). Equation 3.8 reduces to:

$$U|U| = -\frac{\Delta S_{xx}}{\rho C_{da} \Delta x} + \frac{\tau^{sx}}{\rho C_{da}} - \frac{g\Delta\eta D}{C_{da}\Delta x} \quad (3.9)$$

$$U = sgn\left(-\frac{\Delta S_{xx}}{\rho C_{da}\Delta x} + \frac{\tau^{sx}}{\rho C_{da}} - \frac{g\Delta\eta D}{C_{da}\Delta x} \right) \sqrt{\left| -\frac{\Delta S_{xx}}{\rho C_{da}\Delta x} + \frac{\tau^{sx}}{\rho C_{da}} - \frac{g\Delta\eta D}{C_{da}\Delta x} \right|} \quad (3.10)$$

where $\Delta x = x_2 - x_1$. For E3, x_1 and x_2 are E4 and E2, and for E5, they are E6 and E4, respectively.

Equation 3.10 states that for a two-dimensional control volume over the reef, the on-reef flux of momentum due to the incident wave radiation stress, wind stress and pressure gradient is balanced by the bottom stress. Equation 3.10 was used to estimate flow due to surface waves, wind and pressure gradients across the reef using 3 hour low pass filtered observations of water depth, wind speed and direction, and wave parameters. Results are not sensitive to filter cutoff periods between 1 and 6 hours.

The last term on the right-hand side of Equation 3.9 captures pressure gradients on the reef flat due to tides, wind and offshore surface waves. A unified tidal analysis and prediction method (Codiga, 2011) was used to find the tidally driven component of the sea level change ($\Delta\eta_{tide}$). Offshore waves that break on the reef crest (between E1 and E2) also create a pressure gradient which drives flow across the reef. The tidal residual of the pressure gradient term ($\Delta\eta_r = \Delta\eta$ - $\Delta\eta_{tide}$) is assumed to the be driven by the wave setup, but could also have some influence of tides and wind, which is discussed in Section 3.4.1. Wave energy that is not dissipated at the reef crest and is transmitted onto the reef flat contributes to the ΔS_{xx} term in Equation 3.10.

Equation 3.9 can be reorganized to account for the two pressure gradient terms ($\Delta\eta_{tide}$ and $\Delta\eta_r$).

$$U|U| = -\frac{\Delta S_{xx}}{\rho C_{da}\Delta x} + \frac{\tau^{sx}}{\rho C_{da}} - \frac{g\Delta\eta_{tide}D}{C_{da}\Delta x} - \frac{g\Delta\eta_r D}{C_{da}\Delta x} \tag{3.11}$$

The first and fourth term in Equation 3.11 represent the flow driven by surface wave forcing, and the second and third term represent the flow driven by wind and barotropic tides, respectively.

3.2.4 Particle tracking

Residence time was estimated to determine how flow affects the retention of water across the reef and consequently how that relates to various physical and biological features on the reef flat. A quasi-Lagrangian framework, similar to DeCarlo et al. (2017b) was used to determine the residence time (T_{RT}) of a water particle on the reef flat. Using water velocity, pressure and bathymetry data, water particles were tracked from discrete locations across the reef

flat. The residence time was estimated using depth-averaged velocity (in two-dimensions) and water depth ($h(x,t)$) at E3 and E5 (Figure 3.1), and LIDAR-based bathymetry data (resolution = 3 m, Shih et al., 2011) for the reef flat. Velocities across the reef were estimated by linearly interpolating the transport (Equation 3.1) between E3 and E5 when the particle was between the two stations, and applying transport at E3 from the reef crest to E3 and applying transport at E5 from E5 to the lagoon boundary. The tidal difference (η_0) in water depth for each time step was interpolated in the same way, and the water depth relative to mean sea level (h) at each location was used to calculate total depth at any location across the reef flat ($D = \eta_0 + h$). Velocity was not measured at any alongshore locations, so transport on the measured cross section was applied to the north and south in the region that bathymetry data was available ($\sim$ 1500 m to the north, $\sim$ 2000 m to the south of the cross section). The assumption that transport does not vary in the along reef direction is reasonable for an elongated reef (length>>width) where bathymetry does not vary substantially and waves break uniformly along the length of the reef. If the particle reached the north/south boundary, particle tracking was stopped.

Residence time (T_{RT}) was calculated in two different ways to determine (1) where the water at different locations on the reef is coming from, and (2) to determine the effect of varying depth and flow direction on residence time. First, residence time was calculated backward in time from discrete locations across the reef flat to the reef crest or lagoon boundaries to determine where water across the reef flat is coming from. Water particles were tracked across the reef flat until they reach the reef crest or lagoon boundary of the reef flat, as defined in Figure 3.1c,d. Second, particles were started at the reef crest and tracked forward in time to determine the time it takes for water to move across the reef flat with constant (averaged) and actual depth and transport values.

3.3 Results

3.3.1 Oceanographic Conditions

Conditions at the start of the deployment (approximately 04 to 07 June) were calm, with low wind and waves. Tropical Storm Hagibis formed in the northern SCS around 12 June and led to higher wind and wave conditions at the atoll.

Measurements from the meteorological station located on Pratas Island (Figure 3.1b) showed that wind (Figure 3.2a) near the start of the deployment, 04 to 07 June, was on average 1.9 m s^{-1} towards the northeast, and increased from 07 to 10 June, average of 2.9 m s^{-1} with gusts up to 11 m s^{-1}. From 10 to 14 June the wind changed direction towards the southwest, and was on average 3.0 m s^{-1}. The highest wind was seen on 14 to 16 June, on average 5.7 m s^{-1} towards the southeast and then northeast, with peak wind up to 17 m s^{-1}.

Significant wave height, H_S, (Figure 3.2b), measured offshore of the reef crest at E1, (Figure 3.1c), ranged from 0.2 to 3.0 m, with a period of smaller waves from 04 to 08 June and larger waves from 09 to 15 June. Offshore waves, measured at E1, break on the reef crest, dissipating most of their energy and contributing to setup and creating a pressure driven flow over the reef flat. However, some of the offshore wave energy is transferred onto the reef flat, as seen in the wave signal at E2 to E6. Wave height measured at E2 was significantly lower than at E1, ranging from 0 to 0.7 m, and was modulated by the tide. Waves at E4 and E6 are near zero throughout the deployment, however on 15 June wave height at E6 increases to 0.1 m, associated with high tide, strong wind towards the northeast and waves coming from the lagoon.

Spring tides occurred on 29 May (before the deployment began) and 13 June 2014. The
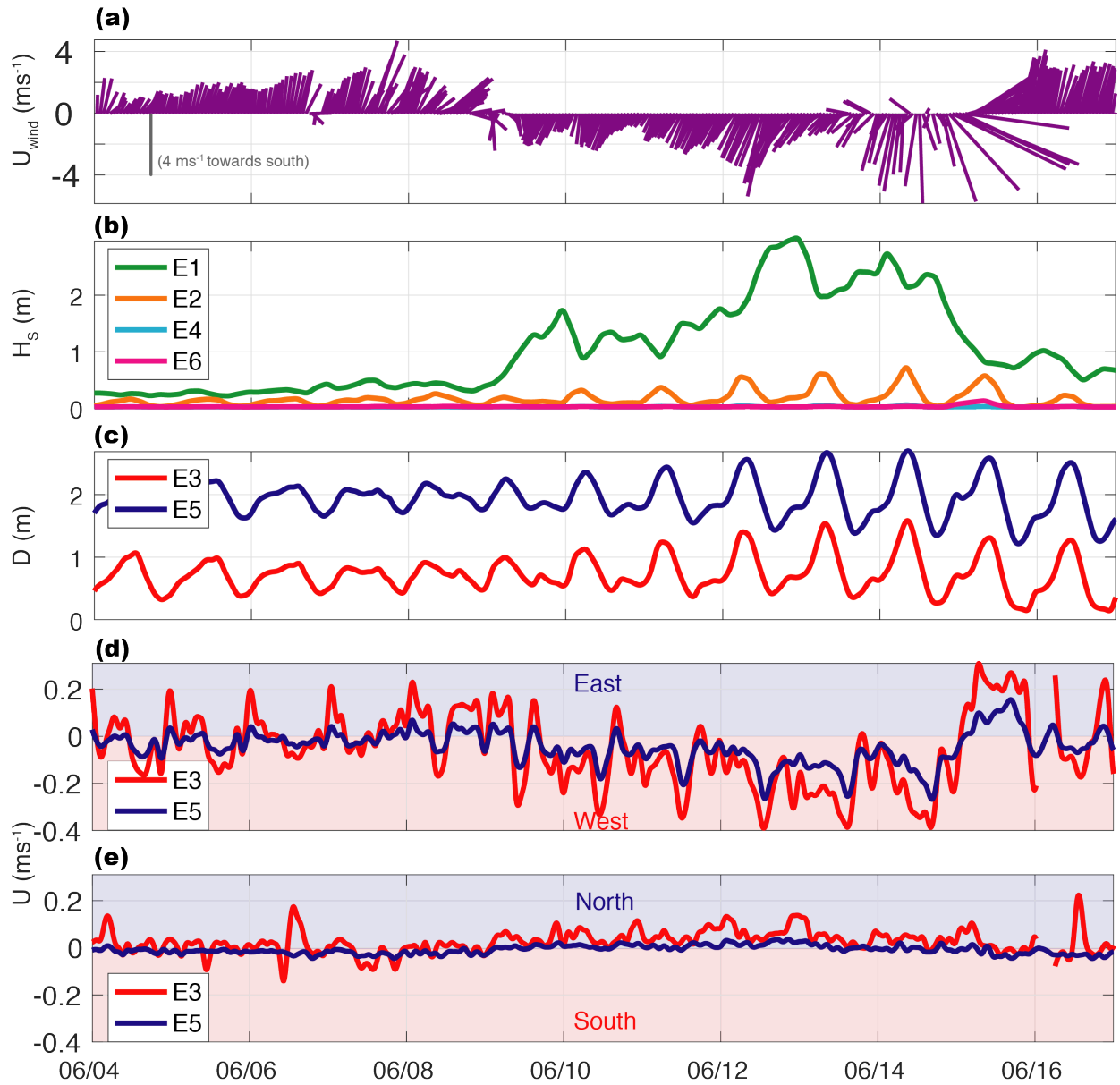
Figure 3.2: Oceanographic conditions during deployment
(a) Wind magnitude and direction (N—S, y axis; E—W, x axis) stick plot with vertical gray bar indicating a magnitude of $4 \, m \, s^{-1}$ towards the south. **(b)** Significant wave height H_s at E1, E2 , E4 and E6. **(c)** Water depth at E3 and E5. **(d)** Depth-averaged cross-shore (positive = eastward) and **(e)** along-shore (positive = northward) currents, at E3 and E5. Observational data in all panels is 3 hour low pass filtered.

daily tidal range during the deployment was between 0.4 and 1.3 m at E3, and between 0.4 and 1.4 m at E5 (Figure 3.2c).

Currents on the reef flat were primarily directed in the cross-reef direction throughout the deployment. Average magnitude of the cross-shore currents were 0.14 m s^{-1} at E3 and 0.06 m s^{-1} at E5 from 04 to 17 June. The average magnitude of cross reef transport is 0.11 m^2 s^{-1} and 0.12 m^2 s^{-1} at E3 and E5, respectively. A small increase in transport at E5 is expected due to the annular shape of the atoll. Average magnitude of the along-shore currents on the reef were 0.03 m s^{-1} at E3 and 0.02 m s^{-1} at E5 (Figure 3.2e). At the start of the study (04 to 08 June), cross-shore currents were slower and tidally reversing, and average cross-shore current magnitudes were 0.07 m s^{-1} at E3 and 0.03 m s^{-1} at E5 (Figure 3.2d). On 08 to 15 June, currents increased and were primarily in the westward direction (towards the lagoon), with average cross-shore current magnitudes of 0.16 m s^{-1} at E3 and 0.08 m s^{-1} at E5.

3.3.2 Variability in Temperature Across the Reef

The high spatial resolution of water temperature available from the DTS data allows us to examine near-bed thermal environments across the reef. Mean temperature over the study period (Figure 3.3b) is highest near the lagoon ($\sim$ 30.0 °C), and lowest at the reef crest ($\sim$ 28.5 °C) where cool offshore water is brought onshore. Large internal waves shoaling on the east forereef of Dongsha Atoll bring cold, nutrient rich water to the near surface, which is then transported westward onto the reef flat by tides, wind and surface waves (Reid et al., 2019). Daily intrusions of cool offshore water are seen in the DTS observations, when currents are directed in the onshore (westward) direction (see Figure 2 in Reid et al., 2019).

Daily temperature range (DTR) has been shown to be an influential metric for characterizing high-frequency temperature variability on coral reefs and thermal resilience (Safaie
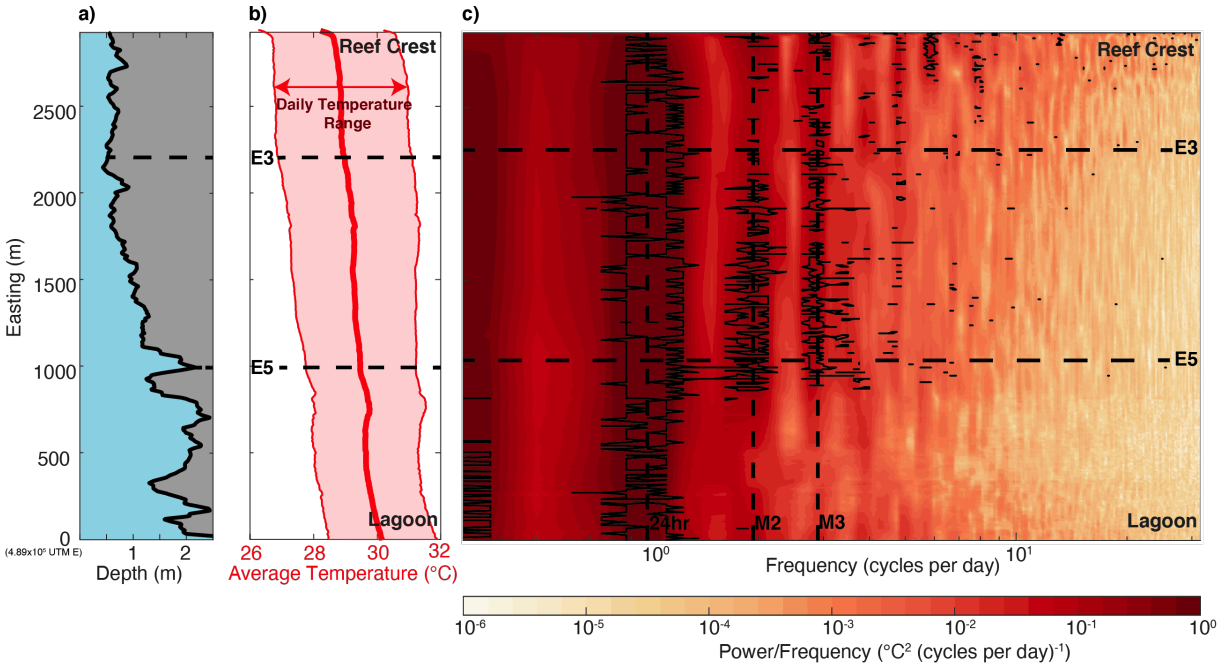
Figure 3.3: Environmental gradients across the east reef flat
(a) Depth below mean sea level associated with each point along the DTS cable. **(b)** Average near-bottom temperature from the DTS data across the east reef flat in red . Average daily temperature range across the east reef flat shown as the shaded area ($\pm$ 0.5 DTR from the mean temperature). **(c)** Power spectral density of near-bottom temperature across the east reef flat from the DTS data. Statistically significant peaks in the spectral analysis are outlined in black. The dashed black lines denote the diurnal (24 hour), semidiurnal (M2 tidal component) and terdiurnal (M3 tidal component) frequencies. All DTS data is averaged in 10 m sections.
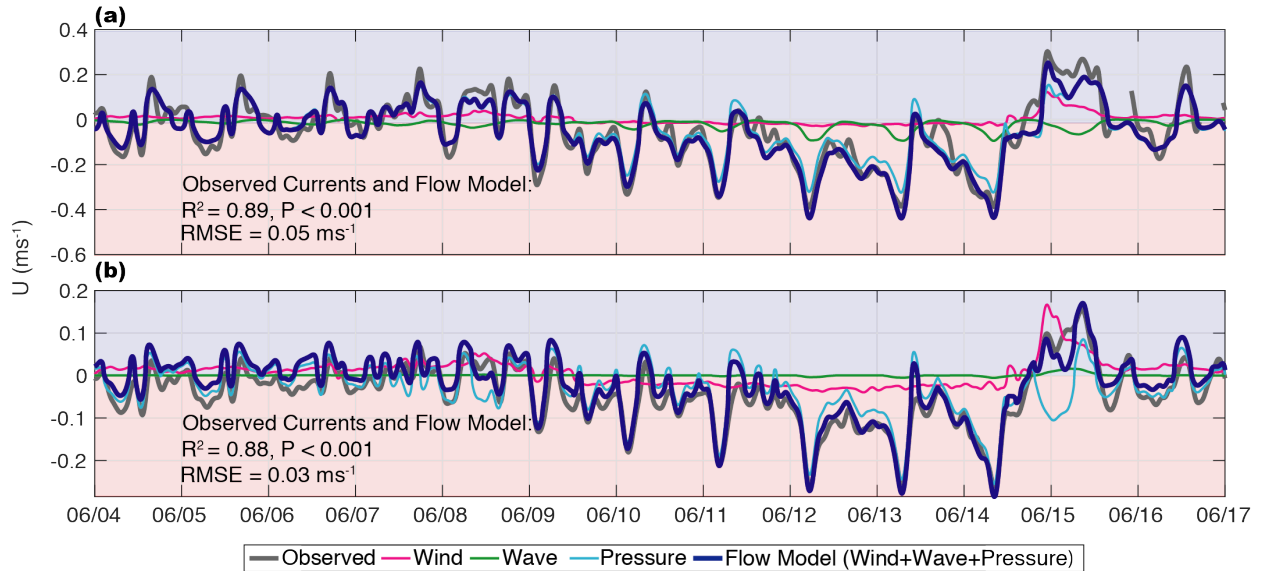
Figure 3.4: Cross-shore flow model
(a) and **(b)** show the observed currents (grey) and the three components of the flow model: wind (pink), waves (green) and pressure gradient (light blue) for E3 and E5, respectively. The sum of the three components of the flow model is shown in dark blue.

et al., 2018). Daily temperature range varies across the reef, ranging from approximately 4.2 °C near the reef crest, where water depth is shallower, to 3.1 °C near the lagoon, the deepest part the reef flat (Figure 3.3a,b).

From the spectral analysis (Figure 3.3c), it is evident that there is significant diurnal variation in water temperature across the entire reef flat. This is likely due to daily heating and cooling from solar insolation of water on the shallow reef and the diurnal component of the tidal flow. Additionally, there are significant peaks at the M2 and M3 tidal frequencies near the middle of the reef flat and towards the reef crest, corresponding to similar spectral peaks in the pressure data which are likely due to the semi-diurnal and higher frequency tidal harmonics present on the shallow reef flat. There is also significant higher frequency variability (>3 cpd) close to the reef crest.

3.3.3 Physical Processes Driving Circulation on the Reef Flat

Reid et al. (2019) completed a heat budget analysis for the Dongsha reef flat, and found that the balance of atmospheric heating and advection of heat across the reef accurately predicts the observed heating rates on the reef flat. The contribution of atmospheric and advective heat flux varied throughout the deployment at E3 and E5 (see Figure 2 for a composite day, and Supplementary Figure S1 for 8 days of the heat budget, Reid et al., 2019), but on average these terms contributed approximately equally to the rate of change of temperature on the reef flat. Tides, wind and waves are driving flow across the reef flat, and subsequently contributing to the advection of heat across the reef. Understanding the physical processes which are contributing to the advective heat flux across the reef can explain the patterns of variability seen in the temperature across the reef flat.

The flow predicted using Equation 3.10 was compared to observed currents on the reef flat at E3 and E5. This simple analytical model (Equation 3.10) reproduced the observed reef flat currents with a R^2 of 0.89 and 0.88 (p <0.001) at E3 and E5, respectively (Figure 3.4). The root-mean-squared error between the model and the observed reef flat currents was 0.05 m s^{-1} and 0.03 m s^{-1} at E3 and E5, respectively.

The terms in Equation 3.11 were used to attribute flow forcing to waves, wind and tides (described in Section 3.2.3). For the entire deployment, the wind stress term accounted for on average 2% of the flow at E3. Waves, driven by the wave radiation stress and residual pressure gradients terms, and tidal pressure gradients each accounted for approximately half of the flow at E3. At E5, surface waves and tide account for 42% and 40% of flow, respectively, and wind accounts for 18% flow. Complications and interdependencies between terms in this simple analytical solution are discussed in Section 3.4.1.

3.3.4 Residence time

The origin (offshore vs. lagoon) of water flowing onto the reef and the residence time of that water on the reef flat both influence the spatial gradients in mean temperature and DTR seen in Figure 3.3. Residence time was estimated by tracking water particles backward in time from six starting locations on the reef (Figure 3.5g, A to F). Only particles that originated from reef crest or the lagoon (as indicated by the dashed lines in Figure 3.5g) were used for residence time estimates. The average residence time was 3.6 hours near the reef crest (Figure 3.5, location F), and increased to 8.6 hours near the lagoon (location A). Particles that end near the reef crest (location F, Figure 3.5f) have short residence times (0 to 3 hours), with a positively skewed tail towards longer residence times. This distribution holds across the middle of the reef flat (location D to F, 3.5d,e,f) but becomes more evenly spread (i.e. a more normal distribution) towards the lagoon (location A to C, Figure 3.5a,b,c). At locations A to C the most common residence times are 3 to 6 hours.

During our study period, near the reef crest (location F) 83% of the particles originated from offshore, and only 3% came from the lagoon. Near the lagoon (location A) the percentage of particles that came from offshore decreases to 50%, while the water particles that came from the lagoon increases to 21%. The remainder of particles could not be tracked to one of these boundaries because they travelled alongshore to the north or south.

Residence time varied throughout the deployment, and the source of the water also varied. At the start of the deployment (04 to 05 June), closer to the spring tide and when wind and waves are small, residence times at point C and D (Figure 3.5g) were on average 11 hours. During this time, 94% of the particles are coming from offshore. During the neap tide (06 to 08 June), residence times were slightly longer ($\sim$ 13 hours), however during this time, 46% of particles were coming from offshore, and 52% are coming from the lagoon (the
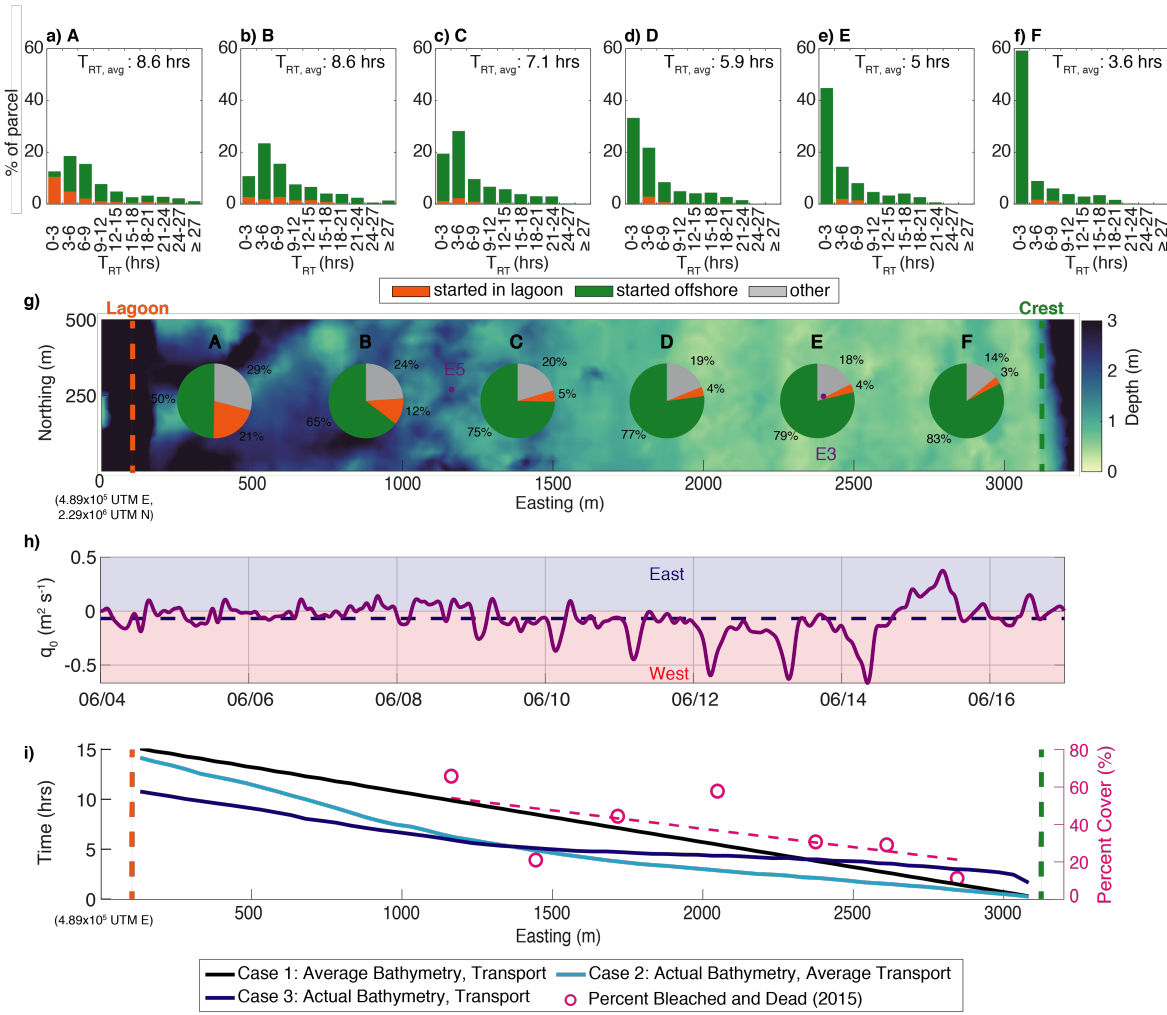
Figure 3.5: Residence time estimates across reef flat

(a) to **(f)** the percentage of particles that started either from the lagoon or offshore from the locations in (g), and the distribution of residence times. **(g)** pie charts show at that location on the reef flat the total percentage of particles that started in either the lagoon or offshore. 'Other' includes tracks that came from the north/south or insufficient data. **(h)** Average cross shore transport in blue dashed line (positive = eastward), and actual cross shore transport across the reef flat in purple. **(i)** the time it takes for a particle started at the reef crest to move across the reef (Section 3.3.4) for case 1 shown in black (average bathymetry and transport across the reef flat), case 2 shown in light blue (actual bathymetry and average transport) and case 3 shown in dark blue (actual bathymetry and transport). The percent of total coral cover that was bleached or dead after a bleaching event in 2015 (DeCarlo et al., 2017a) is shown in pink, with a linear fit to the data.

remainder come from the north/south). Although the residence time was similar when comparing spring and neap, the source of the water changed. When wind and waves picked up (09 to 13 June), residence times were much shorter ($\sim$ 3 hours), and 100% of particles were coming from offshore.

In order to understand how depth and variability in current speed and direction affect residence time estimates on the reef flat, the time for a particle starting at the reef crest to move across the reef flat was determined. Particles are tracked forward in time in three different ways: (1) using an average onshore (westward) transport (Figure 3.5h) and average depth (1.23m) across the entire reef flat, (2) using an average onshore (westward) transport and actual depth across the reef flat, and (3) using actual transport and depth across the reef flat.

Case 1 is the simplest way to think of transit time of a particle from the reef crest to lagoon, and predicts shorter residence times near the offshore (eastern) edge of the reef, and longer times further onshore towards the lagoon (black line, Figure 3.5i. Variability in the depth of water across the reef flat can have a significant impact on the residence time of water (case 2, light blue, Figure 3.5i). For Dongsha, the actual bathymetry decreases the time it takes for a particle to move across the reef flat, because residence times are significantly shorter in the first half of the reef flat where depths are shallower than the average (case 1). The time it takes for a particle to move across the first half ($\sim$ 1500 m) of the reef flat is approximately 5 hours, which is shorter than case 1 ($\sim$ 8 hours). As depth increases towards the lagoon, the slope of the line increases as particles slow down in deeper water (Figure 3.5i), and residence times for case 1 and 2 converge near the lagoon.

Variability in the current speed and direction also lead to complex patterns of residence time across the reef. Tidal fluctuations in flow direction (case 3, dark blue, Figure 3.5i) lead to longer residence times closer to the reef crest, because currents are not always directed
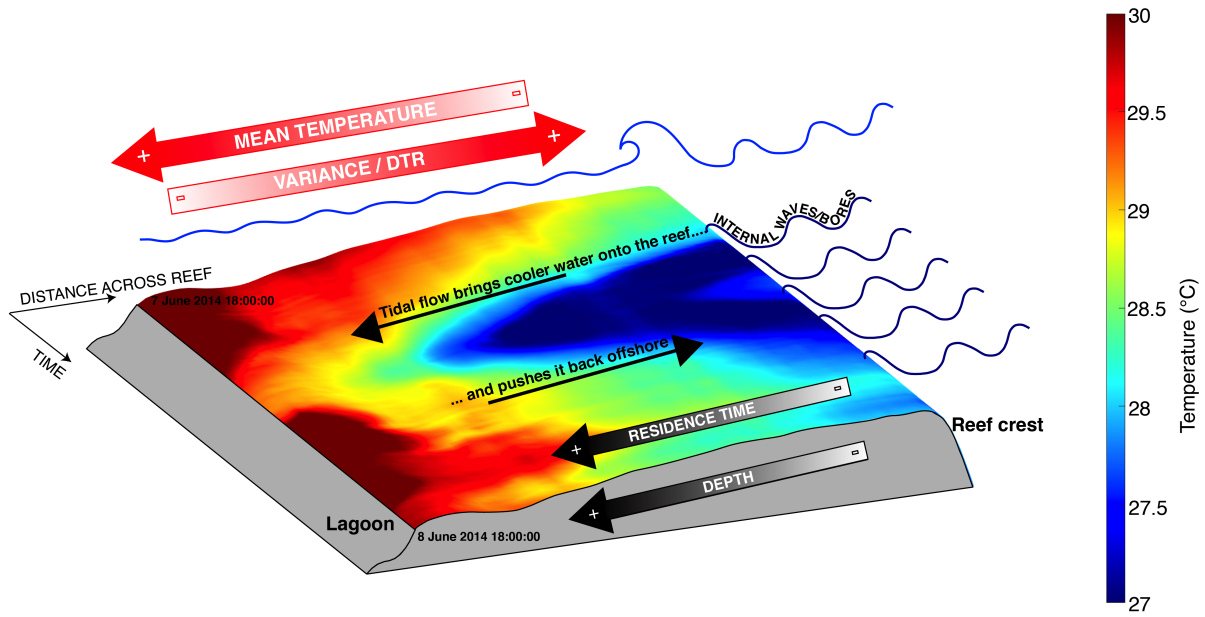
Figure 3.6: Example of DTS data for 07 to 08 June 2014

A quasi-3D view of continuous near-bed temperature measurements across a 3-km cross section of the east reef flat. Bathymetry is smoothed for the cross section of the reef where the DTS is located.

onshore (westward). In the back half of the reef particles slow down in deeper water, similar to case 2, however the time to reach the back of the reef ($\sim$ 11 hours) is shorter than case 1 and 2 ($\sim$ 15 hours), because the observed transport was greater and primarily directed towards the lagoon during the second half of the deployment when wind and waves increased.

3.4   Discussion

The reef flat at Dongsha Atoll is anomalously wide ($\sim$ 3 km), compared to other reefs in the literature (Falter et al., 2013; Goldberg, 2016), and this contributes to the observed patterns of flow and spatial temperature variability (Figure 3.6; also see Figure 2 in Reid et al., 2019, for 8 days of DTS data). Our measurements indicate that flow on the reef flat is driven primarily by tides, wind, and surface waves (Section 3.3.3). These physical processes govern the residence time of water across the reef flat, creating gradients in mean temperature,

diurnal temperature range (DTR) and likely other chemical parameters, although these were not measured.

3.4.1 Physical Processes on a Wide Reef Flat

In Section 3.3.3, Equation 3.11 is used to separate the physical forcings driving flow across the reef flat due to surface gravity waves, tides, and wind stress. The short duration of our field experiment and inherent interdependence in these forces introduce complications to this simple attribution, which we will discuss further in this section.

The pressure gradient term (the last term under the radical in Equation 3.10) represents reef-scale pressure gradients due to tides, wind and surface gravity wave setup. As discussed in Section 3.2.3, surface tides contribute significantly to the pressure gradient term, accounting for 38% and 32% of the variability of $\Delta\eta$ at E3 and E5, respectively. The remainder of the pressure gradient term ($\Delta\eta_r$) was attributed to pressure driven flow from sea level setup by surface gravity waves breaking on the reef crest. From 09 to 15 June significant wave height at E1 is large (>1m, Figure 3.2b), and during this period, there is a large, low frequency pressure gradient at both E3 and E5 due to offshore wave setup (Figure 3.4). The tidal residual pressure gradient ($\Delta\eta_r = \Delta\eta$ - $\Delta\eta_{tide}$) was compared to offshore wave height at E1. The residual pressure gradient term ($\Delta\eta_r$) was significantly correlated with offshore wave height at E3 and E5, R^2 = 0.65 and 0.43, p <0.0001, respectively. This correlation indicates that waves are driving sea surface elevation change, and consequently flow on the reef flat, even as far back on the reef as E5.

The two-week duration of our observations does not permit the resolution and prediction of all tidal constituents, and thus the residual pressure gradient term ($\Delta\eta_r$) likely still includes some influence from tides. Additionally, the tidal response of the lagoon lags the ocean by

approximately 40 minutes - appearing as a pressure gradient between the open ocean and the lagoon. This is also imperfectly captured by our tidal analysis. Tidal modulation of wave radiation stress at the reef crest (e.g. Becker et al., 2014) can be clearly seen in the tidal variations in significant wave heights at E2 relative to the offshore wave heights at E1 (Figure 3.2b). If tidally modulated wave radiation stress dominated the tidal component of the pressure gradient term ($\Delta\eta_{tide}$), we would expect it to peak at low tide; however, $\Delta\eta_{tide}$ exhibits a 90 degree phase difference with the sea level at E3, consistent with tidal forcing.

Previous observations on reefs flats, often with narrower widths than Dongsha, have shown that wind is almost never a dominant force and flow is instead driven primarily by a pressure gradient from surface wave setup or tidal driven flow (Hench et al., 2008; Taebi et al., 2011; Rogers et al., 2016). The average contribution of wind driven flow from 04 to 14 June was 2% and 17% at E3 and E5, respectively. The contribution of wind driven flow increased to 9% and 37% at E3 and E5, respectively, on 15 June, when wind towards the northeast greatly increased. During this windy period, the contribution off the wind stress term at E5 is greater than the wave and tidal forcing.

Wind-driven sea level changes in the lagoon could also be contributing to the pressure gradient driving flow across the reef flat. The wind stress term (in Equation 3.11) only takes into account local wind stress at that location on the reef. For example, an eastward wind, like that which occurred on 15 June, may cause sea level to rise on the east side of the lagoon (on the west side of the reef flat) contributing to pressure driven flow on the reef flat. And, as expected, on 15 June, the strong eastward wind event is accompanied by coincident increase in both the wind stress and the pressure gradient term driving flow across the reef flat. However, on average, the magnitude of the wind was not significantly correlated with the residual pressure gradient term ($\Delta\eta_r$) during our study period.

The internal tide at Dongsha Atoll influences the sea surface height offshore of the reef crest, and subsequently the pressure gradient which is driving flow across the reef flat. The residual between the sea surface height measured offshore of the reef crest at E1 (η_{E1}) and the barotropic tidal sea level variation (η_{tide}), estimated using the OTIS model and TMD toolbox (Egbert and Erofeeva, 2002; Padman and Erofeeva, 2004), was bandpass filtered (10 to 26 hours) and used to estimate the sea level variation due to the internal tide at E1 (η_{IT}). The standard deviation of η_{IT} was 20% of that for η_{tide} on the forereef; however, the spatial gradient in sea level across the reef flat ($\Delta\eta_{IT}$) may be significant, since η_{IT} in the lagoon is likely near zero. This offshore sea level variation due to internal tides is small compared to the barotropic tide, but it may play a significant role in driving flow over the reef flat.

Barotropic tides have a significant effect on flow across the reef flat, accounting for 48% and 41% of the flow variance at E3 and E5, respectively. On the wide reef flat, the tidal excursion, or the distance that a water particle moves over one tidal cycle, varies on fortnightly timescales. From the DTS data, it is evident that cooler offshore water comes onshore during the flood tide and sometimes reaches the lagoon (Figure 3.6; also see Figure 2 in Reid et al., 2019, for 8 days of DTS data). However, on smaller flood tides the cooler offshore water does not make it all the way to the lagoon, but goes back offshore (eastward). For example, on 08 June, during the neap tide and low wave conditions, cold water comes onshore (westward) during the flood, and when currents turn around (eastward), the cold water goes back offshore (Figure 3.6). The contribution of tides to flow (Equation 3.11) on 08 June was on average 38% and 40% at E3 and E5, respectively. On 04 June, when wave conditions were similar to 08 June, stronger tidal currents push cold water all the way across the reef flat (westward) during the flood tide (see Figure 2 in Reid et al., 2019). On 04 June, the contribution of tides to the flow was much greater, 55% and 53% at E3 and E5, respectively.

To understand how tidal excursion of offshore water varies, particles were tracked forward
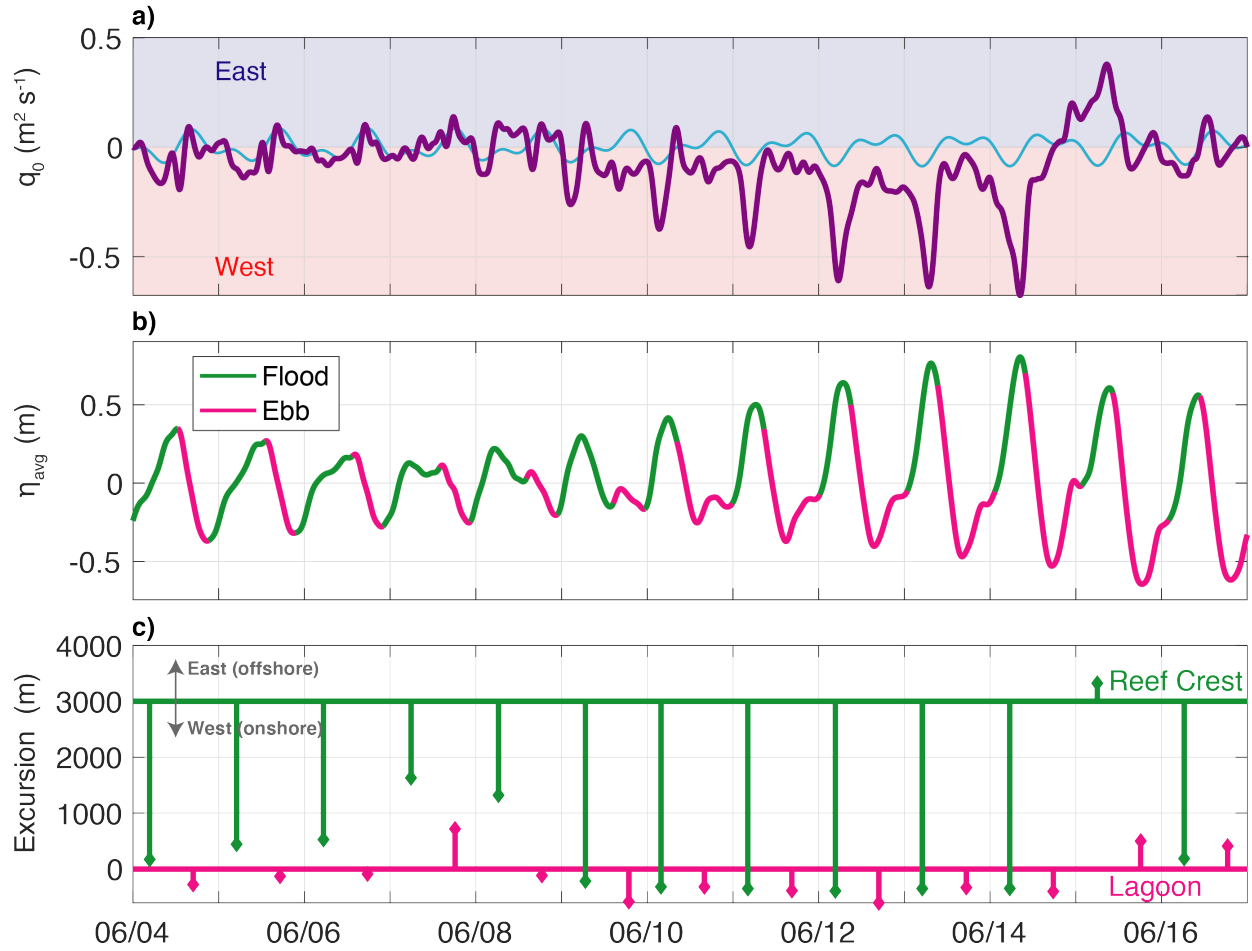
Figure 3.7: Tidal Excursion

(a) Cross-shore transport in purple (positive = eastward), and detrended tidal component of the cross-shore transport in light blue. (b) Average sea level variation across the reef flat, with the flood timing in green and ebb timing in pink. (c) Cross-shore excursion during floods (green) from the reef crest and ebbs (pink) from the lagoon boundary.

in time from the reef crest at the start of every flood tide to estimate the total cross-shore distance the particle travels during a flood. The time of onshore (flood) and offshore (ebb) transport was determined by looking at the detrended tidal diurnal and semi-diurnal component of the average across-shore transport (Figure 3.7a). Particles were tracked from the reef crest when tidal currents were directed onshore (westward), for the duration of the flood.

On average, particles travelled approximately 2570 m (approximately 85% of the reef width) westward towards the lagoon during flood tides (Figure 3.7c). At the start of the

44

deployment (04 to 09 June), there were no significant waves or wind driving flow across the reef flat (Figure 3.2a,b), therefore the flow was largely tidally driven. During the flood tide on 04 and 05 June, near the end of the spring tide, particles travelled westward from the reef crest on average 2700 towards the lagoon. On 06 to 08 June, before wind and waves picked up, particles did not make it into the lagoon, traveling on average 1840 m, during the flood. This is because of weaker currents on the reef flat during the neap tide. On 10 to 14 June, wind and waves picked up, and particles travelled across the reef flat into the lagoon (>3000m). On 15 June, even during the flood tide, high wind toward the northeast pushed water particles at the reef crest offshore (eastward).

Particles were also tracked from the lagoon boundary during the ebb tides to estimate the excursion length during ebb and the influence of lagoon-origin water across the reef flat. During the ebbs on 04 to 08 June, particles stayed near the lagoon boundary, traveling on average 5 m towards the reef crest, and were also carried alongshore (Figure 3.7c). When wind and waves pick up on 09 to 14 June, particles were transported directly into the lagoon during the ebb tide, not entering the reef flat.

There is significant asymmetry in the tidal excursion of water on the reef flat that is evident when tides were primarily driving flow near the start of the deployment (04 to 08 June). During the flood tides, offshore water is moving on average 2200 m onshore (westward); however, during the ebb tides, lagoon water is moving on average 5 m onto the reef flat. This results in more offshore water than lagoon water coming onto the reef flat, which could significantly impact the biogeochemistry on the reef flat. Additionally, in our observations the average tidal excursion length is less than the width of the reef flat, contributing to increased residence time of water on the reef.

3.4.2 Formation of Environmental Gradients

A heat budget analysis for the Dongsha Atoll reef flat (current study site) by Reid et al. (2019) indicates that atmosphere-ocean surface heat flux and advective heat flux contribute in approximately equal parts to the change in temperature across the reef. In this study we examine the physical mechanisms contributing to the advective flux of water on the reef flat and find that surface waves, tides, and wind were all important during our study period. These physical mechanisms combined with variable water depth on the reef flat can create complex patterns in the residence time of water on the reef and correspondingly, environmental gradients in temperature (Figure 3.6).

Daily temperature range (Section 3.3.2) was highest ($\sim$ 4.3 °C), and mean temperatures were lowest ($\sim$ 29.0 °C) near the reef crest. The high DTR near the reef crest and E3 is not only due to daily heating and cooling (surface heat flux) on the shallow reef flat, but also due to high frequency variability in offshore source water and time-variable, tidally forced advective heat flux. Seawater offshore of the reef crest is often cold and highly variable in temperature due to deep water mixed to the surface by shoaling internal waves (Davis et al., 2020). This water is subsequently forced onto the reef flat by tides, wind and waves (see Reid et al., 2019), contributing to the low mean temperature and high variability observed near the reef crest (Figure 3.3). The shallow water depths near the reef crest lead to strong currents and short residence times (Section 3.3.4).

The DTR is lowest ($\sim$ 3.2 °C), and mean temperatures are highest ($\sim$ 30.0 °C) further back on the reef flat near the lagoon. Here, the water is deeper, and has longer residence times. This stagnant water can heat up during the day, contributing to a peak in the temperature spectrum at 1 cycle per day (Figure 3.3) and is subject to less variability in temperature. Also, there is less of an influence of offshore cool water here, leading to higher

mean temperatures.

In the Red Sea, Davis et al. (2011) and Pineda et al. (2013) showed that wave-protected regions on the back of the reef flat had highest mean temperatures, and wave-exposed regions near the reef crest had lower mean temperatures, consistent with observations on Dongsha Atoll. However, these studies also found that the wave-protected regions of the reef flat had the greatest temperature variability - unlike our findings on Dongsha Atoll. On the Red Sea reefs, regions with low temperature variability were located near the reef crest where surface wave forcing was strong, but there were no internal waves. On the east reef flat at Dongsha, we see the opposite spatial pattern in temperature variability, with the surface and internal wave-exposed reef crest having the highest temperature variability. Davis et al. (2011) and Cyronak et al. (2020) also find that shallow regions have the highest temperature variability, consistent with our observations on Dongsha Atoll.

3.4.3 Patterns in Benthic Cover and Bleaching

Thermal tolerance of corals has been shown to vary substantially within an individual reef (e.g. Pineda et al., 2013; Palumbi et al., 2014; Safaie et al., 2018), and studies suggest that reefs that normally experience a variable thermal environment may have a higher temperature tolerance (McClanahan et al., 2005; Oliver and Palumbi, 2011; Palumbi et al., 2014; Safaie et al., 2018). The physical mechanisms driving flow, and resulting residence times across the reef flat are connected to the physical environment and biogeochemistry, and consequently can affect community structure and thermal tolerance of coral reefs. While the physical forcings on the reef flat, primarily tidal and surface waves, and resultant residence times presented here are specific to our two week deployment, we expect that these patterns would be similar outside of our observational period. These results may give some insight into the patterns of benthic cover and bleaching seen at Dongsha Atoll.

In 2015, an ecological survey of the Dongsha Atoll reef flat (current study site) was conducted to quantify coral genera and substrate type both before and after a coral bleaching event (Figure 3.5i) (DeCarlo et al., 2017a). The eastern region of the reef flat, near the reef crest, which had shorter residence times and higher temperature variability during our deployment, had a smaller percentage of corals that bleached or died (Figure 3.5i). This is in contrast to a study by McClanahan et al. (2005) in Mauritius, where they saw that regions with high water flow, that were typically further offshore, experienced higher bleaching intensity. Mean temperature and residence time are both lowest at the reef crest and increase towards the back of the reef (Figure 3.6). On Dongsha Atoll, during this deployment, temperature variability and residence time have an inverse relationship, with short residence times being associated with high variability and long residence times with low variability.

At our study site, DeCarlo et al. (2017b) found relatively low coral cover (6%) near the reef crest, likely due to mechanical breakage from large offshore surface waves breaking on the reef crest (Section 3.3.3). From E3 to E5 coral cover was fairly consistent, at an average 27%, while towards the lagoon side of the reef flat the benthic cover shifts to almost entirely seagrass (78% cover), with very little coral cover (DeCarlo et al., 2017b). A study by Rogers et al. (2016) at Palmyra Atoll showed regions with moderate to high coral cover ($> 10\%$) had lower mean temperatures than regions with low or no coral cover ($< 10\%$). They also observed low coral cover in the back-reef and lagoon, where mean temperatures were higher, and travel times are longer. This trend is consistent with the results seen during this deployment, where the back-reef region (E6) mean temperatures were the highest and there was almost no live coral cover (DeCarlo et al., 2017b).

High frequency temperature variability (i.e. DTR) was shown to be the most influential metric in predicting bleaching prevalence on coral reefs in a global study by Safaie et al.

(2018). On Ofu Island, in American Samoa, Oliver and Palumbi (2011) also showed that environmental variability across an individual reef can lead to variable bleaching responses. Corals living in more variable environments had increased thermal tolerance, and lower rates of mortality. On Dongsha Atoll from the reef crest to the middle of the reef, E2 to E5, there was significant variability in temperature at higher frequencies during our deployment (>24 hours, Figure 3.3c). A survey by DeCarlo et al. (2017a) after a severe bleaching event at Dongsha Atoll in 2015 found that the percentage of coral bleached or dead was lowest near the reef crest, and increased further back on the reef flat (Figure 3.5i).

A study from the Red Sea, documenting reef response to a bleaching event in 2010, showed that bleaching and mortality was most severe on the wave-exposed (offshore) side of the reef platform where mean temperature and variability was lowest (Pineda et al., 2013). The wave-protected (onshore) side of the reef, which has higher mean temperatures, and increased variability, experienced lower mortality. On the Dongsha Atoll reef flat, there are similar patterns in mean temperature (cooler on the offshore/exposed side, warmer on the onshore/protected side), but the opposite pattern in temperature variability seen during this deployment. Pineda et al. (2013) explain the observed pattern in mortality is likely due to previous biological adaptation and acclimatization of corals to high frequency variability, similar to at Ofu (Oliver and Palumbi, 2011). On Dongsha, high temperature variability near the reef crest could lead to low bleaching and mortality in this region.

Safaie et al. (2018) showed that depth was the second most influential metric in predicting bleaching prevalence, with deeper reefs less likely to experience pervasive bleaching. Safaie et al. (2018) note that variability and depth may work in complementary ways to mitigate bleaching, with shallower regions having higher variability and therefore greater thermal tolerance, and deeper regions providing refuge for corals, despite lower variability in temperature. At Dongsha, bleaching and mortality was lowest near the reef crest, where the depth

was shallowest and temperature variability was highest (Figure 3.3 and 3.5i). Bleaching and mortality increased with depth towards the back of the reef, and variability decreased.

3.5   Conclusion

The observations and analyses presented here show that the processes driving flow on the east reef flat at Dongsha Atoll are tidal pressure gradients, wind stress, and surface waves, and that across the reef flat there is variability in both the residence time of water and the thermal environment.

From a simple analytical model of flow on the reef flat, we find that waves and tides each contributed in approximately equal parts to forcing flow on the eastern part of the reef flat (E3) during our study, and wind only contributed significantly during a large wind event. Further back on the reef towards the lagoon (E5), tides and waves also contributed in equal parts, however wind played a more substantial role in driving flow throughout the deployment, especially during the large wind event. Furthermore, the wide reef flat at Dongsha leads to unique patterns of tidal excursion across the reef flat throughout the deployment.

Residence times across the reef flat are shortest near the reef crest, and increase towards the lagoon. The majority of water near the reef crest is coming from offshore (83%), and only a small portion (3%) comes from the lagoon during this deployment, with the remainder unresolved by our particle tracking model. Closer to the lagoon, approximately half of the water originates from the reef crest (i.e. offshore), and only 21% comes from the lagoon. The source of water can influence the thermal and chemical environment across the reef flat.

Understanding the processes driving flow at different locations on the reef, and the sub-

sequent temperature gradients, can help us to understand the distribution of coral across the reef at Dongsha. This elevated thermal variability is a distinguishing feature of shallow reefs compared to the open ocean, and may influence the thermal tolerance of corals. A better understanding of spatial patterns in thermal microclimates and thermal tolerance can help inform which coral reefs may be more resilient in a changing climate and should be prioritized for protection.

Chapter 4

Internal waves influence the thermal and nutrient environment on a shallow coral reef

4.1   Introduction

Internal waves are a persistent feature throughout the world's oceans and can have significant physical and biological impacts on marine ecosystems (Garrett and Munk, 1979; Woodson, 2018). Much attention in the literature has been given to internal waves on the middle and outer continental shelves (Nash et al., 2012; Alford et al., 2015), and increasingly we are learning more about their influence in the inner shelf and nearshore environment (Walter

et al., 2012; Sinnett and Feddersen, 2014; Walter et al., 2014). Shoaling internal waves can transport cold and nutrient-rich water into shallow coastal regions and have been observed to modify water properties and influence the metabolism of benthic communities in coastal ecosystems such as kelp forests and coral reefs (Wolanski and Pickard, 1983; Zimmerman and Kremer, 1984; Wolanski and Delesalle, 1995; Leichter et al., 1996; McPhee-Shaw et al., 2007; Noble et al., 2009; Hofmann et al., 2011; Lucas et al., 2011; Green et al., 2018).

The accelerating degradation of coral reefs over the past 50 years due to rising sea surface temperatures and ocean acidification has led to predictions of a global-scale collapse in reefs within the next few decades (Hoegh-Guldberg et al., 2007; Donner, 2009; Van Hooidonk et al., 2016). However, variation in the physiological responses of individual coral colonies and reefs to environmental stresses suggests critical differences in corals' resilience and/or environmental conditions over small spatial and temporal scales (Riegl and Piller, 2003; Pandolfi et al., 2011; van Woesik et al., 2011, 2012). For example, thermal tolerance can vary substantially across an individual reef (e.g., Pineda et al., 2013; Palumbi et al., 2014; Safaie et al., 2018) and some coral communities thrive in naturally acidified waters (Shamberger et al., 2014; Barkley et al., 2015). Thus, coral organisms with greater resilience and adaptive capacity may persist despite climate change impacts (Pandolfi et al., 2011; Spalding and Brown, 2015). Identifying these resilient corals and prioritizing their protection may be the best strategy for long-term conservation of coral ecosystems (Barshis et al., 2013). Although the factors which confer resilience to coral bleaching are not fully understood, emerging evidence suggests that corals living in areas with naturally variable thermal environments may have higher temperature tolerance (McClanahan et al., 2005; Safaie et al., 2018). Thus, there are strong conservation incentives for investigating the drivers of high-frequency (diurnal or shorter timescales) temperature variability on reefs, including air-sea heat fluxes (e.g., Davis et al., 2011) and internal waves (e.g., Wolanski and Delesalle, 1995; Leichter et al., 1996; DeCarlo et al., 2015).

Dongsha Atoll, a coral reef and Taiwanese National Park in the northern South China Sea (SCS), is directly in the path of some of the world's largest internal solitary waves (with amplitudes of 100-150 m) generated by tidal currents in the Luzon Strait (e.g., Hsu and Liu, 2000; Alford et al., 2015). These internal waves shoal and form bottom-propagating internal bores – internal waves of elevation, where the strongest currents and temperature fronts are near the bed – and boluses on the shallow topography of the reef system and the surrounding shelf, injecting cold, nutrient-rich water onto the forereef (e.g., Wang et al., 2007; Fu et al., 2012; Alford et al., 2015; DeCarlo et al., 2015). We examine benthic thermal environments using a Distributed Temperature Sensing (DTS) system, which resolves spatially-continuous temperature measurements along a fiber optic cable. A 4 km cable was deployed from the east forereef to the lagoon (Figure 4.1). We show that internal waves modify the surface water properties on the forereef and that this water is transported onshore by tides, surface waves and wind. Using the DTS measurements we then quantify the effect of internal waves on the temperature and nutrient environment on the shallow reef flat.

4.2   Methods

4.2.1   Site description

Dongsha Atoll is 28 km in diameter and has an area of approximately 600 km2 (Dai, 2004). The east reef flat, which is the focus of this paper (Figure 4.1b), is roughly 3 km wide, and ranges from 0.6 to 3.5 m depth. The tidal range on the reef flat is approximately 0.9 m. The forereef has a gradual 4% slope down to 25 m depth, beyond which it steepens to 15%. A survey of the benthic composition of the reef flat shows the region is dominated by fleshy
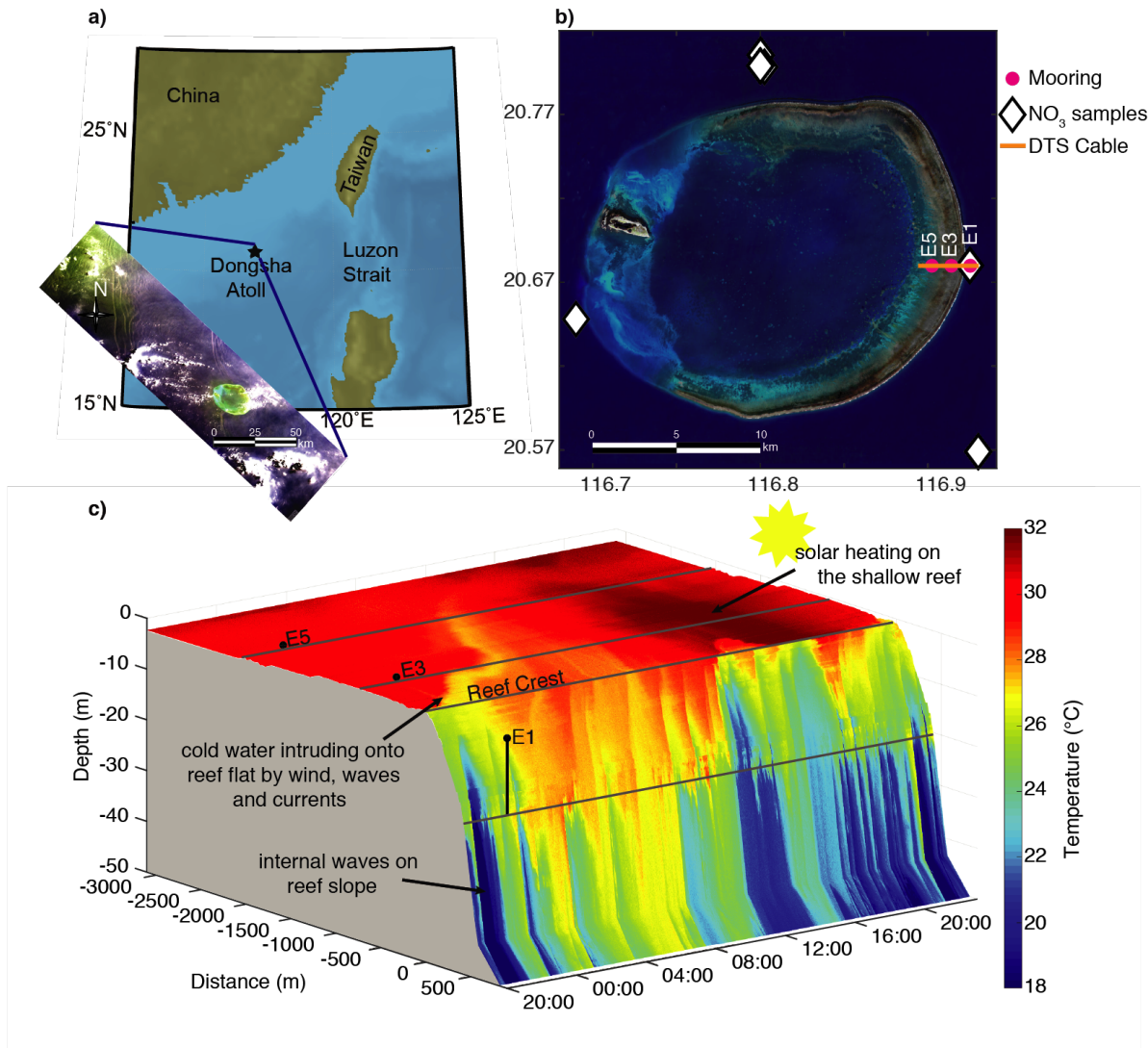
Figure 4.1: Oceanographic setting of the Dongsha Atoll
(a) shows the location of Dongsha Atoll within the northern South China Sea and (b) is a satellite view of the atoll with locations of the DTS cable as an orange line across the east reef flat and slope, and moorings E1, E3 and E5 in pink. Nitrate/temperature sample locations are shown in white diamonds. Two nitrate/temperature sample locations not shown are located at [117.56, 20.760] and [117.63, 20.79]. (c) is a 3-dimensional cross-section of the reef slope and flat with temperature data from the DTS and includes the locations of instrumentation on the reef at E1, E3 and E5.

algae, sea grass and live coral (DeCarlo et al., 2017b). The reef slope has a spur and groove formation, which is dominated by soft corals.

General ocean circulation in the northern SCS during the summer is controlled by monsoon winds (Hu et al., 2000). Winds from the southwest drive surface currents generally to the northeast (Morton and Blackmore, 2001). A seasonally occurring cyclonic eddy, known as the Dongsha Cyclonic Eddy (DCE), typically appears south or southwest of Dongsha Atoll during the late spring and summer, and propagates to the southwest (Chow et al., 2008).

Internal waves generated in the Luzon Strait travel westward as solitary waves of depression, and transform into waves of elevation as they shoal on the shallowing shelf topography in water depths <200 m (Fu et al., 2012). The travel time between generation in the Luzon Strait and Dongsha Atoll is approximately two days (Ramp et al., 2010). When the waves reach depths <30 m, they become highly nonlinear internal bores and boluses, and transport cold, subthermocline water into the nearshore region (Leichter et al., 2003; Wang et al., 2007; Moore et al., 2016). Below, we will consider our study site as two adjacent dynamic systems: 1) the region offshore of the reef crest where shoaling internal waves are dominating cross-shore flows and influencing near surface water properties, and 2) the reef flat region onshore of the reef crest where tides, wind, and surface waves dominate the circulation, and bring offshore water onto the reef. Here we assume that internal waves do not play an important role in driving flow on the reef flat, but instead are important in setting the water properties of the offshore boundary condition.

4.2.2 Experiment

The observations presented here are part of a larger study of coral ecology, reef-scale circulation, and internal wave dynamics at Dongsha Atoll (DeCarlo et al., 2017b). In this study we will focus on measurements of currents, water temperature, nitrate concentrations, and meteorological conditions on the reef slope and flat on the east side of the atoll (Figure 4.1b), collected from 4-11 June, 2014. This study took place during the summer monsoon season in the SCS, and was interrupted by Tropical Storm Hagibis on June 12, when the DTS instrument lost power.

Two 2-MHz Nortek AquaDopp Profilers were placed on the reef flat at E3 and E5 (Figure 4.1b) to measure currents and pressure at 4-minute intervals. The depth at E3 and E5 were on average 0.6 m and 1.9 m, respectively. An upward-looking Acoustic Wave and Current Profiler (AWAC, Nortek AS) was deployed at 18.1 m depth at E1, and recorded current measurements at 1-minute intervals and measured surface wave statistics in 20-minute bursts every three hours.

Water samples were collected using GO-FLO bottles mounted onto a rosette sampling assembly (General Oceanic) aboard the Taiwanese vessel Ocean Researcher 3 (OR3) on 4-5 June 2014 at E1, approximately 450 m from the reef crest, at 2, 5 and 10 m depths every 3 hours and analyzed for nitrate concentrations. Additional discrete water samples for the determination of nitrate were collected in October 2012 at seven locations in the waters surrounding Dongsha (Figure 4.1b), aboard Ocean Researcher 1 (OR1). The samples were quick-frozen with liquid nitrogen onboard ship, and returned to a shore-based laboratory for the determination of nitrate with a precision of about $\pm 0.2 \mu M$ (Wong et al., 2015a,b, 2017).

The meteorological data used in this study was measured from a ēKo Pro Series meteorolog-

ical station on top of a platform located in a sand patch on the reef flat at E5 (Figure 4.1b). The station carries sensor suites for measuring wind speed and direction, air temperature, relative humidity, barometric pressure, incoming shortwave radiation and precipitation, which allow for estimates of the air–sea exchange of heat. Additionally, Level-2 (11 μm) swath sea surface temperature (SST) from the Moderate Resolution Imaging Spectroradiometer (MODIS) instrument aboard the Aqua and Terra satellites, with native spatial resolution of 1x1km2 was used for the heat budget analysis. These data were obtained from the NASA Ocean Color Web (http://oceancolor.gsfc.nasa.gov/, accessed July 2, 2018), and have been observed to compare well to *in-situ* observations at Dongsha Atoll (Pan et al., 2017).

A 19 year (1992-2010) high-resolution (0.1° x 0.1°) ocean reanalysis dataset (called RE-DOS) of the upper ocean in the SCS from Zeng et al. (2014) was used to evaluate the general ocean circulation patterns during summer months.

Tidal velocities in the Luzon Strait were estimated using the Oregon State Tidal Inversion Software, OTIS (Egbert and Erofeeva, 2002), and the TMD toolbox (Padman and Erofeeva, 2004).

4.2.3 DTS set-up and calibration

Raman spectra fiber-optic distributed temperature sensing (DTS) technology was deployed across the Dongsha east reef slope and reef flat to measure temperature at the bed over a 4-km distance. A Sentinel Oryx DTS interrogator collected continuous independent temperature measurements every two meters along a Kaiphone (flexible white, 6mm, steel-reinforced) fiber optic cable at a sampling frequency of one temperature trace per minute, providing a spatially-continuous perspective of near-bed temperature in a cross-shelf section. In DTS, a coherent pulse of light is sent down the cable and continuous measurements of Raman

backscattered light spectra allows for determination of the temperature at each point in the cable (Tyler et al., 2009; Hausner et al., 2011). DTS technology has been used in various environmental monitoring programs in the past, providing high spatial (<1m) resolution temperature measurements at scales of meters to kilometers (Selker et al., 2006; Tyler et al., 2009; Hausner et al., 2011; Suárez et al., 2011; Vercauteren et al., 2011; Van Emmerik et al., 2013; Kobs et al., 2014; Zeeman et al., 2014).

The fiber optic cable was deployed in the cross-shelf direction on the east reef flat, starting near the lagoon and going east across the reef flat and down the reef slope to a depth of approximately 50 m (Figure 4.1c). The Oryx was mounted on a platform set up at E5 (Figure 4.1c), from which a 1 km section of fiber-optic cable was deployed towards the lagoon and a 3-km cable was deployed in the offshore direction. Calibration of the raw DTS data was performed following Hausner et al. (2011). The two cables were deployed in simple single-ended configurations on the reef, with twelve accurate temperature sensors (Seabird Electronics SBE-56s, $\pm$ 0.002°C) placed for calibration (6 sensors) and validation (6 sensors). The calibration sections were held at a relatively constant temperature throughout the deployment; however, due to the dynamic nature of internal waves, obtaining a uniform, steady temperature for the calibration reference point offshore was difficult. The eastern terminal end coil saw dramatic fluctuations in temperature when internal waves arrived at the reef slope. For this reason, a 30-minute low pass filter (LPF) was applied to the calibration coefficients.

The average RMSE and bias calculated for the validation loggers was 0.20 $\pm$ 0.02°C and 0.07 $\pm$ 0.01°C, respectively. When the RMSE value for the validation logger was over a threshold of 0.35°C, the calibration coefficients were removed and linearly interpolated, and temperature was recalculated, along with RMSE and bias of the recalibration.

4.2.4 Estimating tide, wave and wind-driven flow

An analysis of the currents on the Dongsha reef flat at E3, E5 and on the reef slope at E1 was performed to determine the physical processes which govern flow in these regions. On the reef flat, a simple model of tide, wind and surface wave driven flow was created.

Barotropic tidal currents on the reef flat are estimated using the depth averaged currents, and a unified tidal analysis and prediction method (e.g., Codiga, 2011). Wave and wind-driven flow on the reef flat is estimated following Lentz et al. (2016):

$$u = sgn\left(-\frac{S_{xx}}{\Delta x} + \tau^{sx}\right)\sqrt{\frac{-\frac{S_{xx}}{\Delta x} + \tau^{sx}}{\rho C_{da}}} \tag{4.1}$$

where u is the cross shore velocity, positive towards the east, S_{xx} is the cross-reef component of the wave-radiation stress tensor, Δx is the width of the region of wave breaking and reef flat, which is taken as 3000 m, τ_{sx} is the wind stress, and ρ is the density of seawater. C_{da} is the bulk drag coefficient, which is estimated as follows:

$$C_{da} = \kappa^2 \left\{ log\left(\frac{D}{z_0}\right) + (\Pi - 1) \right\}^{-2} \tag{4.2}$$

where $\kappa = 0.4$ is the von Karman constant, h is the time-variable water depth, $z_0 = 3.2cm$ is the hydrodynamic roughness estimated for our site in a previous study (Lentz et al., 2017), and Π is Cole's wake strength, which is taken as 0.2 (Lentz et al., 2016).

The wave-radiation stress tensor, S_{xx} is estimated as follows:

$$S_{xx} = \frac{\rho g H_s^2}{16} \left\{ (\cos^2(\theta_w) + 1)\frac{c_g}{c} - \frac{1}{2} \right\} \tag{4.3}$$

where $g = 9.81ms^{-2}$ is gravitational acceleration, H_s is significant wave height measured at E1, θ_w is wave direction, c_g is group velocity, and c is phase velocity (Lentz et al., 2016).

4.2.5 Heat budget

A heat budget analysis was performed on the reef flat 1) to determine the physical processes that control temperature on the reef flat at Dongsha, and 2) to predict water temperature on the reef flat without the influence of internal wave-induced cooling of the forereef waters. A simple heat budget was estimated following Davis et al. (2011):

$$\frac{\partial \overline{T}}{\partial t} + \overline{u_i}\frac{\partial \overline{T}}{\partial x_i} = -\frac{\partial}{\partial x_i}\overline{u_i'T'} \tag{4.4}$$

where, the summative convention with the index $i = 1 - 3$ and a right-handed coordinate system is adopted with the principle axes defined by x_i: x is the distance across the reef, positive to the east, y is the distance along the reef, positive to the north, and z is positive upward, u_i represents the corresponding velocity components, u, v and w, and T is water temperature. Overbars denote time-averaged quantities (in this case, over 10-minutes), and primed values are the fluctuating components ($u = \overline{u} + u'; T = \overline{T} + T'$). The heat budget is focused on the cross-shore dimension only, because the alongshore flow, v, and vertical velocities, w, are an order of magnitude less than cross shore flow, u. The temperature, T, is assumed to be well mixed in the vertical on the shallow reef flat.

Temporal sampling frequency was not sufficient for measuring turbulent transport of heat. Our results suggest that this term as well as heat flux through the reef bed are likely small, given the approximate balance between advective and atmospheric heat flux; see similar results in Davis et al. (2011).

When Equation 4.4 is vertically integrated over the water column, and the equation is multiplied by the heat capacity per unit volume (ρc_p, assumed to be constant and equal to $4.1 x 10^6 W s m^{-3 \circ} C^{-1}$), we obtain an equation for the heat balance within a volume of water of unit length and width (Equation 4.5, Davis et al., 2011). The left side of Equation 4.5 represents the rate of change of heat storage within the volume, Q_T. The terms on the right side of the equation represent the advective heat flux, ΔF, and atmospheric/ocean heat flux, Q_N.

$$\rho c_p h \frac{\partial \langle \overline{T} \rangle}{\partial t} = -\rho c_p h \langle \overline{u} \rangle \frac{\partial \langle \overline{T} \rangle}{\partial x} + Q_N \tag{4.5}$$

$$OR \quad Q_T = \Delta F + Q_N \tag{4.6}$$

where h represents the depth of the water, and u is the depth-averaged velocity in the cross-shore direction, and angled brackets denote depth averaged quantities. Velocity measurements in the top 1-meter of the water column were missing due to acoustic reflection off the water surface. When the water depth at E3 was too shallow to estimate velocities, a linear relationship between transport at E5 and E3 was used to estimate velocities at E3. Various methods of estimating the velocities for the top of the water column were tested, including applying a log fit or an empirical orthogonal function fit to the data, or applying the available depth averaged currents to the entire water column, and all methods yielded very similar results. We used the latter method for this analysis, where the available depth averaged currents were applied over the entire water column, and a 1-hr low pass filter was applied.

The net heat flux between the atmosphere and the ocean, Q_N, is calculated as follows:

$$Q_N = Q_E + Q_H + Q_S + Q_L \tag{4.7}$$

where the terms on the right-hand side of the equation represent latent, sensible, net short-wave, and net longwave heat flux respectively. The net shortwave heat flux was measured at a meteorological station located on the platform at Station E5. The incoming shortwave radiation was corrected for an additional albedo (10%), to account for reflectance of the coral bed in shallow water (Maritorena et al., 1994). A modified version 2.5 TOGA (Tropical Oceans Global Atmosphere) COARE (Coupled Ocean–Atmosphere Response Experiment) bulk algorithm (Fairall et al., 1996, 2003) was used to compute the latent and sensible heat fluxes. The net long-wave heat flux was calculated as follows (Rosenfeld et al., 1994):

$$Q_b = \epsilon\sigma(T + 273.16)^4(0.254 - 0.00495R_H e_S) \tag{4.8}$$

$$e_S = 6.122 * exp\left(\frac{17.67T_{air}}{T_{air} + 243.5}\right) \tag{4.9}$$

where Q_b is clear sky net long-wave radiation, ϵ is the emissivity of the sea surface, taken as 0.97, σ is the Stefan-Boltzman constant, $5.6697x10^{-8}Wm^{-2\circ}K^{-4}$, T is the sea surface temperature in°C, R_H is the relative humidity measured by the meteorological station, es is the saturated vapor pressure and T_{air} is the temperature of the air in°C. Finally, a linear cloud factor, $(1 - 0.9C)$, from (Reed, 1976), was applied to the net longwave radiation, where C is the cloud cover coefficient, taken as 0.59 for 20°N (Budyko, 1974).

A heat budget focused on the reef flat near E3, where the spatial temperature gradient, $\partial\langle\overline{T}\rangle/\partial x$ in Equation 4.5, is calculated over a 200-meter distance, 100 meters on either side

of the current profiler, using the DTS temperature measurements. The 200-meter spatial averaging is a compromise between resolving spatial gradients on the reef, and measuring differences in temperature over this distance that exceed DTS instrument precision. A heat budget for the entire reef flat is estimated using 200-meter averaged DTS temperature across the reef flat as an initial condition and a boundary condition of 1-hr low pass filtered DTS temperature at the reef crest. Temperature on the reef flat was predicted from Equation 4.5 using a forward differencing scheme for the time derivative and a central difference for the spatial gradient in temperature. Transport at E3 and E5 was calculated, using 1-hr low pass filtered currents, and interpolated for the reef flat in between. The transport from E3 was used from the reef crest to E3, and the transport from E5 was used from E5 towards the lagoon. Atmospheric heat flux at each location on the reef was calculated using temperature from the time step before.

To compare the observed temperatures to the modelled heat budget temperatures, we use the Willmott Skill Score (WSS) (Willmott, 1982), defined as:

$$WSS = 1 - \frac{\frac{1}{N}\Sigma_{i=1}^{i=N}(m_i - o_i)^2}{\frac{1}{N}\Sigma_{i=1}^{i=N}(|m_i - \overline{o}| + |o_i - \overline{o}|)^2} = 1 - \frac{MSE}{\frac{1}{N}\Sigma_{i=1}^{i=N}(|m_i - \overline{o}| + |o_i - \overline{o}|)^2} \qquad (4.10)$$

where o_i is an observation, m_i is the corresponding model value, where there are N paired modeled/observed values and MSE is the mean square error. A WSS value of 1 indicates perfect agreement between the observed and modeled values, and a value of 0 indicates no agreement.
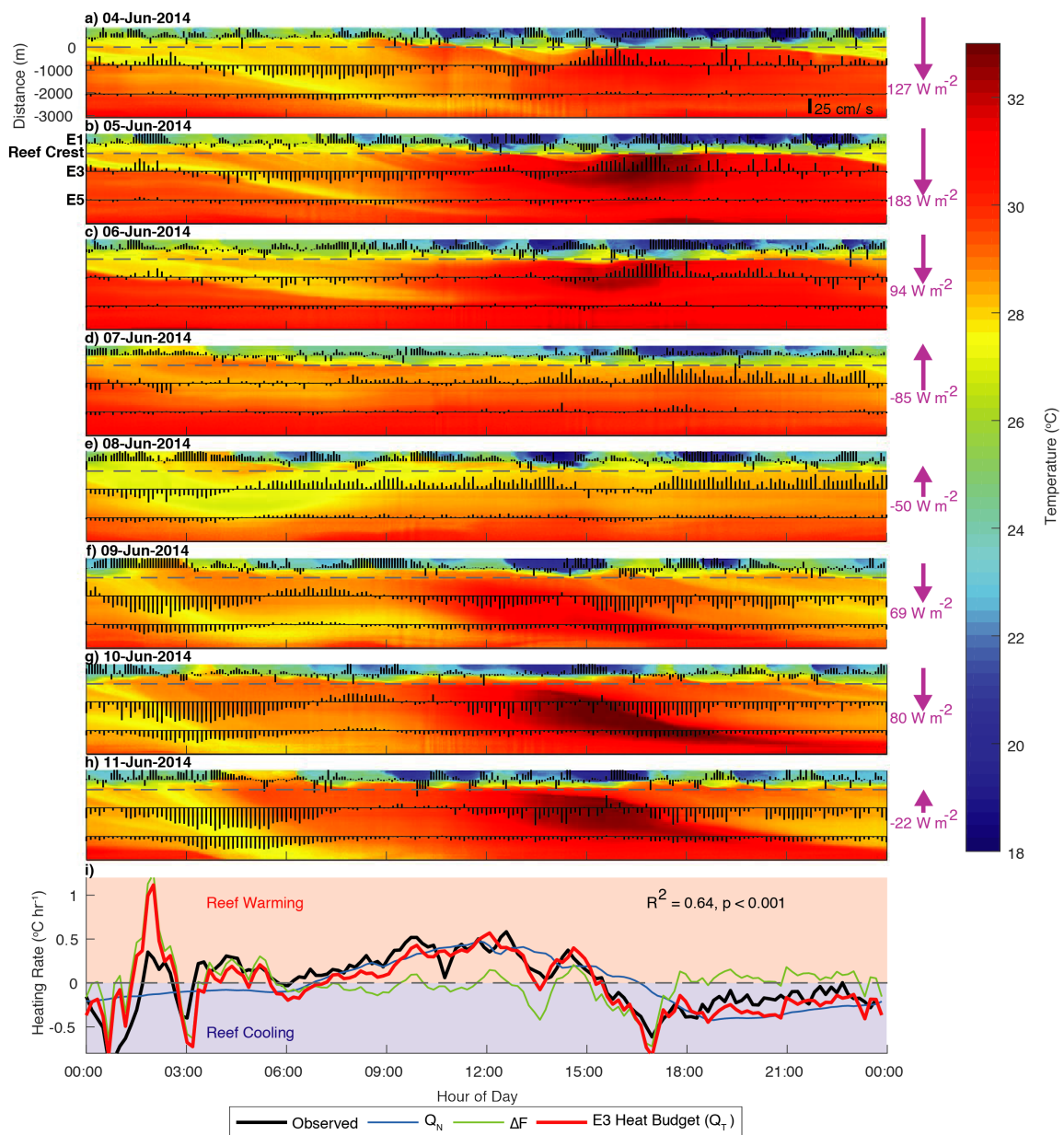
Figure 4.2: DTS temperature data and the heat budget

(a) through (h) show DTS temperature measurements for the 8-day period between 4 June and 11 June, 2014. Across shore currents are shown at E1, E3 and E5 in black quivers, with quivers pointing down indicating onshore flow (to the west), and quivers pointing up indicating offshore flow (to the east). Cumulative net atmospheric heat flux for each day is shown with the magenta arrow indicating net heating (down) or cooling (up). The reef crest is indicated by thick dashed line at distance = 0 meters. (i) shows the daily composite heat budget at E3 for the study period. The black line is the observed heat flux, the blue line is the atmospheric heat flux, the green line is the advective heat flux and the red line is the predicted net heat flux at E3.

4.3   Results

4.3.1   Circulation on the reef

Measurements from the meteorological station located on the reef flat showed that winds at the start of the study period, 4-6 June, were on average 6 $m\,s^{-1}$, and increased on 7-8 June, to an average of 8.5 $m\,s^{-1}$ with gusts up to 22 $m\,s^{-1}$. From 9 to 11 June, winds gradually increased, with an average of 9 $m\,s^{-1}$. Incoming solar radiation showed diurnal heating on the reef, with a maximum of approximately 1000 $W\,m^{-2}$, except on 7-8 and 12 June, when maximum radiation was significantly lower, approximately 200 $W\,m^{-2}$, due to increased cloud cover (Figure 4.2).

Currents on the reef flat (E3) during the study period in June 2014 were influenced by tides, surface waves, and wind stress, and were estimated using tidal analysis and Equation 4.1, where barotropic (surface) tides for 45%, surface waves, 24%, and wind stress, 26% of the variance in across shore flows, with similar results at E5. As might be expected for a shallow reef flat, we did not find any significant relationship between currents on the reef flat and internal wave forcing on the forereef slope offshore. However, offshore on the reef slope (E1, at 20m isobath), the variance in across-shore flows near the reef bed (bottom 8 m) is dominated by bottom-propagating internal bores. Internal waves shoaling on the Dongsha forereef slope have been observed in the form of nonlinear waves of elevation (Fu et al., 2012) and internal bores (Davis et al., 2020). These waveforms can transport dense, cold fluid upslope toward the reef crest. We observed the shoaling of over 500 internal waves on the Dongsha forereef in 11 days. The internal bores appear as a strong, cold temperature front in the DTS signal with apparent phase speeds of approximately 0.4 ms^{-1} and often transport cold water all the way to the surf zone. The focus of this study is what impact the internal-wave modified water has on the reef flat community.
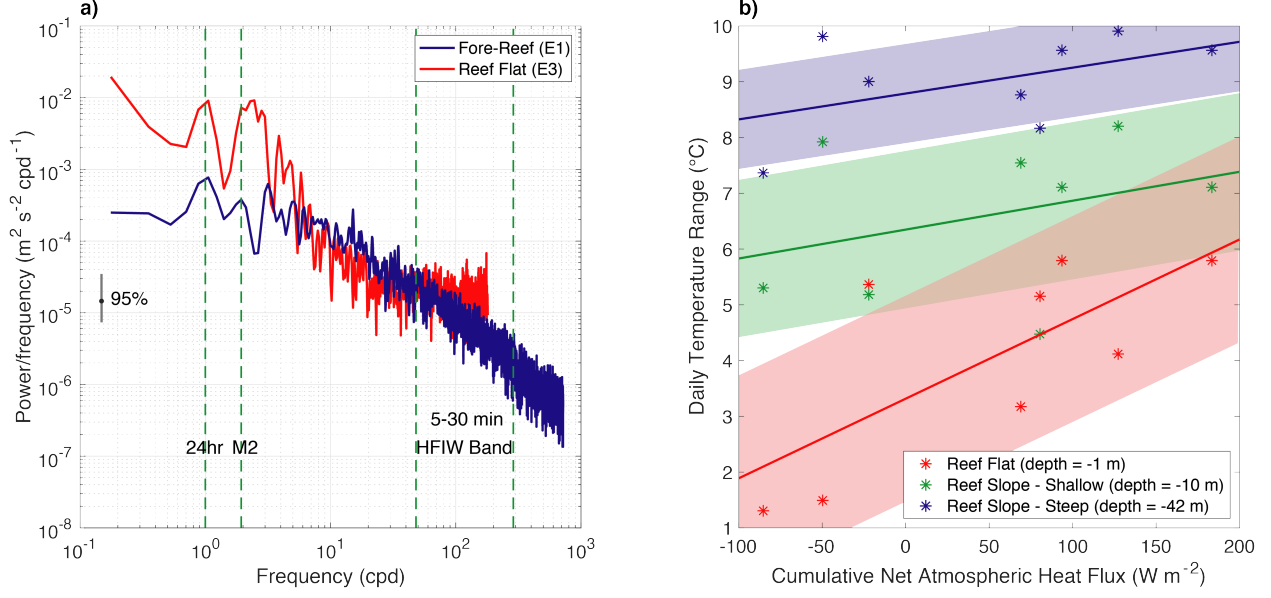
Figure 4.3: DTS daily temperature range and power spectra of currents
(a) shows the power spectra of currents on the reef flat at E3 (red), and on the forereef at E1 (blue). The 24 hour, M2 and high frequency (5-30 minute) internal wave band frequencies are plotted in green dashed lines.(b) shows the daily temperature range at different locations and the cumulative net atmospheric heat flux for each day. The shaded area represents one standard deviation of the data in the linear fit.

Spectral analysis of the across-shore component currents at E1 and E3 reveals a significant peak at the diurnal and semidiurnal frequency (Figure 4.3a) on both the reef flat and reef slope. During a period of low winds (June 4-6), the depth averaged currents on the reef flat were primarily tidal from the ocean to the lagoon on flood and reversing on ebb. During a period of higher winds and waves, depth-averaged currents were directed primarily offshore on 07 and 08 June and onshore from 09 to 11 June. For this deployment, when significant wave height, Hs, was greater than 1.5 meters, depth averaged currents on the reef were directed towards the lagoon, and did not reverse with the tide.

Flushing time, Tf, was estimated for the reef flat at E3 and E5 as:

$$T_f = \frac{V}{Q} \tag{4.11}$$

where V is the volume of water on the reef from the crest to 3-km towards the lagoon, and Q is the volumetric flow rate through the system (Monsen et al., 2002). Daily average flushing time during the study period ranged from 0.7 days to 2.1 ±0.2 days, with the shorter flushing times occurring when wind and waves were stronger, forcing more flow across the reef.

4.3.2 Near-bed temperature across the reef

While corals are typically thought to thrive in thermally-stable environments (Glynn, 1993; Goreau and Hayes, 1994; Hoegh-Guldberg, 1999), there is a large amount of temperature variability in both time and space on the reef flat (Figure 4.2). The mean temperature on the reef flat from the lagoon to the reef crest is 29.4°C. The forereef experiences a natural topographic slope break at about 25 m depth, with a shallow slope (4%) from the reef crest to the 25-m isobath (approximately 425 m offshore of the reef crest), and a steep slope (15%) from 25-50 m depth (the end of the cable). The mean temperatures on these two sections are 27.2°C and 23.6°C, respectively. The steep section of the forereef experiences strong internal wave action and has a diurnal temperature range of 7.4-9.0°C, while corals on the shallow section of the forereef, experience a range of 4.5-8.2°C, because fewer internal waves propagate shoreward beyond the slope break.

In this time series, internal waves arriving at the atoll are seen on the forereef slope as pulses of cold water accompanied by temperature decreases of approximately 4-8°C in less than 1 minute. Typically, there are more frequent internal waves, with larger (6-8°C) temperature decreases evident near the spring tides (new moon on 29 May, and full moon on 13 June), and there are fewer internal waves, with smaller (2-4°C) temperature decreases arriving during the neap tide. The diurnal timescale variability of near bed temperature on the forereef does not appear to be controlled by atmospheric heating and cooling (Figure 4.3b), unlike the reef flat, discussed below.

Water temperature on the reef flat exhibits much smaller diurnal temperature ranges than water on the internal wave-exposed forereef slope. During the 8-day study period, corals on the reef flat (near E3) experienced diurnal temperature ranges of 1.3-5.8°C, primarily due to solar heating cycles. For example, in Figure 4.2a-h, the reef flat (between -3000 and 0 meters) experiences maximum temperatures (red patches) in the afternoon and this heating is modulated by the intensity of solar insolation (purple arrows on the right-hand side of Figure 4.2 and also Figure 4.3b). On 07 to 08 June when cloudy conditions caused reduced atmospheric heating, there was reduced heating on the reef flat (Figure 4.2d-e) and the diurnal temperature range was 1.4°C, on average, while during days with clearer skies and increased solar forcing, daily temperature ranges averaged 4.9°C. When cumulative atmospheric heat flux was -85 $W\,m^{-2}$ (due to clouds) on 07 June, the temperature range on the reef flat was 1.3°C. Whereas, on 06 June, when cumulative atmospheric heat flux was 94 $W\,m^{-2}$, and circulation on the reef flat was similar, the temperature range on the reef flat was 5.8°C. The relationship between atmospheric heating and daily temperature range of the near-bed waters was much stronger in shallow reef flat waters than on the deeper forereef slope (slope of red line in Figure 4.3b is approximately three times larger than blue and green).

There are cold water intrusions evident on the reef flat, which generally occur when currents on the reef flat are directed onshore in the morning. During these intrusions, approximately 2-3°C cooler water from the forereef is drawn onto the reef flat by tide, wave and wind driven currents, and is transported towards the lagoon. In certain cases, (such as on the 8 June), a cold-water intrusion begins, and the cold-water mass is quickly pushed back offshore by changing tidal currents (Figure 4.2e).

4.3.3 Reef flat heat budget

A heat budget (Equation 4.5) was constructed for the reef flat using near bed temperature from the DTS and velocity and water depth measurements at E3 and E5 (Figure A.1). Figure 4.2i shows the heating rate observed on the reef at Mooring E3 and the heating rate predicted from the heat budget estimation for a composite-day average. A simple balance of atmospheric heating and advection of heat across the reef flat was found to adequately predict observed heating rates for a composite day (Figure 4.2i, $R^2 = 0.64$, p <0.001). The advective (ΔF) and atmospheric (Q_N) heat flux are similar in magnitude, and both vary substantially on times scales of days. The atmospheric heat flux (Q_N) is dominated by net shortwave (Q_S) and latent (Q_E) heat flux. Solar heating is large on 04 to 06 June and 09 to 11 June due to clear skies, and smaller on 07 to 08 June due to clouds. Advective heat flux increases near the end of the deployment due to larger tidal currents and increased wind and wave driven flow across the reef.

Over the whole reef flat (Figure 4.4), the heat budget reproduces DTS-observed reef-flat temperatures with an average Wilmott Score of 0.91 (Equation 4.10), for the 8-day study period. The heat budget for 5 June (Figure 4.4b) shows similar patterns to the observed (Figure 4.4a) onshore flow of cold water in the morning, and solar heating on the reef flat midday. From our observations during this deployment, the advection of offshore water onto the reef flat, and surface heat flux from solar heating control the variability of temperature on the reef flat. From a simple balance of atmospheric and advective heat flux, given an offshore boundary condition, initial condition across the reef flat, and circulation on the reef, we can predict spatial variability in temperature on the reef flat.
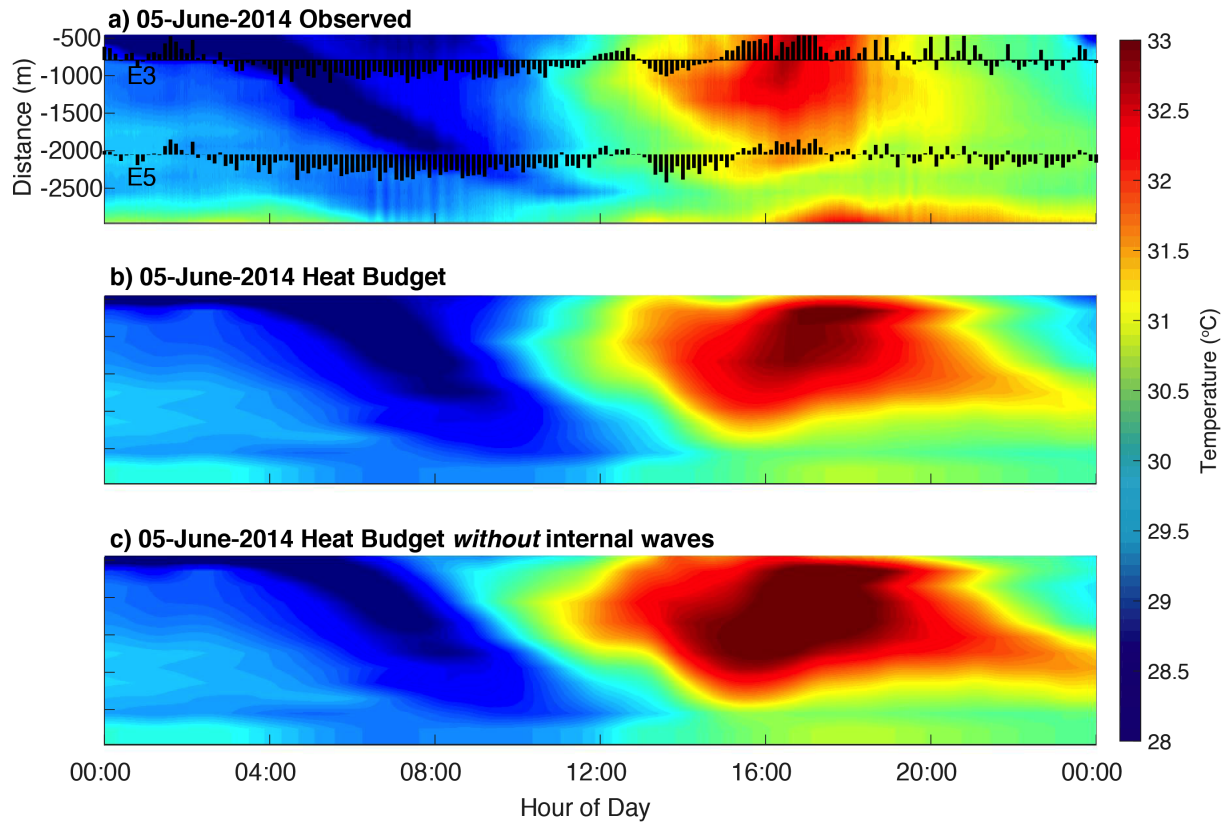
Figure 4.4: DTS temperature and heat budget model

(a) shows the observed DTS temperature on the reef for 5 June, 2014. The data is averaged in 200m sections. Across shore currents are shown at E3 and E5 in black quivers, with quivers pointing down indicating onshore flow (to the west), and quivers pointing up indicating offshore flow (to the east). **(b)** shows the modeled reef flat temperature using the model described in Section 4.2.4. **(c)** shows the modeled reef flat temperature without internal waves.

4.4 Discussion

4.4.1 Influence of internal waves on reef flat temperatures

For our study period, advective heat flux is important in driving cooling on the reef flat, by bringing offshore water from the forereef onto the reef flat. In addition to direct observations of the shoreward transport of cold subthermocline waters all the way to the surf zone on Dongsha by internal bores (Davis et al., 2020), internal wave cooling of the forereef water is suggested by an average MODIS SST image for June to August 2002-2017 (Figure 4.5a). A cold crescent on the northeast side of the atoll, where internal waves directly impinge, is evident. We averaged MODIS SST in a 3 km2 area at a location 700 m offshore of the reef crest (point A, Figure 4.5a), and a location approximately 6.5 km offshore of the reef crest (point B). At the deeper offshore location (point B), shipboard observations by Fu et al. (2012), have shown that the internal waves are still in coherent form as waves of depression, and have not yet forced cool water to the surface as they do further onshore on the shallow slope (point A). Observations during this experiment near point A (approximately 50 m depth) indicate that the internal waves are in highly nonlinear form (Davis et al., 2020), and can transport cold subthermocline water shoreward all the way to the reef crest (1m depth, e.g. Figure 4.2). During summer months (June to August), when internal wave forcing is strongest in the SCS (Ramp et al., 2010), the average difference in SST between points A and B (ΔSST_{AB}) is 0.22 $\pm$0.01°C, with offshore waters being warmer (Figure 4.5a). This difference is smaller during the winter months ($\Delta SST_{AB} = 0.10 \pm 0.01$°C) when the internal wave field in the SCS is diminished. Further evidence that the cooling on the forereef is driven by remote internal wave forcing, is that ΔSST_{AB} is largest two days after the maximum tidal currents in the Luzon straight (Figure 4.5b), which corresponds to the approximate travel time for internal waves between the Luzon Strait and Dongsha Atoll (Ramp et al., 2004, 2010).
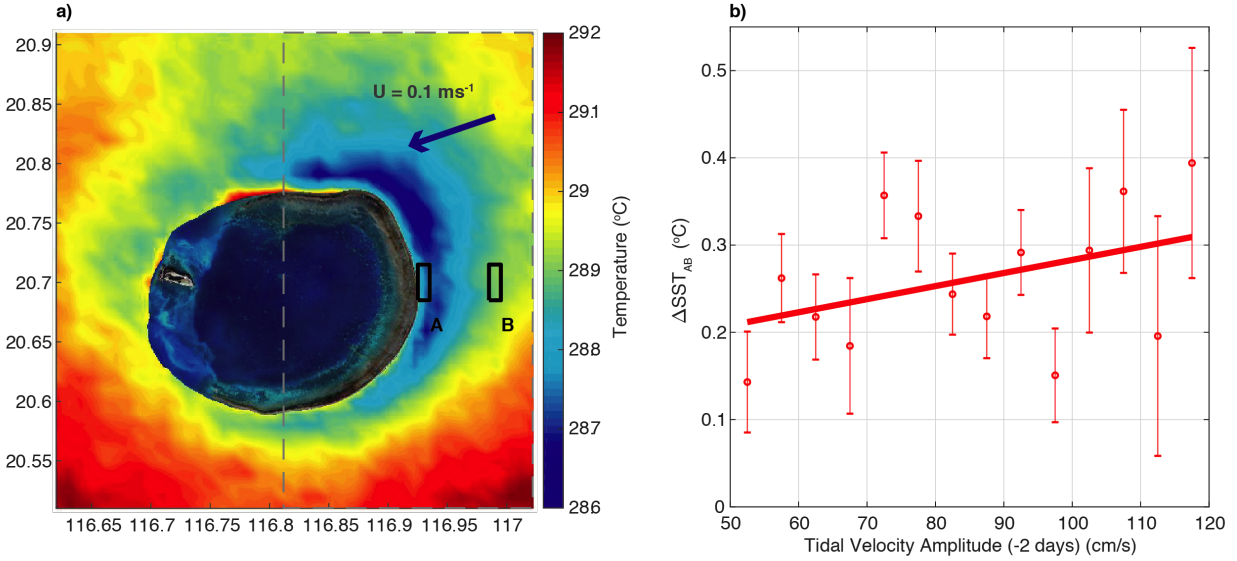
Figure 4.5: Sea surface temperature difference and Luzon tidal amplitudes
(a) shows the average MODIS SST data for summer (June to August 2002- 2017). The blue arrow shows modeled depth averaged currents from REDOS within the grey dashed box for summer (June to August 1992-2010) (Zeng et al. 2014). **(b)** shows the bin averaged SST difference between B and A for summer months (June to August 2002-2017) and the daily range of tidal velocity in the Luzon Strait, 2 days prior to the SST measurements (Egbert and Erofeeva 2002; Padman and Erofeeva 2004).

In addition to internal waves, here we discuss other oceanographic processes that could explain the observed cooling on the north-east reef slope. Nineteen years (1992-2010) of REDOS data output (Section 4.2.2) from Zeng et al. (2014), show depth averaged currents during the month of June east of Dongsha Atoll are 10 c $m\,s^{-1}$ to the south-west, consistent with currents observed at E1 during this study. Southward-directed currents along the east forereef slope would lead to downwelling, due to Ekman transport, so we do not expect this to be a source of cold water to the east side of Dongsha Atoll during our deployment. The Dongsha Cyclonic Eddy (Section 4.2.1) originates near the south/southwest side of the atoll and travels south/southwest, driving upwelling in the center of the eddy and downwelling on the outside. Due to the location and direction of propagation of the eddy, it does not seem likely to be driving the pattern of observed cooling on the east side of Dongsha. Island wakes can also be a source for upwelled waters (Heywood et al., 1996; Coutis and Middleton,

73

2002; Dong et al., 2007). However, since flow around Dongsha is on average towards the southwest from REDOS output, we would expect a wake to develop on the lee (southwest) side of the atoll (Coutis and Middleton, 2002) and this is not consistent with the observed SST pattern. Thus, we conclude that the observed cooling pattern seen on the east forereef of Dongsha Atoll in the MODIS SST data is primarily due to shoaling large-scale internal waves generated in the Luzon Strait region. Further, we posit that if internal waves were not present, the forereef water would be warmer, and this would make a significant difference in the heat budget on the reef flat.

The important role of advective heat transport in the reef flat heat budget suggests that even though internal waves are not of first-order importance in driving currents on the reef flat, their influence on water properties (e.g. temperature, nutrient concentrations) on the forereef slope could affect communities on the reef flat when these waters are forced onto the reef flat by local tidal currents and surface gravity waves. In order to estimate the temperature of the forereef waters without the influence of internal waves, the difference between the temperature on the reef crest and the mean offshore (point B) SST during our deployment (T_{IW}) was added to the forereef temperature (boundary condition) in the heat budget (Figure 4.4c). The difference between the mean temperature at the reef crest (from the DTS measurements), and the mean offshore SST during our deployment was 0.6°C with offshore SST being higher. Over the 8-day observation period, the composite heat budget suggests that cold subthermocline water delivered to the shallow forereef by internal waves makes its way onto the reef and contributes to cooling of the reef flat. The location of point B was chosen because we know the form of the wave there, but we acknowledge that a different offshore point would affect our results. We consider the choice of point B to be conservative, because it may already be in a region of internal wave influenced cooling (Figure 4.5a). If we chose a point further offshore where temperature is warmer, the influence would be greater.

74
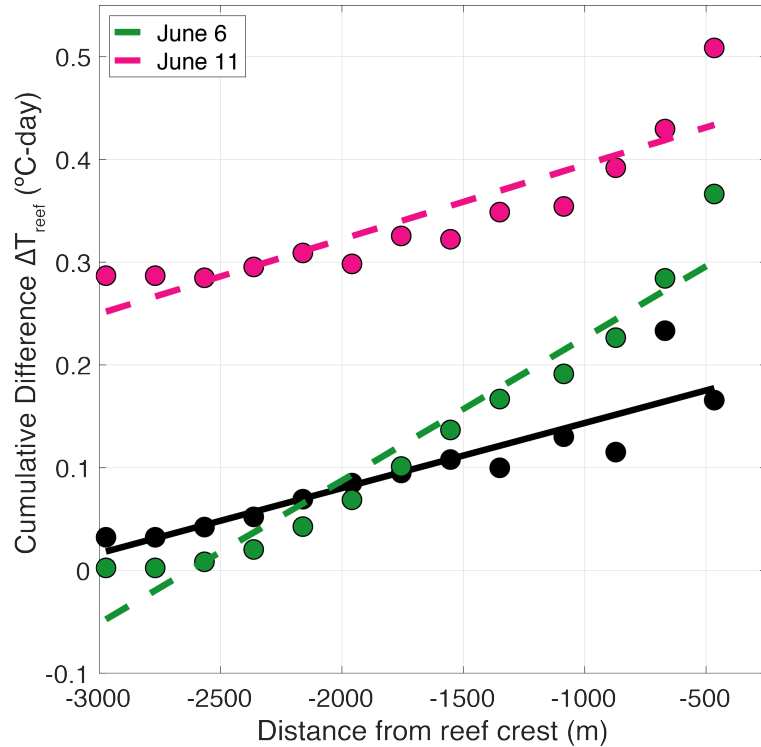
Figure 4.6: Cumulative difference without internal waves
The composite daily average of the cumulative difference between the heat budget with internal waves and without internal waves at each location across the reef flat with 0m representing the reef crest, and -3000m as the closest location to the lagoon. The black points represent the average for the whole deployment, and the green and pink points represent the test cases where only currents are changed, and other forcing is kept the same.

To quantify the impact of internal waves on the reef flat, the estimated temperature from the heat budget with and without internal waves was compared. This simple model suggests that without internal waves, instantaneous predicted temperatures can be as high as 2.0 $\pm 0.2°$C warmer on the reef flat, and on average 0.1 $\pm 0.2°$C warmer. The cooling effect of the internal waves on the reef flat water temperatures may have important consequences for the coral community inhabiting the reef flat. For example, it has been shown that thermal stress accumulates over time, and large positive cumulative temperature anomalies can cause bleaching (Glynn and D'croz, 1990).

The cumulative difference in predicted temperatures with and without internal waves (ΔT_{reef}) over a composite day is 0.2°C-day near the reef crest and decreases linearly to-

wards the lagoon (Figure 4.6). While it may be intuitive that the section of the reef near the changed boundary condition sees a bigger effect from internal waves, the influence of the offshore boundary on the reef is highly dependent on the cross-reef flow, which in turn depends on the magnitude and direction of the overall flow across the reef. The only way for ΔT_{reef} to vary with distance across the reef flat in our simple model (neglecting mixing and assuming the effect of water temperature on the surface heat flux is negligible), is for changes in cross-reef current strength and direction to drive spatially variable flushing of reef-flat waters over the course of a day. To test this, we calculated the heat budget for two days with very different currents (06 June which had smaller magnitude currents that were tidally reversing and 11 June when currents were stronger, forced by wind and waves and primarily directed towards the lagoon) but held the atmospheric forcing and ΔT_{IW} the same for both days, set to average conditions. The only difference between these two experimental days were the currents, to test the effect of advection on the spatial variability in internal wave driven cooling across the reef flat. It is evident that when currents on the reef flat were tidally forced and smaller magnitude (for example 06 June, Figure 4.6), the spatial gradient in ΔT_{reef} across the reef flat was greater. In this case, the internal waves were not influencing the temperature near the lagoon because the ocean water does not reach the lagoon edge of the reef. When currents were unidirectional onshore and higher magnitude (for example 11 June, Figure 4.6), the gradient in ΔT_{reef} was smaller. Also, with stronger flow across the reef flat due to surface waves, we see an increased influence of internal waves towards the lagoon. These tests illustrate the importance of circulation in driving spatially variable residence times which determine the influence of the offshore boundary condition (internal waves) across the reef.

Temperatures near the reef crest exceeding the maximum monthly mean (28.9°C for Dongsha Atoll) + 1°C threshold were integrated for one week, to estimate the Degree Heating Weeks (DHW) metric, commonly used in coral bleaching predictions. The difference be-

tween the DHW with and without internal waves (ΔDHW) is 0.7°C-weeks. A synthesis study of factors influencing coral bleaching (Safaie et al., 2018) predicts that an increase in cumulative thermal anomaly, $\Delta DHW = 0.7$°C-weeks, would result in approximately four times the probability of a more severe bleaching event on this reef without the influence of internal waves.

Cool offshore (on the forereef) water can provide an important source of cooling for the reef flat, as was seen in June 2015, when low flow on the reef flat, caused by low wind and wave conditions, prevented offshore water from coming onshore (DeCarlo et al., 2017a). This led to high residence times and intense heating on the reef flat. Temperatures were 6°C above normal on the reef flat, and widespread bleaching occurred despite no change in internal wave activity in the SCS. This highlights the role of advection on reef flat temperatures, in bringing offshore, internal wave cooled water, and preventing intense heating due to stagnation of water. The increase in probability of a bleaching event, and direct observations of bleaching when internal wave cooled water was not influencing the shallow reef flat, suggest that a reef which experiences internal wave driven cooling may have corals with increased resilience.

4.4.2   Influence of internal waves on reef flat nutrients

Nitrate (NO_3^- measurements from water samples taken on the east reef slope and surface waters (<40 m depth) around Dongsha were used to construct a temperature-nutrient relationship (Figure 4.7b). Nitrate concentrations below the detection limit (0.1 μM) of the sample analysis were not included in the temperature-nutrient relationship. When internal waves shoal on the forereef slope, cold, high-nutrient water is transported into shallow waters. Shipboard observations on the shallow reef slope (near E1) from 4 June 2014, show when an internal wave arrives, water temperature decreases approximately 4°C and nitrate
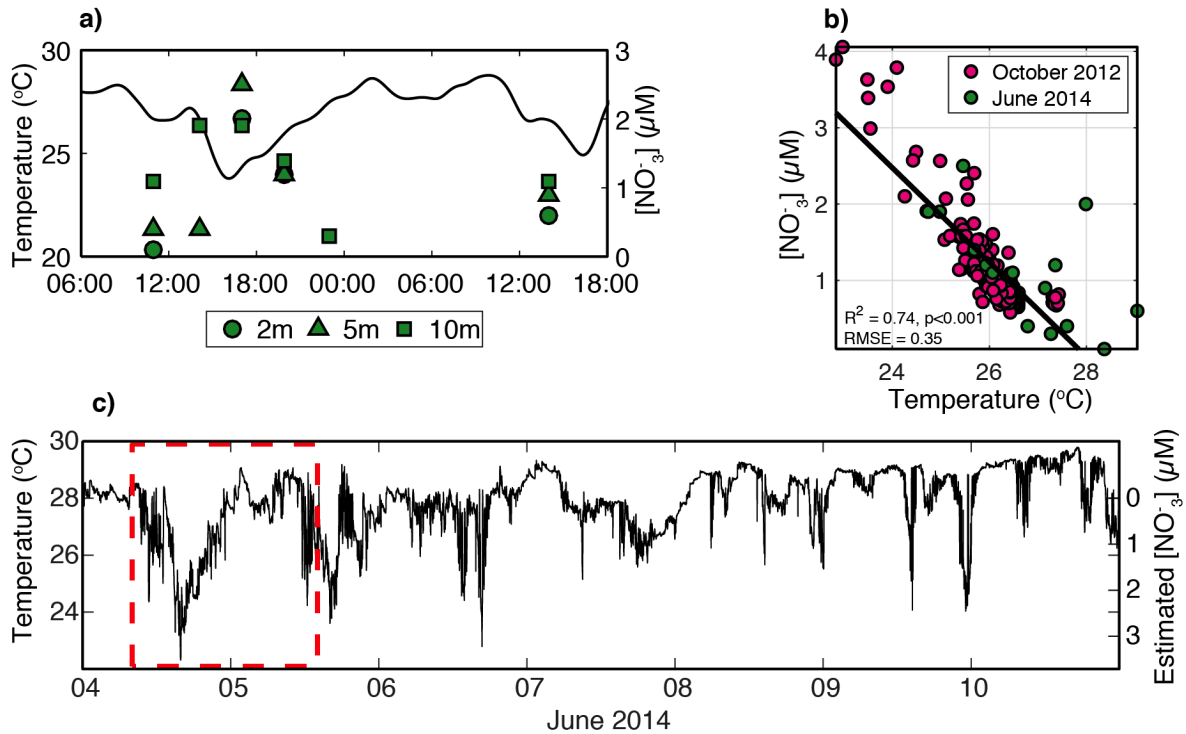
Figure 4.7: Temperature Nutrient relationship
(a) shows 3-hr low pass filtered temperature measurements taken at E1 (depth of 10 meters), and nutrient measurements taken at 2, 5 and 10 meters' depth on 4 and 5 June, 2014. **(b)** shows the temperature-nutrient relationship for measurements taken at locations shown in Figure 1. **(c)** shows the temperature at E1 (depth of 10 meters) for the whole study period. Nutrient approximations, using the relationship from (b) are shown on the right axis.
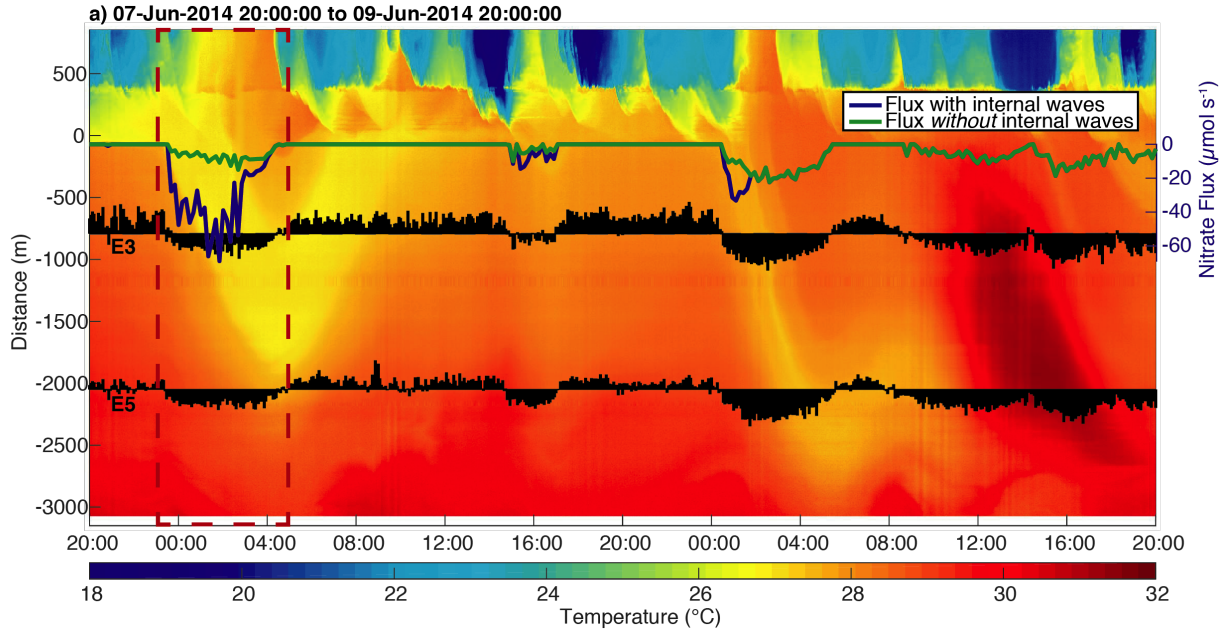
Figure 4.8: Nutrient flux
DTS temperature measurements for the 7 June 20:00:00 to 9 June 20:00:00, 2014. Across shore currents are shown at E3 and E5 in black quivers, with quivers pointing in the direction of flow across the reef flat. Onshore nutrient flux with internal waves is shown in blue, just onshore of the reef crest, with negative values indicating an onshore flux of nutrients. Onshore nutrient flux without internal waves is shown in green.

concentrations 2-meters below the surface increase from $<0.1\mu M$ to approximately 2.0 μM (Figure 4.7a). This high-nutrient water is then available to be transported onto the reef flat by tidal and wave driven flow. The temperature-nitrate relationship, DTS temperatures at the reef crest, onshore currents and depth from E3 were used to estimate nitrate concentration and flux (Figure 4.8) at the reef crest. Like the heat budget, ΔT_{IW} was added to the reef crest temperature to estimate the nitrate concentration and flux without internal waves.

In our observations, nitrate flux onto the Dongsha reef flat is episodic in time, peaking when cold water from the forereef comes onshore past the reef crest. For example, on 07 June, 2014 at 23:00:00, there is a spike in nitrate flux as offshore water flows onto the reef, but this pulse only lasts for a couple of hours before returning to values below detection level (Figure 4.8). Without internal wave influence on the forereef, we estimate that nitrate

fluxes to the reef flat are not significantly above detection level, i.e. are near zero. This is because water coming onto the reef in the no-internal wave case is warmer and has thus lower nitrate concentrations, commonly having values of zero when water temperature at the reef crest is above the zero-crossing in the derived temperature-nitrate relationship. If a conservative limit of nitrate minimum concentration (0.1 μM) is applied, the maximum flux of nitrate onshore through a unit width of the water column was 100.93 ± 20 $\mu Mols^{-1}$, and without internal waves was 21.60 ± 20 $\mu Mols^{-1}$. If we consider a 6-hour period on 07 June 2014 when a pulse of offshore water is coming onto the reef (red dashed box, Figure 4.8), the cumulative flux of nitrate transported onshore through a unit width of the water column was $5.7 \pm 4.5x10^5$ $\mu Mols^{-1}$ with internal waves, and $1.3 \pm 4.5x10^5$ $\mu Mols^{-1}$ without internal waves.

While the noise in the temperature-nitrate relationship and the detection limit of the nitrate analysis technique introduce uncertainties in the cumulative difference in nitrate fluxes to the reef flat with and without internal waves, our observations suggest that internal waves increase the episodic flux of nitrogen to the reef, and thus play an important role in reef flat productivity. For example, with increased levels of atmospheric CO_2, ocean acidification continues to threaten coral reefs as decreased availability of carbonate ions hinders calcification and skeletal growth (Raven et al., 2005). However, studies have shown that increased heterotrophic feeding or inorganic nutrient availability boosts the energy of corals, which allows them to continue to calcify in low pH seawater (Cohen and Holcomb, 2009; Holcomb et al., 2010).

4.4.3 Consequences for reef ecosystems globally

In this study we show that internal waves can significantly influence the temperature and nutrient environment on the shallow reef flat of Dongsha Atoll and these changes can have

implications for the thermal resilience and calcification rates of the reef community. During the 1997-1998 El Niño event, and a 2015 bleaching event, corals on the slopes of Dongsha Atoll that receive internal waves had low mortality, whereas the corals in the lagoon not exposed to internal wave influence had high mortality rates (Dai, 2004; DeCarlo et al., 2017a). A study by Tkachenko and Soong (2017) showed that the forereef was dominated by thermally-susceptible coral genera, potentially due to the influence of internal waves, and they classified Dongsha as a thermal refuge for corals. The environmental conditions driven by the internal wave influence on the shallow reef at Dongsha likely contribute to the resilience of the coral community there.

The reef at Dongsha Atoll has higher net ecosystem calcification rates than any other coral reef studied to date, and the internal waves are one of the mechanisms that may contribute to this (DeCarlo et al., 2017b). This study showed that net ecosystem production and net ecosystem calcification are tightly linked on the reef flat; therefore, the flux of nutrients onshore due to internal waves could be influencing the net ecosystem calcification rates (DeCarlo et al., 2017b). Although Dongsha Atoll is a unique case, due to the large amplitude internal waves that shoal there, internal waves are prominent features throughout the world's oceans, and these temperature and nutrient effects may be common on other coral reefs with internal wave influence. Furthermore, warming of the upper layer of the ocean, due to climate change, has led to an increase in stratification, that is likely accompanied by an increase in internal wave activity in the northern SCS since 1900 (DeCarlo et al., 2015), and this could be occurring in other locations as well.

A literature review documents observations of internal waves in the vicinity of reefs in at least 44 different locations globally, with about half of these being *in-situ* measurements and the other half remote-sensing studies (e.g. Jackson and Apel, 2004; Jackson, 2007, see Table B.1 for detailed list of other papers). There have been various studies that have shown

the effect of internal waves on coral communities at deeper sites (10 m depth and greater). Wall et al. (2015) showed that in the Andaman Sea, post-bleaching mortality of corals was higher in regions unaffected by internal waves compared to internal wave-influenced regions. Furthermore, enhanced growth rates of suspension feeding corals has been observed where IWs are present (Leichter et al., 1998). Leichter and Genovese (2006) showed that there were higher growth rates of coral in Florida than in Jamaica, due to greater internal wave activity there, and in Florida they saw 10-40 fold increases in nutrient concentrations with the arrival of internal waves (Leichter et al., 2003). Internal wave influence on shallow reefs is likely more extensive than has been directly observed. Further research may reveal similar conclusions of the effect on the heat budget and nutrient concentrations on shallow coral reefs worldwide. Understanding these impacts can help identify which reefs may be a thermal refuge due to internal wave influence.

4.5 Conclusion

The observations and analyses presented here indicate that internal waves arriving at Dongsha Atoll are modifying water properties on the forereef and significantly affecting the water temperature and nitrate concentrations on a wide, shallow reef flat. Spatially-continuous measurements of water temperature across the forereef and 3-km wide reef flat from the DTS instrument make it possible to connect offshore processes to water properties in nearshore benthic communities and allow for a spatially-resolved heat budget.

We find that internal waves shoaling on Dongsha Atoll cool the near surface waters on the east forereef by 0.2°C in summer and that this internal wave influence is both tidally and seasonally modulated (Figure 4.5a). Internal wave-influenced water on the forereef is transported onto the shallow reef flat by tides and surface waves and our analysis shows that

it can cool the reef by as much as 2.0 $\pm$0.2°C and increase instantaneous nitrate fluxes by approximately four-fold. Thus, internal waves generated over 500 km away from Dongsha may play an important role in mediating thermal stress and the metabolism of a very shallow reef ecosystem. For example, estimates from a statistical model of bleaching factors (Safaie et al., 2018) indicates that without internal wave cooling of the Dongsha reef flat, there would be four times the probability of more severe bleaching.

Quantifying the impact of internal waves on the temperature and nutrient budget of a coral reef will help us to understand resilience of corals and why corals thrive in different environments. Internal waves likely play a role in modifying the water properties on other shallow ecosystems and understanding the magnitude of these impacts is important in a changing climate.

Chapter 5

Physical forcing determines temperature gradients and improves predictions of diurnal variability in shallow coastal ecosystems: observations from three coral reefs

5.1 Introduction

Rising ocean temperatures and acidification are substantial threats to coral reefs worldwide (Hoegh-Guldberg et al., 2007; Donner, 2009; Van Hooidonk et al., 2016). There has been significant variation, over small spatial and temporal scales, of the physiological response of coral colonies and reefs to environmental stressors observed (Riegl and Piller, 2003; Pandolfi et al., 2011; Oliver and Palumbi, 2011; van Woesik et al., 2011, 2012; DeCarlo et al., 2017a). The temperature tolerance and subsequent resilience of corals, is greater in regions of natural thermal variability (McClanahan et al., 2005; Palumbi et al., 2014; Safaie et al., 2018; Schoepf et al., 2020). Currently, reef-scale (<750m) and diurnal patterns of temperature variability are not available from global satellite products. Corals may exhibit different physiological responses to environmental stresses over small spatial and temporal scales, and understanding the physical processes which are driving small scale variability could be important for understanding resilience to current and future environmental changes.

Temperature variability on diurnal timescales has been shown to be one of the most important metrics for predicting bleaching severity (Safaie et al., 2018). Corals living in regions with a history of higher diurnal temperature range have lower odds of severe bleaching occurring. Cyronak et al. (2020) found that water depth was a good predictor of of the diurnal range of temperature and pH on a reef. Understanding which reefs experience high-frequency temperature variability (here, defined as frequencies $\leq 1/\text{day}$), and why they experience this variability, may be important for future conservation efforts.

The processes driving circulation on coral reefs shape their physical and chemical environments. Dynamical scales on coral reefs can range from millimeters to kilometers, and the geometry of coral reefs leads to complex flows (Monismith, 2007; Lowe et al., 2005). Hydrodynamic processes which drive flow on coral reefs are primarily tides, waves, and winds

85

(Lowe and Falter, 2015; Reid et al., 2020). Physical mechanisms that could be driving high-frequency variability of temperature, and other environmental parameters, could include flow on the reef due to wind (DeCarlo et al., 2017a), waves (Pineda et al., 2013; Rogers et al., 2016), tides (Schoepf et al., 2015, 2020), atmospheric heat flux (Davis et al., 2011; Pineda et al., 2013; Guadayol et al., 2014), and internal waves (Leichter et al., 2003; Leichter and Genovese, 2006; Leichter et al., 2006; Wyatt et al., 2020).

The three study sites which are included in this study are Dongsha Atoll, in the northern South China Sea, Kaneohe Bay, on Oahu, Hawaii, and Ofu-Olosega, American Samoa. The physical mechanisms which drive variability at these sites are very different, as are their morphologies. Here we compare the spatial and temporal variability in temperature from our high-resolution measurements at these reefs, and expand our understanding of the mechanisms which are determining the thermal environment in these different coral ecosystems, and improve predictability of temperature variability through the application of a simplified heat budget.

5.2 Methods

5.2.1 Study Sites

The observations presented here are part of larger studies of coral ecology and reef-scale circulation, conducted on three coral reefs. Deployments were conducted at Dongsha Atoll (latitude: $20.7°N$) during June 2014 (see DeCarlo et al., 2017a,b; Reid et al., 2019; Davis et al., 2020), Kaneohe Bay (latitude: $21.5°N$) during January 2017 (see Kealoha et al., 2019)
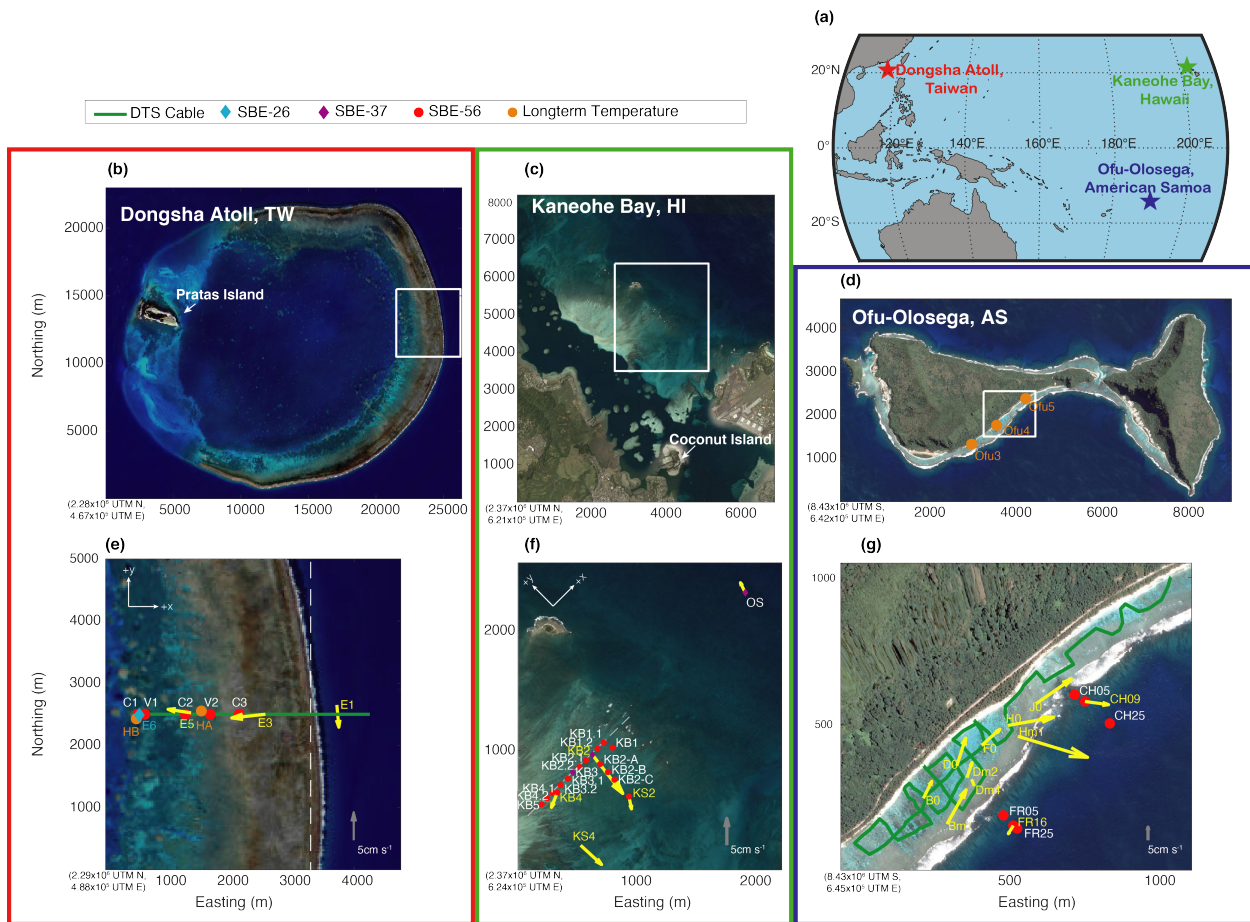
Figure 5.1: Oceanographic setting of the study sites.
(a) Map showing the location of the three sites. (b) Satellite image of Dongsha Atoll from the Taiwan National Space Organization. White box indicates region covered by (e). (b) Satellite image of Kaneohe Bay from Google Earth, Maxar Technologies. White box indicates the region covered by (f). (d) Satellite image of Ofu-Olosega from Google Earth, CNES/Airbus. White box indicates the region covered by (g). (e) East reef flat of Dongsha Atoll, where the location of the DTS cable is shown as a green line. The location of SBE-56 thermistors are shown as red circles. Depth-averaged currents during the deployment at E1, E3, and E5 are shown with yellow quivers at their respective locations on the reef. (f) Reef flat of Kaneohe Bay, where the location of SBE-56 thermistors are shown as red circles and SBE-37 MicroCATs as purple diamonds. Depth-averaged currents during the deployment are shown with yellow quivers at their respective locations on the reef. (g) Back reef lagoons at Ofu, where the location of the DTS cable is shown with a green line and offshore SBE-56 thermistors are shown as red circles. Depth-averaged currents during the deployment are shown with yellow quivers at their respective locations on the reef. Grey quivers shown in (e), (f) and (g) indicate the scale of the currents. Longer term temperature thermistors at Dongsha ((e)), Ofu ((d)) are shown as orange circles.

87

and Ofu-Olosega (latitude: $14.2°S$) during March 2017 (see Rogers et al., 2018; Hefner et al., 2019).

Dongsha Atoll (Figure 5.1a,e) is a a ring-shaped coral reef ecosystem, approximately 28 km in diameter and has an area of approximately 600 km^2 (Dai, 2004). Kaneohe Bay is a semi-enclosed embayment, bounded by a barrier reef, on the eastern side of the island of Oahu, Hawaii (Figure 5.1c,f). The site at Ofu-Olosega (Figure 5.1d,g), in American Samoa, is a fringing reef on the south side of the island.

5.2.2   Dongsha Atoll Experiment

In this study we focus on measurements of currents, pressure and water temperature taken on the reef flat on the east side of Dongsha Atoll and meteorological conditions measured on Pratas Island (Figure 5.1b), collected from 04 to 17 June, 2014. This study took place during the summer monsoon season in the South China Sea. Details of all instrumentation are listed in Table 5.1.

 Temperature and circulation measurements were made here on the east reef flat and forereef slope. The east reef flat (Figure 5.1e), is approximately 3km wide, and ranges from 0.3 to 4.0 m depth. The fore reef has a 4% slope down to 25 m depth, beyond which it steepens to 15% to 50 m depth, after which it flattens slightly to 7% to 300 m depth. Internal waves arriving on the forereef slope at Dongsha Atoll can contribute to thermal variability across the atoll (Wang et al., 2007; Fu et al., 2012; Reid et al., 2019). The reef at Dongsha Atoll has higher net ecosystem calcification rates than any other coral reef studied to date, and the internal wave induced variability is one mechanism that could contribute to this (DeCarlo et al., 2017b).

Table 5.1: Deployment instrumentation for Dongsha Atoll

Location	Instruments	Depth (m)	Sampling Rate	Dates (dd/mm/yy)	
Reef Flat & Slope	Sensornet Oryx DTS	0.3 to 50	1 min	4-12/06/14	
E1	Nortek AWAC	18.1	profile: 1-min, 50cm bins, waves: 512 bursts at 2Hz every 3hrs	1-17/06/14	
E3	Nortek ADP	0.4	profile: 4-min, 10cm bins	1-17/06/14	
E5	Nortek ADP	1.5	profile: 4-min, 10cm bins	1-17/06/14	
E6	Sea-Bird SBE-26	1.6	10-min	1-17/06/14	
C1	Sea-Bird SBE-56	2.4	0.5 sec	1-17/06/14	
C2	Sea-Bird SBE-56	2.2	0.5 sec	1-17/06/14	
C3	Sea-Bird SBE-56	0.5	0.5 sec	1-17/06/14	
V1	Sea-Bird SBE-56	2.4	0.5 sec	1-17/06/14	
V2	Sea-Bird SBE-56	1.4	0.5 sec	1-17/06/14	
HA	Hobo U22	1.4	15 min	18/06/13 - 20/06/14	-
HB	Hobo U22	1.8	15 min	18/06/13 - 23/05/14	-

Two 2-MHz Nortek AquaDopp Profilers (ADPs) were placed on the reef flat at E3 and E5 (Figure 5.1e) to measure currents and pressure at 4-minute intervals. A Seabird Electronics Seagauge (SBE-26) was placed on the reef flat at E6 to measure presure at 10-min intervals. The depth at E3, E5 and E6 was on average 0.4 m 1.5, and 1.6 m, respectively. At times, water depth at E3 was too shallow for the AquaDopp to accurately measure currents. Gaps in velocity data were interpolated if the gap was less than 6 hours. When water depth was less than 0.25 m, velocity data is not shown or used in this study. An upward-looking Acoustic Wave and Current Profiler (AWAC, Nortek AS) was deployed at 18.1 m depth at E1 on the forereef (Figure 5.1e), and recorded current measurements at 1-minutes intervals and measured surface wave statistics in 20-minute bursts every three hours.

The meteorological data used in this study were measured from the weather station located on Pratas Island (Figure 5.1b).

Raman spectra fiber-optic Distributed Temperature Sensing (DTS) technology was deployed at Dongsha Atoll from 04 to 11 June 2014 to measure near bed water temperatures across the east reef flat and forereef slope over a 4 km distance. A Sensornet Oryx DTS interrogator collected continuous independent temperature measurements every two meters along a Kaiphone (flexible white, 6 mm, steel-reinforced) fiber optic cable at a sample frequency of one temperature trace per minute.

The fiber optic cable was deployed on the sea floor in the cross-shelf direction on the east reef flat starting near the lagoon and extending east across the reef flat and down the reef slope to a depth of approximately 50 m (Figure 5.1e). The DTS measurements started on 04 June 2014, and continued until the machine lost power due to Tropical Storm Hagibis on 12 June 2014. Details of deployment and calibration are found in Reid et al. (2019). The average bias and root-mean-square difference between the validation loggers (SBE-56s) and

the DTS was 0.07 ± 0.01°C and 0.20 ± 0.02°C, respectively.

Five Sea-Bird Electronics temperature sensors (SBE-56) which were placed along the DTS cable for calibration and validation (C1, C2, C3, V1, and V2), were used for estimates of DTR in Section 5.3.3 and 5.3.4 because they were still logging after the DTS lost power on 12 June. They were logging from 04 June to 17 June, 2014. They measured temperature at 0.5-second intervals, and were in depths of 0.5 to 2.4 m.

5.2.3 Kaneohe Bay Experiment

Measurements of currents, pressure, and water temperature on the reef flat and offshore at Kaneohe Bay (Figure 5.1f), and meteorological conditions on Coconut Island (Figure 5.1c), were made from 15 to 27 January, 2017. Details of all instrumentation are listed in Table 5.2.

The reef flat (Figure 5.1f), is approximately 1.5 km wide, and ranges from 0.2 to 3.0 m depth. The dynamics in Kaneohe Bay have been extensively studied (Lowe et al., 2005, 2009a,b), and it has been shown that surface wave driven flow is the dominant mechanism driving flow over the reef. Spatial temperature variability has been studied on the fringing reefs at Coconut Island (Figure 5.1c) in Kaneohe Bay, which showed that total variance of temperature, pH and oxygen decreased in an offshore direction (Guadayol et al., 2014). In this study, they also found that diurnal variability was more significant in shallow regions, and decreased in deeper waters offshore.

Fifteen Sea-Bird Electronics temperature sensors (SBE-56), and three Sea-Bird Electronic MicroCATs (SBE-37 SMP-ODO) were deployed on the bottom in along-reef and cross-reef

Table 5.2: Deployment instrumentation for Kaneohe Bay

Location	Instruments	Depth (m)	Sampling Rate	Dates (dd/mm/yy)
OS	Teledyne ADCP	13.1	profile: 1-min, 60cm bins, waves: 512 bursts at 2Hz every 3hrs	15-27/01/17
	Sea-Bird SBE-37		60 sec	
KB1	Sea-Bird SBE-56	1.5	0.5 sec	15-27/01/17
KB1.1	Sea-Bird SBE-56	1.3	0.5 sec	15-27/01/17
KB1.2	Sea-Bird SBE-56	1.4	0.5 sec	15-27/01/17
KB2	Sea-Bird SBE-37 Nortek ADP	1.5	60 sec profile: 4-min, 10cm bins	15-27/01/17
KB2.1	Sea-Bird SBE-56	1.4	0.5 sec	15-27/01/17
KB2.2	Sea-Bird SBE-56	1.3	0.5 sec	15-27/01/17
KB2.A	Sea-Bird SBE-56	1.9	0.5 sec	15-27/01/17
KB2.B	Sea-Bird SBE-56	1.8	0.5 sec	15-27/01/17
KB2.C	Sea-Bird SBE-56	2.1	0.5 sec	15-27/01/17
KB3	Sea-Bird SBE-37	1.3	60 sec	15-27/01/17
KB3.1	Sea-Bird SBE-56	1.2	0.5 sec	15-27/01/17
KB3.2	Sea-Bird SBE-56	1.2	0.5 sec	15-27/01/17
KB4	Sea-Bird SBE-56 Nortek ADP	0.9	0.5 sec profile: 4-min, 10cm bins	15-27/01/17
KB4.1	Sea-Bird SBE-56	0.9	0.5 sec	15-27/01/17
KB4.2	Sea-Bird SBE-56	0.6	0.5 sec	15-27/01/17
KB5	Sea-Bird SBE-56	0.5	0.5 sec	15-27/01/17
KS2	Sea-Bird SBE-56 Nortek ADP	2.7	0.5 sec profile: 4-min, 10cm bins	15-27/01/17
KS4	Nortek ADP	3.1	profile: 4-min, 10cm bins	15-27/01/17

transects on the reef flat and offshore (Figure 5.1f) to measure temperature at 0.5-second (SBE-56) and 1-minute (SBE-37) intervals. The depth of the temperature sensors ranged from 0.5 to 2.7 m on the reef flat and 13.1 m offshore. Three 1-MHz and one 2-MHz Nortek AquaDopp Profilers (ADPs) were placed on the reef flat at KB2, KB4, KS2 and KS4 (Figure 5.1f) to measure currents and pressure at 4-minute intervals. Offshore, an upward-looking Teledyne Sentinel V Acoustic Doppler Current Profiling (ADCP) was deployed at 13.1 m depth on the forereef (Figure 5.1f), and recorded current measurements at 1-minute intervals and measured surface wave statistics in 3-minute bursts every three hours.

The meteorological data used in this study were measured from the weather station located on Coconut Island (Figure 5.1c).

5.2.4 Ofu-Olosega Experiment

The deployment on Ofu-Olosega Island included measurements of currents, pressure and water temperature in the back reef pools and on the forereef slope (Figure 5.1d,g) from 15 to 25 March, 2017. Details of all instrumentation are listed in Table 5.3.

The deployment site has a shallow and wide reef flat, coral filled lagoons, and a break in the reef crest that creates a strong channel outflow (called an "ava"). Measurements of temperature and circulation were made in the back reef lagoons, reef flat and on the forereef slope. Flow is largely driven by tidal modulation of breaking waves on the reef crest (Koweek et al., 2015). The Ofu lagoons have been shown to have substantial small-scale heterogeneity in temperature, water chemistry (pH, dissolved O2), and flow (Craig et al., 2001; Smith et al., 2008; Monismith, 2014). The coral reef ecosystem at Ofu has high biodiversity (Craig

Table 5.3: Deployment instrumentation Ofu-Olosega

Location	Instruments	Depth (m)	Sampling Rate	Dates (dd/mm/yy)
Back reef	Silixa XT-DTS	0.1-2.1	2-10 min	15-25/03/17
FR5	Sea-Bird SBE-56	5.8	0.5 sec	15-25/03/17
FR16	Nortek ADP	15.4	profile: 5-min, 50 cm bins, waves: 1024 burst samples at 1Hz, every 30 min	15-25/03/17
	Sea-Bird SBE-56		0.5 sec	15-25/03/17
FR25	Sea-Bird SBE-56	24.4	0.5 sec	15-25/03/17
CH5	Sea-Bird SBE-56	6.2	0.5 sec	15-25/03/17
CH9	Nortek ADP		profile: 5-min, 50 cm bins, waves: 1024 burst samples at 1Hz, every 30 min	15-25/03/17
	Sea-Bird SBE-56	8.5	0.5 sec	15-25/03/17
CH25	Sea-Bird SBE-56	21.3	0.5 sec	15-25/03/17
B0	Nortek ADP	2.3	profile: 3-min, 15 cm bins, waves: 2048 burst samples at 2Hz, every 30 min	15-25/03/17
B-1	Teledyne vADCP	0.8	profile: 0.33Hz, 3 cm bins	15-25/03/17
D0	Nortek ADP	1.7	profile: 3-min, 15 cm bins, waves: 2048 burst samples at 2Hz, every 30 min	15-25/03/17
D-2	Nortek ADV	1.7	profile: 1024 burst samples at 4Hz, every 10 min	15-25/03/17
D-4	Teledyne vADCP	0.7	profile: 0.33Hz, 3 cm bins	15-25/03/17
F0	Nortek ADP	1.6	profile: 3-min, 15 cm bins, waves: 2048 burst samples at 2Hz, every 30 min	15-25/03/17
H0	Nortek ADP	1.5	profile: 3-min, 15 cm bins, waves: 2048 burst samples at 2Hz, every 30 min	15-25/03/17
H-1	Teledyne vADCP	0.6	profile: 0.33Hz, 3 cm bins	15-25/03/17
J0	Nortek ADP	0.7	profile: 3-min, 15 cm bins, waves: 2048 burst samples at 2Hz, every 30 min	15-25/03/17
Ofu3	Hobo UTBI/U22	0.8	30 min	02/01/04 - 08/09/11
Ofu4	Hobo UTBI/U22	1.5	30 min	18/12/03 - 01/09/11
Ofu5	Hobo UTBI/U22	0.9	30 min	25/08/02 - 11/07/09

et al., 2001), and the lagoons here have shown to have distinct thermal environments, with small pools experiencing higher diurnal variability and extreme temperatures (Oliver and Palumbi, 2011). The corals in the back reef pools have demonstrated high variability in bleaching responses, with corals in the high variability pools having a higher heat tolerance (Barshis et al., 2010; Oliver and Palumbi, 2011; Barshis et al., 2013; Bay and Palumbi, 2014; Palumbi et al., 2014).

A DTS system and fiber optic cables were deployed in the back reef pools in an along and cross-reef pattern to measure near bed water temperature (Figure 5.1g). A Silixa XT-DTS interrogator collected continuous independent temperature measurements every 0.25 m along two Kaiphone (flexible white, 6 mm, steel-reinforced) fiber optic cables at a sample frequency ranging from 2 to 10 minutes, which was interpolated in post processing to one temperature trace per 2 minutes. Each cable was 2 km in length, and was deployed in a simple single-ended configuration on the reef with 12 accurate temperature sensors (Sea-Bird Electronics SBE-56s, $\pm 0.02°$C) placed for calibration (6 sensors) and validation (6 sensors). Calibration procedures outlined in Hausner et al. (2011) were followed, similar to Reid et al. (2019); Sinnett et al. (2020). The average bias and root-mean-square difference calculated for the validation loggers was $0.04°$C$\pm 0.02°$C and $0.07°$C$\pm 0.02°$C, respectively. Bathymetry data was not available for the back-reef pools, however the cables were surveyed during the deployment, and mean sea level measurements were recorded.

Eleven current meters (7 Nortek Aquadopp Profilers, 3 Teledyne vADCP's, 1 Nortek ADV) were deployed in the back reef pools, and on the forereef slope (Figure 5.1g). Offshore of the reef crest, on the forereef slope (Figure 5.1g), six Sea-Bird Electronics temperature sensors (SBE-56) were deployed to measure temperature at 0.5-second intervals. The sensors were deployed in two cross-shore transects, at depths ranging from 4.2 to 24.4 m depth. Details of sampling rates can be found in Table 5.3.

5.2.5 Temperature Analysis

Spectral analysis of temperature data at the three sites was completed using the multitaper method (Thomson, 1982; Lilly, 2019). The 95% confidence interval is found from the χ^2_k distribution with the 6 degrees of freedom given by orthogonal Slepian tapers (Thomson, 1982). DTS temperature data from Dongsha Atoll and Ofu was averaged in 10 m sections before spectral analysis was performed. The spectra was integrated between specified ranges representing weekly (27 hours to 7 days), daily (21 to 27 hours), 2 times daily (10 to 14 hours), 3 times daily (6 to 10 hours) and internal wave frequencies (5 to 30 minutes), similar to Guadayol et al. (2014). Total variance is calculated in these ranges.

Empirical Orthogonal Function (EOF) analysis was completed to describe the dominant spatial patterns of variance in the temperature data at the three sites. The gradient EOF was calculated in order to highlight gradients in the temperature data following Keiner and Yan (1997). First, the spatial mean was removed from the temperature data, as follows:

$$T'(x,t) = T(x,t) - \frac{1}{M} \sum_{x=1}^{M} T(x,t) \tag{5.1}$$

where T(x,t) is the temperature at each location and time, T'(x,t) is the spatially demeaned temperature at each location and time, and M is the number of elements in the spatial dimension. The gradient EOF was solved for the spatially demeaned temperature data at the three sites to determine the spatial pattern functions (or the eigenvector), the temporal amplitude functions and the amount of variance in the modes (or the eigenvalues). Gradient EOF's can be used to show where strong spatial gradients (such as fronts) exist in

the temperature data (Keiner and Yan, 1997). All data was averaged in 10-minute intervals before completing the EOF analysis. Results at each site were scaled so the eigenvectors were within the same range.

5.2.6   Longer-term Data

To understand how physical forcing drives temperature variability at these sites, longer-term data was gathered for Dongsha Atoll and Ofu-Olosega. At Dongsha Atoll, Onset Corporation HOBO U22 loggers (accuracy $\pm 0.2°C$ after calibration in an isothermal bath) were deployed on the east reef flat at two locations, HA and HB, (Figure 5.1e), at 1.4 and 1.8 m depth, respectively, from June 2013 to June 2014. At Ofu-Olosega, three loggers (HOBO UTBI and U22, accuracy $\pm 0.2°C$) were deployed in the back reef lagoons in depths ranging from 0.8 to 1.5 m (Figure 5.1d) between 2002 and 2011 (see Table 5.3 for specific dates).

To estimate the tidal depth on these reefs when there are not *in-situ* observations, the Oregon State Tidal Inversion Software (Egbert and Erofeeva, 2002) and the TMD toolbox (Padman and Erofeeva, 2004) was used. Wave and weather data were accessed from the Copernicus Climate Data Store ERA5 dataset, European Centre for Medium-Range Weather Forecasts (ECMWF), a climate reanalysis model (hourly data, spatial resolution = $0.25°$ for atmospheric data, $0.5°$ for ocean wave data, doi: 10.24381/cds.adbb2d47).

5.2.7 Particle Tracking

Residence time was estimated to determine how the retention of water across the reef affects temperature variability across the reef flat at Kaneohe Bay and Dongsha Atoll. A quasi-Lagrangian framework, similar to DeCarlo et al. (2017b) was used to determine the residence time (T_{RT}) of a water particle on the reef flat. Using water velocity, pressure and bathymetry data, water particles were tracked from discrete locations across the reef flat. The residence time was estimated using depth-averaged velocity (in two-dimensions) and water depth ($h(x,t)$). At Dongsha Atoll, measurements of velocity and depth at E3 and E5 (Figure 5.1e), and LIDAR-based bathymetry data (resolution = 3 m, Shih et al., 2011) for the reef flat were used. At Kaneohe Bay, measurements of velocity and depth at KB2, KB4, KS2 and KS4 (Figure 5.1f), and LIDAR-based bathymetry data (resolution = 4 m, NOAA Pacific Islands Fisheries Science Center, Coral Reef Ecosystem Division, Pacific Islands Benthic Habitat Mapping Center, 2011) were used. Velocities across the reef were estimated by linearly interpolating the transport between sites:

$$U(\eta + \eta_0 + h) = U(\eta + D) = q_0 \qquad (5.2)$$

where $U(x,t)$ is the depth-averaged cross-reef current including the Stokes velocity due to waves, $\eta(x,t)$ is the sea level variation over the scale of the reef due to wave forcing (wave setup), η_0 is the sea level variation on spatial scales that are large compared to the reef, which include tides, wind forcing and seasonal buoyancy forcing, $h(x)$ is the water depth relative to mean sea level when currents are weak, and $D(x,t) = \eta_0(t) + h(x)$. Based on our observations, $\eta << D$, so that $\eta + D \approx D$, as variations in η are typically centimeters and D is about 1 m. The tidal difference (η_0) in water depth for each time step was interpolated between sites on the reef flat, and the water depth relative to mean sea level (h) at each location was used to calculate total depth at any location across the reef flat ($D = \eta_0 + h$).

For Dongsha, transport was interpolated between E3 and E5 when the particle was between the two stations, and applying transport at E3 from the reef crest to E3 and applying transport at E5 from E5 to the lagoon boundary. Velocity was not measured at any alongshore locations, so transport on the measured cross section was applied to the north and south in the region that bathymetry data was available ($\sim$ 1500 m to the north, $\sim$ 2000 m to the south of the cross section). The assumption that transport does not vary in the along reef direction is reasonable for an elongated reef (length $>>$width) where bathymetry does not vary substantially and waves break uniformly along the length of the reef. If the particle reached the north/south boundary, particle tracking was stopped.

For Kaneohe Bay, transport was interpolated between the four sites, and when the water particle was outside the bounds of the four stations, nearest-neighbor extrapolation was used. Since many of the particles originated to the north of our sampling sites, more information was needed to determine the transport in that section of the reef. When particles were outside of the bounds of the four current meters, nonphysical results were seen due to the nearest-neighbor extrapolation method. Measurements completed by Lowe et al. (2009a) from a site north of the transect (see Location A2 in Lowe et al., 2009a), and the current magnitude and direction at KB4 was similar to site A2. The currents measured during the deployment at KB4 were applied at the location of site A2 to expand the area where current data and depth could be interpolated for the particle tracing (see Kealoha et al., 2019, Supporting Information (S1) for more details).

Residence time (T_{RT}) was calculated backward in time from discrete locations across the reef flat to the reef crest to determine where water across the reef flat is coming from, and how long it takes to move across the reef flat. Water particles were tracked across the reef flat until they reach the reef crest boundary. For Kaneohe Bay, particles were tracked until particles reached 4m depth offshore (eastward of reef flat, see bathymetry in Figure 5.2b).

At Dongsha, particles were tracked until they reached the reef crest (as defined by the white dashed line in Figure 5.1e). Particles that did not travel towards the reef crest were not included in the results. The distance from the reef crest at each site to the location across the reef flat (Δx_{RC}) was also determined.

5.2.8   Estimating Tide, Wave and Wind-Driven Flow

A simple analytical flow model was used to determine the cross-shore flow on the reef flat at Dongsha Atoll and Kaneohe Bay, which is then used in the heat budget model described below (Section 5.2.9). Flow was predicted following Lentz et al. (2016); Reid et al. (2020). Assuming steady state flow and neglecting along-shore variations (i.e. that along-reef variations in bathymetry are negligible and waves break uniformly along the length of the reef) continuity in depth-averaged flow implies that cross-reef transport, $q_0(t)$, does not vary across the reef (Equation 5.2). The steady, depth-averaged cross-reef momentum balance becomes:

$$\frac{\partial(U^2 D)}{\partial x} = -gD\frac{\partial \eta}{\partial x} - \frac{1}{\rho}\frac{\partial S_{xx}}{\partial x} + \frac{\tau^{sx}}{\rho} - \frac{\tau^{bx}}{\rho} \tag{5.3}$$

where $g = 9.81\ m\,s^{-2}$ is gravitational acceleration, S_{xx} is the cross-reef component of the wave-radiation stress tensor, in $kg\,s^{-2}$, ρ is the density of seawater, in $kg\,m^3$, τ^{sx} is the wind stress and τ^{bx} is the bottom stress, in Pa (Mei, 1989; Lowe et al., 2009b). The wave-radiation stress tensor, S_{xx} is estimated as follows:

$$S_{xx} = \frac{\rho g H_s^2}{16}\left\{(\cos^2(\theta_w) + 1)\frac{c_g}{c} - \frac{1}{2}\right\} \tag{5.4}$$

where H_s is significant wave height, in m, and θ_w is wave direction, c_g is group velocity, and c is phase velocity (Longuet-Higgins and Stewart, 1962, 1964). Offshore significant wave statistics were taken from ERA5 data. Significant wave height in the lagoon was assumed to be zero.

Bottom stress is estimated as:

$$\tau^{bx} = \rho C_{da} U |U| = \rho C_{da} \frac{q_0 |q_0|}{D^2} \tag{5.5}$$

where $C_{da}(x, t)$ is a bulk drag coefficient for the depth-averaged current (Rosman and Hench, 2011). The depth-dependence of drag has been shown to be important on coral reefs (Lentz et al., 2017) and is estimated as follows:

$$C_{da} = \kappa^2 \left\{ log \left(\frac{D}{z_0} \right) + (\Pi - 1) \right\}^{-2} \tag{5.6}$$

where $\kappa = 0.4$ is the von Karman constant, z_0 is the hydrodynamic roughness, and Π is Cole's wake strength, which is taken as 0.2. Hydrodynamic roughness, z_0, was estimated for the Dongsha Atoll reef flat in a previous study by Lentz et al. (2017), as 3.2 cm for E3 and 1.4 cm for E5 (Figure 5.1a). The value for z_0 at Kaneohe Bay has not been measured, however, a reef with similar bottom roughness, Qita Dukais in the Red Sea, had an average value of z_0 of 6.0 cm (Lentz et al., 2017), so this value was applied at Kaneohe Bay. A smaller value of z_0 of 2.0 cm was tested, and results were not significantly different.

Dividing Equation 5.3 by D and using Equation 5.2 yields:

$$-\frac{q_0^2}{D^3} \frac{\partial D}{\partial x} = -g \frac{\partial \eta}{\partial x} - \frac{1}{\rho D} \frac{\partial S_{xx}}{\partial x} + \frac{\tau^{sx}}{\rho D} - C_{da} \frac{q_0 q_0}{D^3} \tag{5.7}$$

Integrating Equation 5.7 from x_1 to x_2 to estimate the sea level difference $\Delta\eta = \eta(x_2) - \eta(x_1)$:

$$g\Delta\eta = -q_0|q_0|\left(\int_{x_1}^{x_2} C_{da}D^{-3}\mathrm{d}x + \frac{1}{2}sgn(q_0)D^{-2}\Big|_{x_1}^{x_2}\right) + \int_{x_1}^{x_2}\left(-\frac{1}{\rho D}\frac{\partial S_{xx}}{\partial x} + \frac{\tau^{sx}}{\rho D}\right)\mathrm{d}x \quad (5.8)$$

Solving for q_0 yields:

$$q_0|q_0| = \left(\int_{x_1}^{x_2}\left(-\frac{1}{\rho D}\frac{\partial S_{xx}}{\partial x} + \frac{\tau^{sx}}{\rho D}\right)\mathrm{d}x - g\Delta\eta\right) \Big/ \left(\int_{x_1}^{x_2} C_{da}D^{-3}\mathrm{d}x + \frac{1}{2}sgn(q_0)D^{-2}\Big|_{x_1}^{x_2}\right) \quad (5.9)$$

Similar to Lentz et al. (2016), Equation 5.9 can be simplified by recognizing that the bathymetric slope on the reef flat is very small (i.e. the magnitude of dD/dx is negligible). Equation 5.9 reduces to:

$$U|U| = -\frac{\Delta S_{xx}}{\rho C_{da}\Delta x} + \frac{\tau^{sx}}{\rho C_{da}} - \frac{g\Delta\eta D}{C_{da}\Delta x} \quad (5.10)$$

$$U = sgn\left(-\frac{\Delta S_{xx}}{\rho C_{da}\Delta x} + \frac{\tau^{sx}}{\rho C_{da}} - \frac{g\Delta\eta D}{C_{da}\Delta x}\right)\sqrt{\left|-\frac{\Delta S_{xx}}{\rho C_{da}\Delta x} + \frac{\tau^{sx}}{\rho C_{da}} - \frac{g\Delta\eta D}{C_{da}\Delta x}\right|} \quad (5.11)$$

where $\Delta x = x_2 - x_1$. For the reef flat, x_1 and x_2 are assumed to be offshore of the reef crest and near the lagoon, respectively. For each site, Δx was taken as the width of the reef flat.

Equation 5.11 states that for a two-dimensional control volume over the reef, the on-reef flux of momentum due to the incident wave radiation stress, wind stress and pressure gradient is balanced by the bottom stress. Equation 5.11 was used to estimated flow on the reef flat for the longer-term data, and used in the heat budget estimates of DTR (see Section 5.2.9). Average depth on the reef, and average z_0 were used in Equation 5.11 to estimate mean flow on the reef flat. The estimated mean flow across the reef was multiplied by the

average depth to find mean transport on the reef flat. This transport was applied across the reef flat to find flow at each location, and input to the heat budget model.

In order to estimate flow when we do not have measurements on the reef flat, input data was gathered from a tidal model and a climate reanalysis model. Sea level variation (η_0) was estimated using the Oregon State Tidal Inversion Software (Egbert and Erofeeva, 2002) and the TMD toolbox (Padman and Erofeeva, 2004). This was then used to estimate time varying depth across the reef flat for Dongsha Atoll and Kaneohe Bay using LIDAR bathymetry data at each site. All other inputs to the flow model (Equation 5.11), including wind and wave data, were gathered from the Copernicus Climate Data Store ERA5 dataset, described in Section 5.2.6.

Significant wave height (H_S) from the ERA5 dataset at Dongsha Atoll and Kaneohe Bay was greater than observed values during the deployments. The closest location in the ERA5 dataset was approximately 8 km offshore of the east reef flat at Dongsha, and 5.5 km offshore at Kaneohe Bay. The offshore wave field was different than the nearshore wave field at both sites. This leads to overestimates of flow on the reef flat at both sites when the ERA5 significant wave height is used. A factor was applied to the significant wave height (cH_S), and compared to significant wave height observations when they were available at each site. The absolute error between the observations and ERA5 data was found for a range of factors ($c = 0.25 - 0.99$), to find the minimum error. The optimal decreasing factor for Dongsha Atoll was $c = 0.82$ and for Kaneohe Bay was $c = 0.65$. This is further discussed in Section 5.4.2.

The last term on the right-hand side of Equation 5.11 captures pressure gradients on the reef flat due to tides, wind and offshore surface waves. This term can be separated into tidally driven sea level change ($\Delta\eta_{tide}$ and residual sea level change $\Delta\eta_r$), driven by offshore waves

that break on the reef crest and could also include some influence of tides and wind (see Reid et al., 2020, for a full analysis of this term). To estimate the tidally driven pressure gradient term ($\Delta\eta_{tide}$), a unified tidal analysis and prediction method (Codiga, 2011) was used to find the coefficients for the tidal model of the pressure gradient when we had measurements at Dongsha Atoll and Kaneohe Bay. Offshore pressure and near lagoon pressure (E6 for Dongsha Atoll, KB4 for Kaneohe Bay) were used as inputs for $\Delta\eta_{tide}$. This tidal model was then applied to find $\Delta\eta_{tide}$ when we do not have measurements pressure on the reef flat. The residual pressure gradient term ($\Delta\eta_r$) cannot be estimated from the tidal model, and is therefore not included in the flow model. This could lead to an underestimate of flow on the reef, and is discussed in Section 5.4.2. The tidal prediction of sea level variation $\Delta\eta_{tide}$ was used in Equation 5.11 to find cross-shore flow due to pressure gradients on the reef flat.

5.2.9   Heat Budget Model

A heat budget was completed to estimate the daily temperature range (DTR) across the reef flat at Dongsha Atoll and Kaneohe Bay. Using the heat budget, we are able to incorporate more physical forcings acting on the reef flat, to estimate DTR for a specific day and location on the reef. In order to estimate the DTR using the heat budget for times when we do not have observational data on these reefs, the inputs are taken from a tidal model and climate reanalysis model, both described above (Section 5.2.6). The heat budget estimate of DTR is compared to the temperature observations during the January 2017 deployment at Kaneohe Bay and longer-term temperature data from Dongsha Atoll, to see how well the heat budget model is performing.

The simple heat budget was estimated following Davis et al. (2011); Reid et al. (2019):

$$\frac{\partial \overline{T}}{\partial t} + \overline{u_i} \frac{\partial \overline{T}}{\partial x_i} = -\frac{\partial}{\partial x_i} \overline{u_i' T'} \tag{5.12}$$

where, the summative convention with the index $i = 1, 2, 3$ and a right-handed coordinate system is adopted with the principle axes defined by x_i: x is the distance across the reef, y is the distance along the reef, and z is positive upward, u_i represents the corresponding velocity components, u, v and w, and T is water temperature. Figure 5.1e and 5.1f show the corresponding across-reef (x) and along-reef (y) axes used for each site. Overbars denote time-averaged quantities, and primed values are the fluctuating components ($u = \overline{u} + u'; T = \overline{T} + T'$). The heat budget is focused on the cross-shore dimension only, because the along-shore flow, v, and vertical velocities, w, are an order of magnitude less than cross-shore flow, u. At Kaneohe Bay, along-shore flow, v, is significant, however, the results of the predicted temperature are similar to the observed, so only the cross-shore dimension x, was considered to simplify the analysis. The temperature, T, is assumed to be well mixed in the vertical on the shallow reef flat.

Estimates for the cross-shore flow on the reef flat are completed using the tidal, wind and wave driven flow model described above (Section 5.2.8. Estimates of turbulent transport were not possible, because the temporal frequency of the inputs for the model from the tidal model and climate reanalysis model were not sufficient for measuring turbulent transport of heat. Our results suggest that this term as well as heat flux through the reef bed are likely small, given the approximate balance between advective and atmospheric heat flux; see similar results in Davis et al. (2011); Reid et al. (2019).

When Equation 5.12 is vertically integrated over the water column, and is multiplied by the heat capacity per unit volume (ρc_p, assumed to be constant and equal to $4.1 x 10^6 \, W s m^{-3 \circ} C^{-1}$),

we obtain an equation for the heat balance within a volume of water of unit length and width (Equation 5.13) (Davis et al., 2011; Reid et al., 2019). The left side of Equation 5.13 represents the rate of change of heat storage within the volume, Q_T. The terms on the right side of the equation represent the advective heat flux, ΔF, and atmospheric/ocean heat flux, Q_N.

$$\rho c_p D \frac{\partial \langle \overline{T} \rangle}{\partial t} = -\rho c_p D \langle \overline{u} \rangle \frac{\partial \langle \overline{T} \rangle}{\partial x} + Q_N \tag{5.13}$$

$$OR \quad Q_T = \Delta F + Q_N \tag{5.14}$$

where D represents the depth of the water, and u is the depth and time-averaged, velocity in the cross-shore direction, and angled brackets denote depth averaged quantities.

The net heat flux between the atmosphere and the ocean, Q_N, is calculated as follows:

$$Q_N = Q_E + Q_H + Q_S + Q_L \tag{5.15}$$

where the terms on the right-hand side of the equation represent latent, sensible, net short-wave, and net longwave heat flux respectively. The incoming shortwave radiation was corrected for an additional albedo (10%), to account for reflectance of the coral bed in shallow water (Maritorena et al., 1994). A modified version 2.5 TOGA (Tropical Oceans Global Atmosphere) COARE (Coupled Ocean–Atmosphere Response Experiment) bulk algorithm (Fairall et al., 1996, 2003) was used to compute the latent and sensible heat fluxes. The net

long-wave heat flux was calculated as follows (Rosenfeld et al., 1994):

$$Q_b = \epsilon\sigma(T + 273.16)^4(0.254 - 0.00495R_H e_S) \tag{5.16}$$

$$e_S = 6.122 * exp\left(\frac{17.67T_{air}}{T_{air} + 243.5}\right) \tag{5.17}$$

where Q_b is clear sky net long-wave radiation, ϵ is the emissivity of the sea surface, taken as 0.97, σ is the Stefan-Boltzman constant, $5.6697x10^{-8}Wm^{-2\circ}K^{-4}$, T is the sea surface temperature in $^\circ C$, R_H is the relative humidity measured by the meteorological station, es is the saturated vapor pressure and T_{air} is the temperature of the air in $^\circ C$. Finally, a linear cloud factor, $(1-0.9C)$, from (Reed, 1976), was applied to the net longwave radiation, where C is the cloud cover coefficient, taken as 0.59 for 20°N (Budyko, 1974).

The heat budget for the reef flat was calculated daily, and compared to *in-situ* observations of temperature at Dongsha Atoll and Kaneohe Bay. The model needs an initial condition of temperature in the cross-section that the heat budget is being calculated for. The initial condition for temperature at the reef crest was estimated using offshore sea surface temperature (SST) from the ERA5 data. To estimate the initial temperature gradient for the reef flat, the observations of temperature gradients (DTS data for Dongsha Atoll, SBE-56 thermistors for Kaneohe Bay) were used. The gradient was estimated as the average difference between the reef crest and the lagoon temperature $(\Delta T_{avg} = \overline{T_{RC}} - \overline{T_{LG}})$. The temperature at the reef crest was assumed to be equal to offshore SST, and the temperature at the lagoon end was estimated as the SST - ΔT_{avg}. Temperature in between the reef crest and lagoon was interpolated. The initial condition of temperature was re-initialized at the start of each day of the model calculations. The offshore SST was used as the reef crest boundary condition for the heat budget model. The heat budget was calculated in 50 m sections across the reef

flat, and bathymetry on the reef flat was averaged in these sections.

Temperature on the reef flat was predicted from Equation 5.13 using a forward differencing scheme for the time derivative and a upwind differencing scheme for the spatial gradient in temperature $(\partial\langle\overline{T}\rangle/\partial x)$. Depth on the reef flat at each location and time was estimated using the bathymetry and the sea level variation from the TMD model. Transport across the reef flat was calculated using the tide, wave and wind-driven flow model described above (Section 5.2.8). Atmospheric heat flux at each location on the reef was calculated using temperature from the time step before. All inputs were interpolated to 30-second intervals for the heat budget calculations.

Overestimates of flow on the reef (see Section 5.2.8 and discussion in Section 5.4.2) lead overestimates of the advective flux term (ΔF, Equation 5.14). This leads to large, unrealistic temperature changes on the reef flat. When the change in temperature on the reef is greater than two times the maximum observed DTR on the reef, results for that day are not included in the estimates of average DTR.

5.3 Results

5.3.1 Oceanographic Conditions

Conditions at Dongsha Atoll were calm, with low wind and waves near the start of the deployment (approximately 04 to 07 June), and Tropical Storm Hagibis formed in the SCS around 12 June, which led to higher wind and wave conditions at the atoll. Daily average

atmospheric heat flux (Q_N), ranged from -70 to 234 W m^2, with lower values on 07 to 08 June when there was low solar radiation. Mean wind speed at the start of the deployment (04 to 10 June) was 2.4 m s^{-1} towards the northeast, and increased from 10 to 14 June, to 3.0 m s^{-1} towards the southwest. Peak winds occurred from 14 to 17 June, towards the southeast, and then northeast (average = 4.9 m s^{-1}). Significant wave height, H_S, was measured offshore of the reef crest at E1 (Figure 5.1e), and ranged from 0.2 to 3.0m, with smaller waves from 04 to 08 June, and increased wave height from 09 to 15 June. The barotropic (surface) tide at Dongsha Atoll is microtidal, and mixed semidiurnal. Daily tidal range on the reef flat was between 0.4 and 1.3 m at E3, and between 0.4 and 1.4 m at E5, with a spring tide before the deployment (29 May 2014), and again on 13 June. Circulation on the east reef flat was primarily in the cross-shore (east-west) direction (Figure 5.1e). More details on oceanographic conditions during the deployment are found in Reid et al. (2019, 2020).

At Kaneohe Bay, oceanographic conditions were calm near the start of the deployment, and wind and waves were stronger at the end of the deployment. Daily average atmospheric heat flux (Q_N), ranged from 21 to 149 W m^2. Average wind speed was 3.8 m s^{-1} towards the southwest at the start of the deployment (15 to 20 January, 2017), and increased to 8.8 m s^{-1} from 21 to 23 January. Wind decreased to 4.8 m s^{-1} near the end of the deployment (24 to 27 January). Average significant wave height, H_S, was 1.0 m at the start of the deployment (15 to 20 January), and increased to 2.6 m from 21 to 23 January, and decreased again to 1.5 m for the end of the deployment (24 to 27 January). At Kaneohe Bay, the barotropic tide is microtidal, and mixed semidiurnal. Daily tidal range on the reef flat at KB2 was between 0.3 and 0.9 m, with spring tide occurring before the deployment on January 12 and again on January 27. Average flow across the reef flat is towards the south/south-east (Figure 5.1f). More details on the oceanographic conditions during the deployment are found in Kealoha et al. (2019).

At Ofu, wind and waves were small throughout the deployment, with several longer pe-
riod swell events. Daily average atmospheric heat flux (Q_N), ranged from -97 to 160 W m^2.
Average wind speed throughout the deployment was 2.5 m s^{-1} towards the west and average
significant wave height during the deployment was 0.7 m. Flow is primarily in the along-
shore (north-east) direction, and turns offshore (eastwards) near the ava (Figure 5.1g). The
barotropic tide at Ofu is microtidal, and semidiurnal. In the lagoon, daily tidal range was
between 0.4 and 0.7 m, with a spring tide before the deployment on 12 March and again
after the deployment on March 27. More details on the oceanographic conditions during the
deployment are found in Rogers et al. (2018); Hefner et al. (2019).

5.3.2   Variability in Temperature Across the Three Sites

There was significant variability in mean temperature and daily temperature range (DTR)
between the three reefs, as well as within each site. The high spatial resolution of water
temperature data from the DTS at Dongsha and Ofu, and the individual thermistors at
Kaneohe Bay allow us to examine patterns of temperature variability across the three sites.

Mean offshore SST close to each site was determined for the same month as the deploy-
ments for five years from the ERA5 dataset (described in Section 5.2.6). The mean offshore
SST at Dongsha in June from 2010 to 2014 was 28.4°C, which is significantly warmer than
the mean near-bed temperature offshore at Dongsha during the study period (22.9°C, Fig-
ure 5.2a). At Kaneohe Bay, mean offshore SST in January from 2013-2017 was 24.1°C,
similar to the offshore mean near-bed temperature during the deployment (Figure 5.2b).
At Ofu, mean offshore SST in March from 2013 to 2017 was 29.7°C, which is cooler than
the offshore mean near-bed temperature at Ofu during the deployment (30.0°C, Figure 5.2c).

Mean near bed water temperature during the study period at Dongsha ranged from 30.3°C
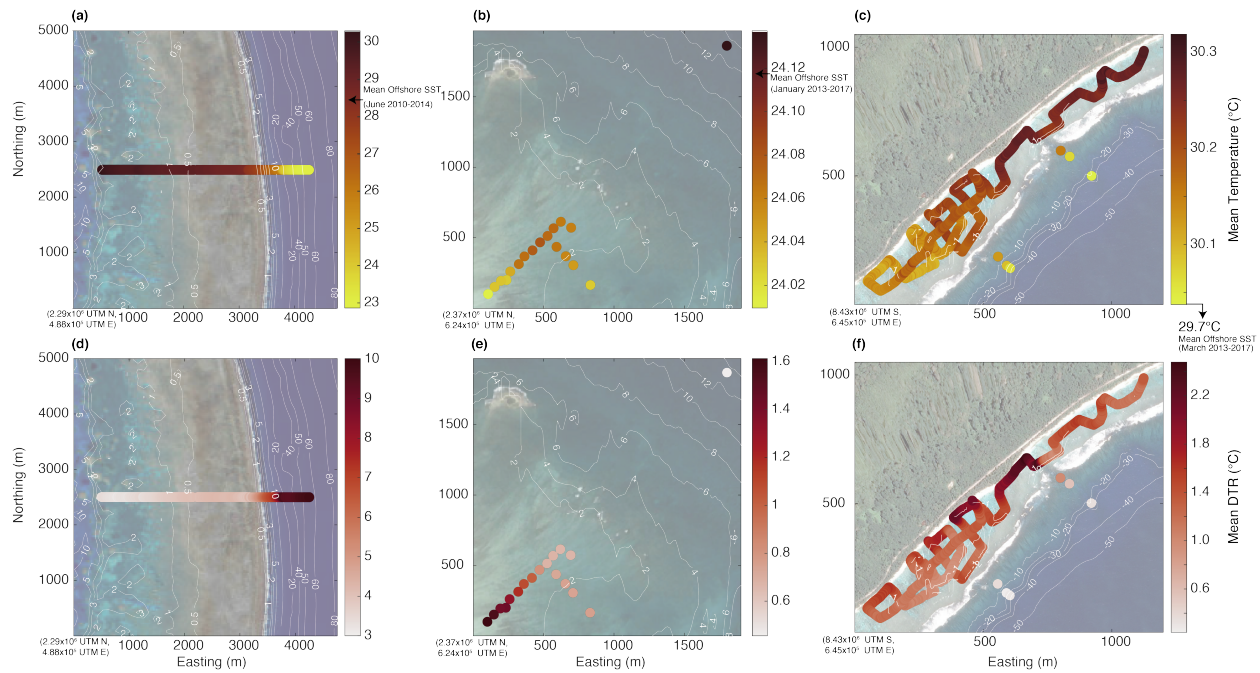
Figure 5.2: Mean Water Temperature and Daily Temperature Range.
Mean water temperature during the deployment at **(a)** Dongsha Atoll, **(b)** Kaneohe Bay, and **(c)** Ofu. Mean offshore sea surface temperature (SST) for the same month as the deployment for 5 years prior is shown on the corresponding colorbars. Daily temperature range (DTR) at **(d)** Dongsha Atoll, **(e)** Kaneohe Bay, and **(f)** Ofu. Bathymetry for Dongsha Atoll is from Shi-Ming Chen (personal communication). Bathymetry for Kaneohe Bay is from NOAA Pacific Islands Fisheries Science Center, Coral Reef Ecosystem Division, Pacific Islands Benthic Habitat Mapping Center (2011). Bathymetry data for Ofu is a combination of data from NOAA Pacific Islands Fisheries Science Center, Coral Reef Ecosystem Division, Pacific Islands Benthic Habitat Mapping Center (2010) and measurements of depth from surveys and pressure measurements in the back reef lagoons.

111

near the lagoon to 22.9°C on the forereef slope, at approximately 30.0 m depth (Figure 5.2a). At Kaneohe Bay, mean water temperature ranged from 24.0°C near the lagoon to 24.1°C offshore at approximately 13.1 m depth. (Figure 5.2b). At Ofu, mean temperature ranged from 30.3°C in the back reef pools to 30.0°C on the forereef slope at approximately 24.4 m depth (Figure 5.2c).

Average DTR varied significantly between the three reefs, and in some cases, varied substantially within a reef. DTR was calculated as the difference between the maximum and minimum daily temperature at each location, and average DTR values for each location are shown in Figure 5.2d,e, and f. At Dongsha, average DTR ranged from 3.1°C near the lagoon to 4.2°C at the reef crest (Figure 5.2d). On the reef slope, average DTR was as high as 10.0°C at 30 m depth due to the large internal waves arriving on the forereef slope (Reid et al., 2019; Davis et al., 2020; Reid et al., 2020). At Kaneohe Bay, average DTR was 1.6°C near the lagoon, and 0.7°C near the reef crest (Figure 5.2e). Offshore, in approximately 13.1 m depth, average DTR was 0.5°C. In the back reef pools at Ofu, average DTR ranged from 0.8°C to 2.5°C (Figure 5.2f). On the forereef slope, average DTR was 0.2°C at approximately 24.4 m depth.

5.3.2.1   Spectral Analysis

The total variance in the water temperature data at Dongsha Atoll is low near the lagoon (0.7°C^2 at point 1), and increases in the offshore (eastward) direction to 2.0°C^2 at point 10 (Figure 5.3d). There is a sharp increase on the forereef slope where the total variance is 4.8°C^2 (point 11). Higher values of total variance towards the reef crest are likely driven by the shallower water depths, and the influence of internal waves. At Kaneohe Bay, total
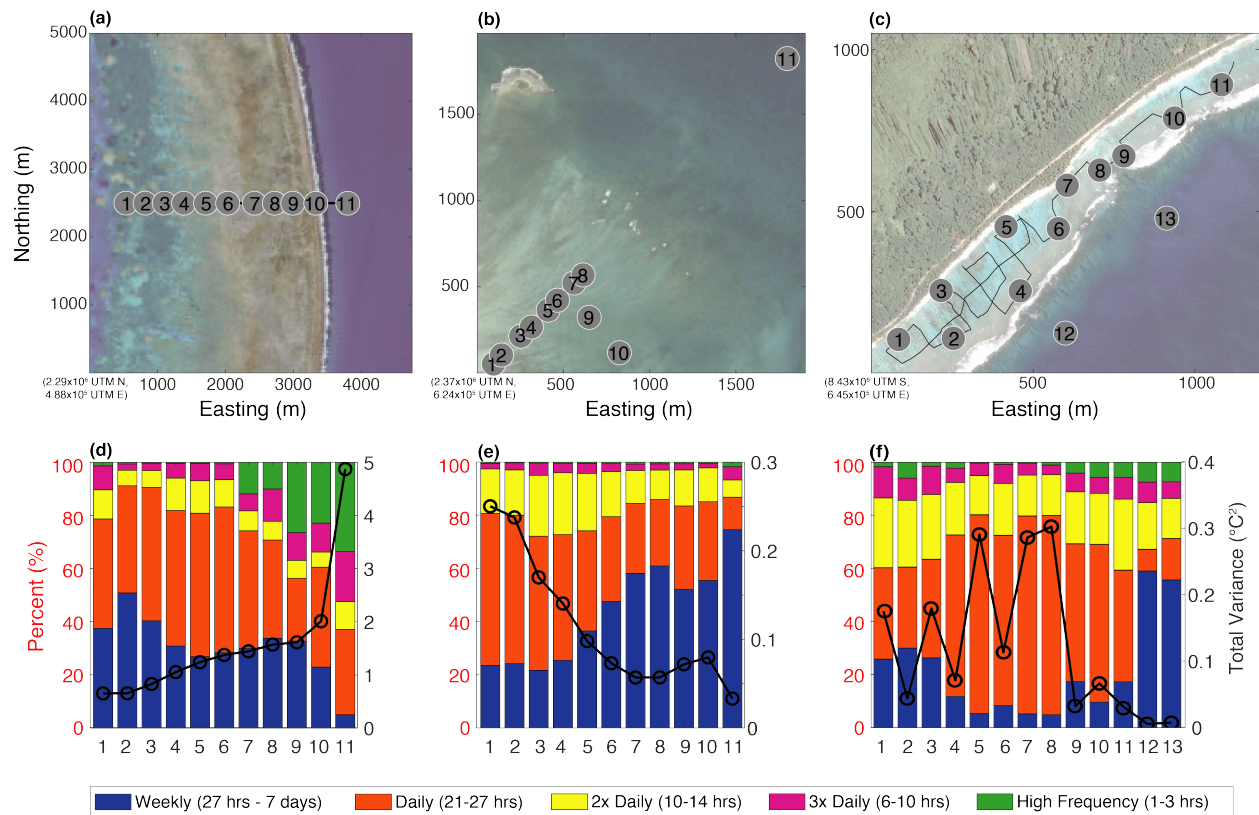
Figure 5.3: Spectral Analysis of Temperature.
Location of spectral analysis results at **(a)** Dongsha Atoll **(b)** Kaneohe Bay, and **(c)** Ofu. Locations of spectral analysis corresponding to results in **(d)**, **(e)** and **(f)** are labelled with grey circles. Percentage of variance (on the left side axis) at each location integrated in weekly, daily, 2 times daily, 3 times daily, and internal wave frequencies shown as stacked bars at **(d)** Dongsha Atoll, **(e)** Kaneohe Bay, and **(f)** Ofu. Total variance (on the right side axis) at each location shown in black circles, with total variance.

variance decreases in the cross-shore direction (Figure 5.3e) with higher values near the lagoon ($0.3°C^2$ at point 1), and lower values near the reef crest ($0.1°C^2$ at point 1). Offshore at Kaneohe Bay (point 11), total variance is near zero. There is also a small increase in the along-shore towards the southern reef pass channel from point 7 to 10. Here, higher values of total variance are associated with longer residence times near the lagoon, and in the alongshore direction towards the south. The shallow depth at the back of the reef, near the lagoon, is likely also contributing to higher values of total variance. At Ofu, there are gradients in the total variance in the cross-shore and along-shore direction. Close to shore (points 1, 3, 5, and 7, Figure 5.3) total variance ranged from 0.2 to $0.3°C^2$, however at offshore locations (points 2, 4, 6), total variance is less than half (from near zero to $0.1°C^2$). Total variance increases in the along-shore direction towards the ava, with a sharp decrease in total variance from $0.3°C^2$ (point 8) to near zero (point 9). On the east side of the ava (points 9, 10, and 11), total variance is small, approximately $0.1°C^2$ (Figure 5.3f). Offshore in 24.4 and 21.3 m depth (points 12 and 13, respectively), total variance is near zero.

The dominant frequencies of temperature variability are spatially variable across the reef as evident from the spectral analysis of the temperature data at Dongsha Atoll. Close to the lagoon (point 1, Figure 5.3a), the weekly (27 hours to 7 days) and daily (21 to 27 hours) frequency bands represent about equal percentage of the variance in the temperature signal (38% and 41%, respectively, Figure 5.3). The percentage of variance in the weekly frequency band decreases in the offshore (eastward) direction to 23% near the reef crest, and 5% offshore. The percentage of variance in the daily frequency band (21-27 hours) increases from the lagoon (point 1, 41%) to the middle of the reef (point 6, 55%), where it decreases from point 7 to 11 (from 44 to 32%). In the middle of the reef, (at point 7, Figure 5.3a), the percentage of variance in the high frequency (1 to 3 hours) band increases from 11 to 33% of the variance, likely due to small scale fronts, surface wave events and the influence of internal waves.

At Kaneohe Bay, 24% of the variance is in the weekly frequency band at point 1 (Figure 5.3b,e), and the percentage increases in the offshore (north-eastward) direction to close to the rest crest (point 8, 61%). Offshore (point 11), there is a large percentage of variance (75%) in the weekly frequency band. The percentage of variance in the daily frequency band is highest near the lagoon (point 1, 51%) and decrease in the offshore direction to 25% (point 8). In the along-shore direction (points 7, 9, 10), the percentage of variance in the daily frequency increases towards the southeast (from 26 to 30%).

At Ofu, gradients in the along-shore and cross-shore direction are evident from the spectral analysis (Figure 5.3f). The percentage of variance in the weekly frequency band is highest towards the south-west (point 1 to 3, $\sim 25\%$), and decreases towards the north-east (point 8, 5%). The percentage of variance in the daily frequency band is low near point 1 (34%), and increases towards the north-west (point 8, 75%). On the north side of the ava the percentage of variance in the weekly frequency band increases to between 8 and 10%, and the energy in the daily frequency band is between 42 and 61%.

5.3.2.2 Gradient Empirical Orthogonal Functions

The first mode of the gradient EOF can show where strong spatial gradients exist in the temperature data. The first gradient mode represents 71% of the total spatial temperature variance in the cross reef section at Dongsha Atoll (Figure 5.4a). The spatial pattern function shows a large gradient between offshore on the forereef slope, and the reef flat near the reef crest, changing sign at the reef crest. The temporal amplitude indicates that the reef flat is always warmer than the forereef, and has large fluctuations daily (Figure 5.4d).
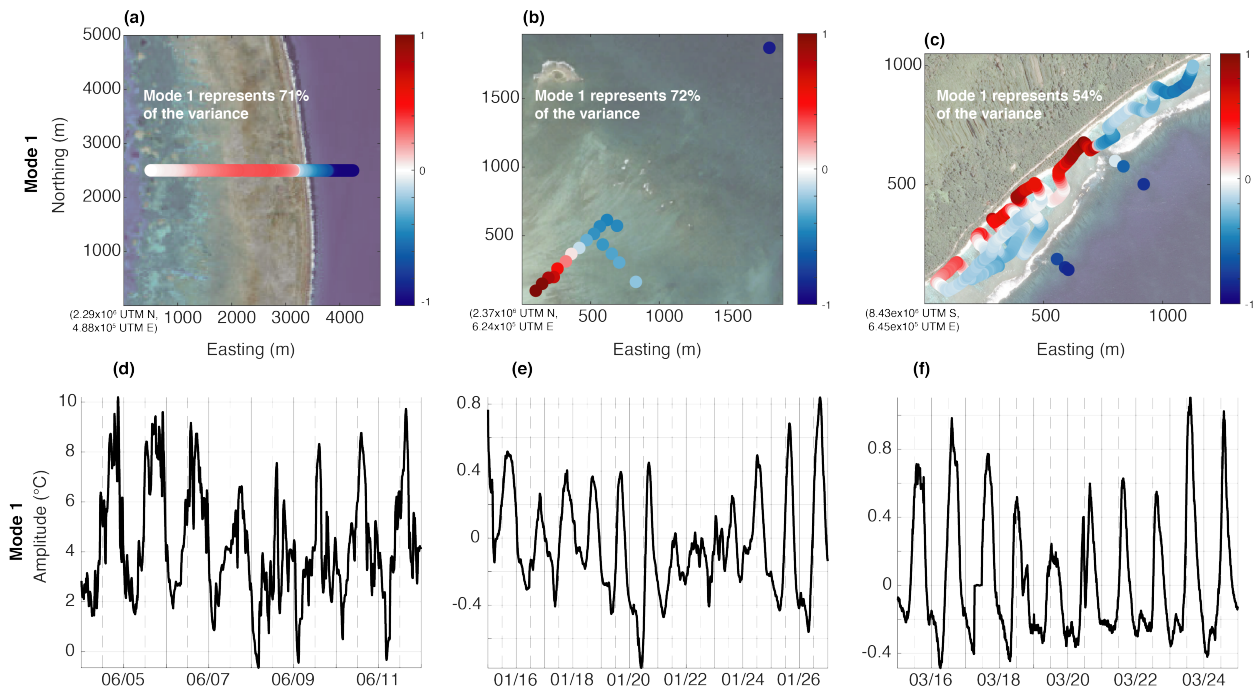
Figure 5.4: Gradient Empirical Orthogonal Functions.
Spatial pattern function (eigenvector) of Mode 1 of the gradient EOF for **(a)** Dongsha **(b)** Kaneohe Bay and **(c)** Ofu. Temporal amplitude of Mode 1 of the gradient EOF for **(d)** Dongsha **(e)** Kaneohe Bay and **(f)** Ofu. Solid lines in the vertical indicate 12:00am, and dashed lines indicate 12:00pm (local).

The magnitude of the amplitude indicates the size of the gradient. In the afternoon, the amplitude is largest, indicating a stronger gradient between the reef flat (which heats in the afternoon) and the forereef (Figure 5.4d).

At Kaneohe Bay, the first mode of the gradient EOF represents 72% of the total spatial temperature variance, a gradient between offshore and the lagoon (Figure 5.4b). The temporal amplitude fluctuates between positive and negative values, over a daily cycle (Figure 5.4e). The gradient between the shallow reef flat near the lagoon and offshore is the greatest in the early morning and afternoon. In the morning, the shallow reef flat near the lagoon is cooler than the mean, and offshore is warmer than the mean. In the afternoon, the shallow reef flat is warmer than the mean, and offshore is cooler.

At Ofu, the first gradient mode represents 54% of the total spatial temperature variance (Figure 5.4c). There is a large gradient evident as the eigenvector sharply changes sign at the ava. Also, there is a gradient between near the shore region to offshore. Near the reef crest and to the north-east of ava, the eigenvector is the same sign, which indicates that these regions experience similar thermal environments. The temporal amplitude fluctuates daily, and is the largest in the early morning and the afternoon (Figure 5.4f). Paired with the eigenvector, this indicates that in the morning the shallow regions close to shore are cooler than the offshore region, and the region to the north-east of the ava. In the afternoon, the opposite trend is seen, the shallow regions close to the shore are warmer than the other regions.
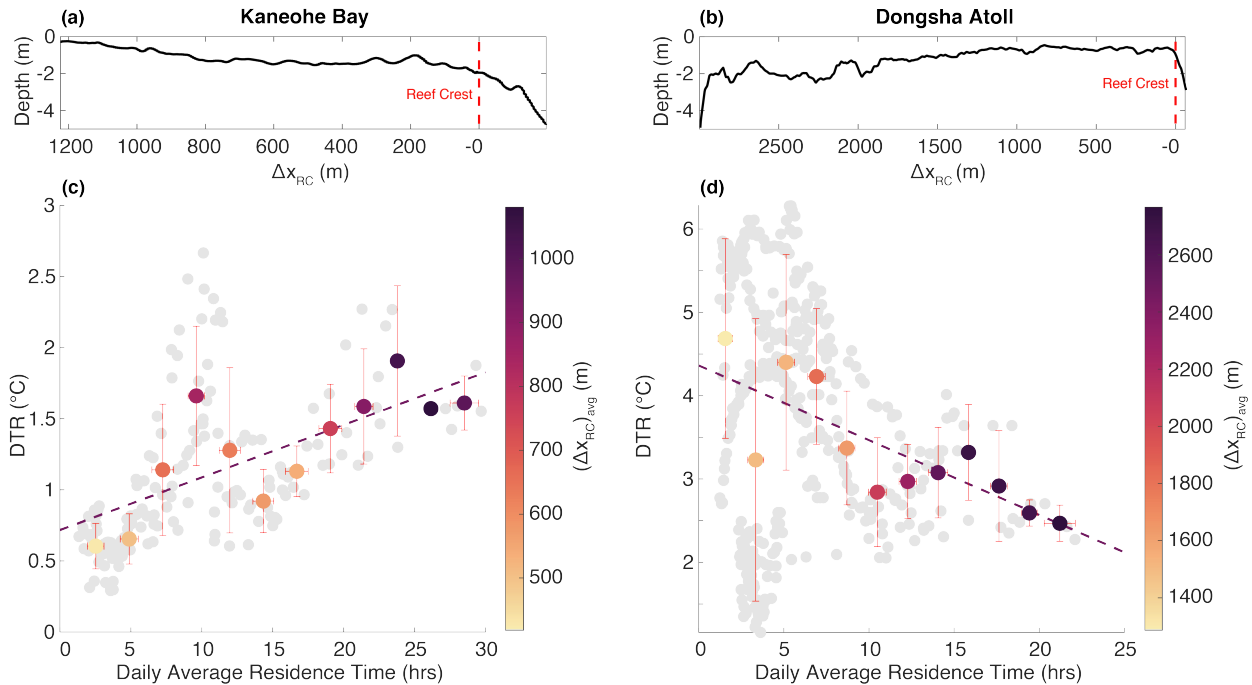
Figure 5.5: Residence Time and Daily Temperature Range.
Bathymetry cross-section which shows distance from the reef crest at **(a)** Kaneohe Bay and **(b)** Dongsha Atoll. Residence time results from the particle tracking and the corresponding average daily temperature for each location particles were tracked from. Grey circles show all results of particle tracking, and colored circles show bin averaged residence times and DTR and corresponding average distance from the reef crest. Error bars indicate one standard deviation of the bin averages. The linear fit between bin averaged DTR and residence times is shown with the dashed line.

5.3.3 Residence Time

Residence time was estimated by tracking particles backwards in time from locations on the reef at Kaneohe Bay and Dongsha Atoll (see Section 5.2.7) to determine how long it takes for a water particle to reach that region of the reef flat. The relationship between residence time of water and DTR was different for Kaneohe Bay and Dongsha Atoll.

At Kaneohe Bay, the water depth, for the locations where particles were tracked, is shallower close to the lagoon ($\sim$ 0.5m), and deeper closer to the reef crest ($\sim$ 2m, Figure 5.5a). Daily average residence times ranged from 1.3 to 29.7 hours. The daily average residence time of particles tracked at each location was shortest near the reef crest, and longest further back

118

on the reef towards the lagoon (Figure 5.5c). The associated DTR for each location on the reef flat showed low DTR (~ 0.6°C) associated with short residence times, and larger DTR (~ 1.6°C) associated with longer residence times. Near the deeper reef crest, residence times are shorter and DTR was smallest. Further back on the reef, in shallow water, residence times were longer and DTR was highest.

At Dongsha, the relationship between residence time and DTR was more complicated. At Dongsha, the water depth is shallower close to the reef crest (~ 0.5m) and deeper near the lagoon (~ 2m, Figure 5.5b). Daily average residence times ranged from 0.6 to 22.1 hours. The daily average residence time of particles was shorter near the reef crest, and longer further from the reef crest towards the lagoon (Figure 5.5d). The DTR close to the reef crest had a large range of values; however the bin averaged DTR was large (~ 4.5°C). Further back on the reef flat, towards the lagoon, the bin averaged DTR was smaller (2.5°C), with a smaller range of average DTR included in the bin averages. The DTR near the reef crest, where residence times were shorter and the depth was shallow, was largest, likely due to the internal wave cooled water coming onshore (Reid et al., 2019). The DTR decreases towards the back of the reef where residence times are longer, and water is deeper. The opposite relationship between DTR and residence time at Kaneohe Bay and Dongsha Atoll is further discussed in Section 5.4.3.

5.3.4   Physical Mechanisms Driving Temperature Variability

In order to understand the physical mechanisms which influence residence time of water and drive temperature variability on coral reefs, the daily temperature range at Dongsha Atoll, Kaneohe Bay and Ofu-Olosega was compared to metrics which quantify contributions
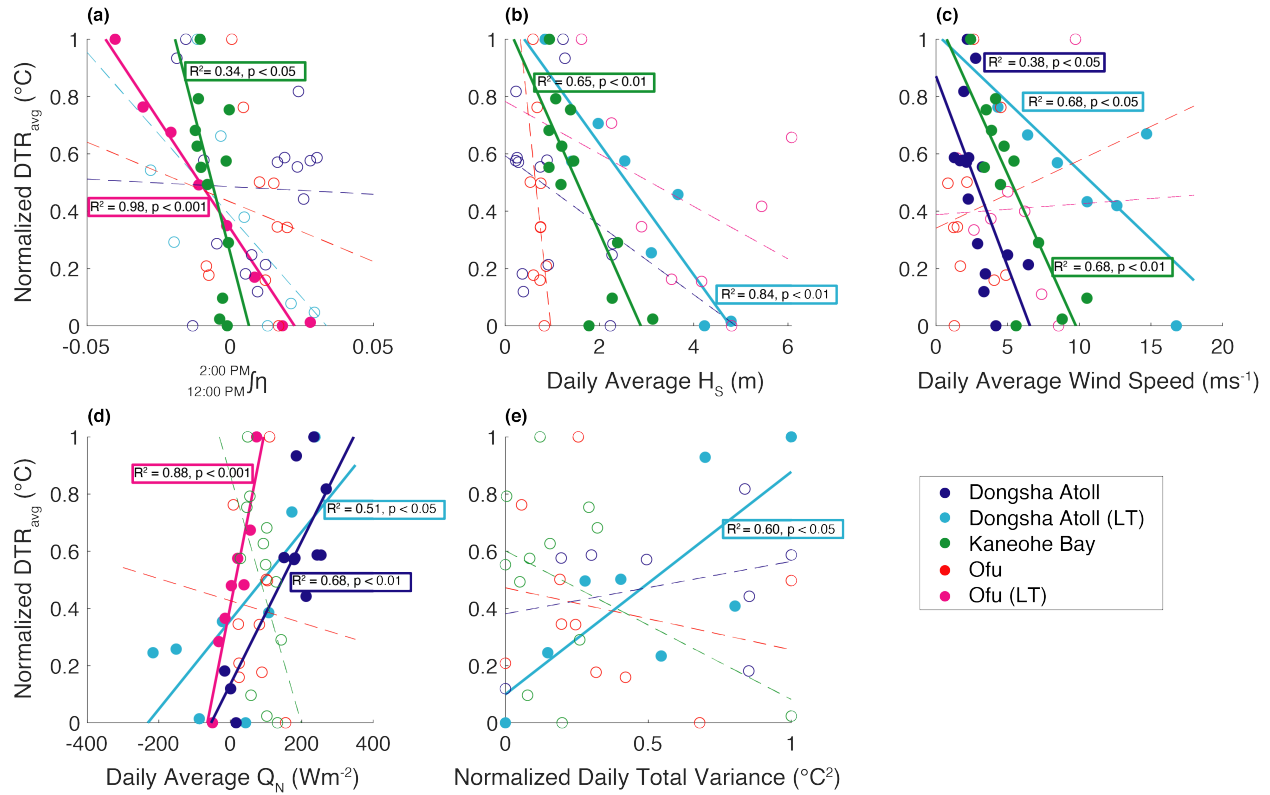
Figure 5.6: Physical Mechanisms driving Temperature Variability.
(a) Integrated sea level variation (η) from 12:00 to 2:00pm (local) and normalized daily temperature range (DTR). **(b)** Daily average offshore significant wave height (H_S) and normalized DTR. **(c)** Daily average wind speed and normalized DTR. **(d)** Daily average net atmospheric flux (Q_N) and normalized DTR. **(e)** Normalized daily total offshore variance and normalized DTR. Longer-term data from Dongsha Atoll and Ofu is denoted with LT. Statistically significant linear fits are shown with filled circles and solid lines, and statistically non-significant linear fits are shown with empty circles and dashed lines.

of various physical forcing to water level and circulation on the reefs. In order to further assess the physical mechanisms driving variability on these coral reefs, the longer-term (LT) temperature data (described in Section 5.2.6) was compared to the various physical mechanisms. Longer-term data was available for Dongsha Atoll and Ofu-Olosega (Figure 5.1d,e). All long-term data was bin averaged.

The first physical mechanism that was considered was the influence of tide. We predict that if low tide occurs at midday, there would be more heating on the reef. If the water depth on the reef is smaller during the time of day when surface heat flux is the largest,

120

there would be greater heating of the water column. Sea level variation η for each site was integrated between 12:00 and 2:00pm (local) for each day of observations. To estimate the integrated sea level $\int \eta$ for the long-term data, results from the Oregon State Tidal Inversion Software (Egbert and Erofeeva, 2002) and the TMD toolbox (Padman and Erofeeva, 2004) were used. More negative values of $\int \eta$ are expected to be associated with high DTR, positive values of $\int \eta$ are expected to be associated with lower DTR. This metric was compared to the normalized daily average DTR for each site (Figure 5.6a). At Dongsha Atoll, only DTS data 500 m back (west) of the reef crest, and in depths less than 3 m were used to find DTR. A linear fit was found for the daily average DTR and $\int \eta$. Dongsha Atoll (short and longer-term data), Kaneohe Bay and Ofu (short and longer-term data) all had higher average DTR with more negative values of $\int \eta$ (negative relationship), however only the Kaneohe Bay and longer-term Ofu relationships were significant (Kaneohe: $R^2 = 0.34, p <0.05$ and Ofu: $R^2 = 0.98, p <0.001$, respectively). See Table 5.4 for all correlations.

The next physical mechanism that was considered was wave forcing. We predict that with smaller waves, there would be less flow on the reef, and consequently higher DTR, and with higher waves we would expect lower DTR. Daily average wave height (H_S) was compared to normalized daily average DTR for each site (Figure 5.6b). Daily average wave height for the longer-term data was estimated from the ERA5 dataset. A linear fit was found for the daily average DTR and wave height, and all three sites (short and longer-term data) had higher DTR with lower values of daily average wave height (negative relationship). The data from Ofu had a negative relationship with wave height, however the relationships were not significant. Temperature data from Dongsha Atoll (longer-term) Kaneohe Bay had significant correlation with waves (Dongsha: $R^2 = 0.84$, $p <0.01$ and Kaneohe: $R^2 = 0.65$, p <0.01, respectively).

Wind forcing at each reef was also considered. We predict that with low wind conditions,

Table 5.4: Relationship between DTR and Physical Mechanisms.

Significant correlations are **bolded**. Longer-term data from Dongsha Atoll and Ofu is denoted with LT.

Mechanism	Site	Slope	R^2	p-value
Dongsha Atoll	Tide	Negative	0.00	p >0.05
	Waves	Negative	0.09	p >0.05
	Wind	**Negative**	**0.38**	**p <0.05**
	Atmospheric Flux	**Positive**	**0.68**	**p <0.01**
	Offshore Boundary	Positive	0.09	p >0.05
Dongsha Atoll (LT)	Tide	Negative	0.43	p >0.05
	Waves	**Negative**	**0.84**	**p <0.01**
	Wind	**Negative**	**0.68**	**p <0.05**
	Atmospheric Flux	**Positive**	**0.51**	**p <0.05**
	Offshore Boundary	**Positive**	**0.60**	**p <0.05**
Kaneohe Bay	Tide	**Negative**	**0.34**	**p <0.05**
	Waves	**Negative**	**0.65**	**p <0.01**
	Wind	**Negative**	**0.68**	**p <0.01**
	Atmospheric Flux	Negative	0.27	p >0.05
	Offshore Boundary	Negative	0.19	p >0.05
Ofu	Tide	Negative	0.02	p >0.05
	Waves	Negative	0.31	p >0.05
	Wind	Positive	0.01	p >0.05
	Atmospheric Flux	Negative	0.00	p >0.05
	Offshore Boundary	Negative	0.05	p >0.05
Ofu (LT)	Tide	**Negative**	**0.98**	**p <0.001**
	Waves	Negative	0.18	p >0.05
	Wind	Positive	0.00	p >0.05
	Atmospheric Flux	**Positive**	**0.88**	**p <0.001**
	Offshore Boundary	n/a	n/a	n/a

there would be less flow on the reef, and higher DTR. Daily average wind speed was compared to the normalized daily average DTR for each site (Figure 5.6c). Daily average wind speed for the longer-term data was estimated from the ERA5 dataset. A linear fit was found for daily average DTR and wind speed, and Dongsha Atoll (short and longer-term data) and Kaneohe Bay had higher DTR with lower values of daily average wind speed (negative relationship), and both had a significant correlation (Dongsha: $R^2 = 0.38$ (short-term), 0.68 (longer-term), p <0.05 and Kaneohe: $R^2 = 0.68, p$ <0.01, respectively).

The influence of net atmospheric flux on DTR was considered. We predict that with net atmospheric flux, there would be low DTR, and with atmospheric flux, there would be higher DTR. Daily average net atmospheric heat flux (Q_N) was compared to the normalized daily average DTR for each site (Figure 5.6d). Daily net atmospheric heat flux for the longer-term data was estimated from the ERA5 dataset. A linear fit was found for the daily average DTR and Q_N, and Dongsha Atoll and Ofu both had higher values of DTR associated with higher values of Q_N (positive relationship), and both were significant (Dongsha: $R^2 = 0.68$, p <0.01 (short-term), 0.51 p<0.05 (longer-term), and Ofu: 0.88 p<0.001).

Finally, the influence of the offshore boundary condition was considered. We predict that with larger values of temperature variance offshore of the reef crest, DTR on the reef flat would be greater. Normalized daily total variance of the offshore near bottom temperature at each site was compared to the normalized daily average DTR (Figure 5.6e). DTS temperature at 20 m depth was used for the short term Dongsha Atoll DTS data, and the longer-term data at HC (in 20 m depth) was compared to the longer-term data (HA and HB). The offshore data at Kaneohe Bay (OS) was in 13.1 m depth. At Ofu, offshore data at FR25 (in 24.4 m depth) was compared to the short term DTS data, and longer-term data offshore at Ofu was not available. A linear fit was found for the daily average DTR and daily total variance offshore, and Dongsha Atoll had higher values of DTR with higher values of total

variance in the boundary condition. Only the longer-term data had a significant relationship with DTR ($R^2 = 0.60$, p <0.05). At Dongsha Atoll, the mechanism which is likely setting the boundary condition offshore is the strong internal tide and internal wave influence. This is not expected to be an important mechanism at Kaneohe Bay or Ofu-Olosega.

5.4   Discussion

5.4.1   Neglecting advection in the prediction of DTR

Daily temperature range has been shown to be an important metric for characterizing high-frequency temperature variability on coral reefs and predicting bleaching prevalence (Safaie et al., 2018). The ability to predict diurnal time scale temperature variability on coral reefs could be important for understanding how a reef may respond to future anomalies.

Cyronak et al. (2020) found that DTR could be predicted from bathymetry data using a power function relationship ($DTR = 3.478 * h^{-1.000}$, where h is the water depth relative to mean sea level). The relationship had a high correlation ($R^2 = 0.926$) with observations from five different reefs. The reefs studied included Hog Reef, Bermuda and Kaneohe Bay, Hawaii (both barrier reefs), Heron Island, Australia and Bocas del Toro, Panama (both fringing reefs), and Palmyra, a coral atoll. This depth-DTR relationship predicts that shallow water environments experience high DTRs, and deeper water environments have low DTRs. For a stagnant volume of water of unit horizontal area and variable depth, this is what we might expect for heating due to surface heat flux. Although this may be a good first-order estimate of DTR, the relationship may not hold if there are other physical mechanisms which could contribute to the advection of heat across the reef.

Although the depth-DTR relationship does have a connection to surface heat flux, it does not take into account seasonal variations. A consideration for prediction of DTR is the amount of solar radiation the coral reef is receiving during the study period. For example, the temperature data from Kaneohe Bay was collected in the winter season (January 2017), and the average DTR is lower than the predicted values using the Cyronak et al. (2020) relationship (average RMSE = 2.6°C). The depth-DTR relationship could lead to overestimates of DTR when atmospheric forcing is low. In order to test this, the heat budget (described in Section 5.2.9) was used to estimate water temperature on the reef flat during the deployment at Kaneohe Bay. For this estimate, the advective term (ΔF, Equation 5.14) was not included in the heat budget estimates, to see the influence of the atmospheric term on the change in temperature. The actual atmospheric heat flux during the deployment was estimated, using data from the meteorological station. Offshore SST from the ERA5 dataset was used to initialize the temperature in the heat budget each day. The heat budget, neglecting the advective term, was used to predict DTR in a stagnant volume of water with 1 m depth. The average predicted DTR was 1.8°C, which is much lower than the (Cyronak et al., 2020) prediction of DTR (3.5°C). This highlights the importance of using actual meteorological data in the prediction of DTR.

Another situation when the depth-DTR relationship may not accurately predict DTRs is in very shallow depths. Without including advection in the estimate of DTR, the depth-DTR relationship may lead to overestimates of DTR in shallow water. For example in the back reef pools at Ofu, the Cyronak et al. (2020) estimate of DTR is much larger than observed values of DTR (average RMSE = 6.7°C). The predicted values of DTR at <1.0 m depth are >3.5°C; however, at Ofu, where the depth ranged from $\sim$ 0.1 to 2.1 m in the back reef pools, average DTR ranged from 0.8°C to 2.5°C (in the locations where depth was available from snorkel surveys). The difference between the predicted and observed DTR could be due to the advection of heat. If water was stagnant, the observed values of DTR

125

may be closer to the predicted values from the (Cyronak et al., 2020) relationship. Similar to above, the heat budget was used to predict DTR on the reef, without the advective heat flux term, using the data from the meteorological station to predict atmospheric heat flux at Ofu during the study period. Temperature was predicted for a a stagnant volume of water, with 1 m depth, and the average predicted DTR was 3.2°C. Similar to the (Cyronak et al., 2020) prediction of DTR (3.5°C), but much higher than the observed DTR at Ofu during the study period. This highlights the importance of including advective flow in the estimates of DTR. If advection was included in the heat budget estimate, the DTR would likely be lower, and similar to the DTR observed at Ofu.

The depth-DTR relationship also does not take into account the effect of tides, wind and waves. As discussed in Section 5.3.4, when low tide occurs near noon, we would expect higher atmospheric heating of the water column, leading to higher values of DTR. The static estimate of DTR from the depth-DTR relationship does not take into account the varying tidal influence of heating on the reef. Similar to above, the heat budget was used to predict DTR for a stagnant volume of water, without the advective heat flux term, and with and without tidally varying water depth. The atmospheric forcing, and observed values of sea level change from the deployment at each reef was used to predict DTR with a constant water depth, and with a tidally varying water depth. At all three sites, the influence of tidally varying water depth increases the average DTR. On average, the DTR is 0.1°C smaller at Dongsha Atoll and Kaneohe Bay, and 0.2°C smaller at Ofu without the influence of tides. This is further evidence that including actual advective and atmospheric heat flux terms in the estimate of DTR would improve estimates.

Finally, at Dongsha Atoll, large internal waves arriving on the forereef slope (Reid et al., 2019; Davis et al., 2020; Reid et al., 2020) lead to high DTR (10.0°C at 30.0 m depth, Figure 5.2d). The depth-DTR estimate at 30 m depth is 0.1°C, and Cyronak et al. (2020) acknowl-

126
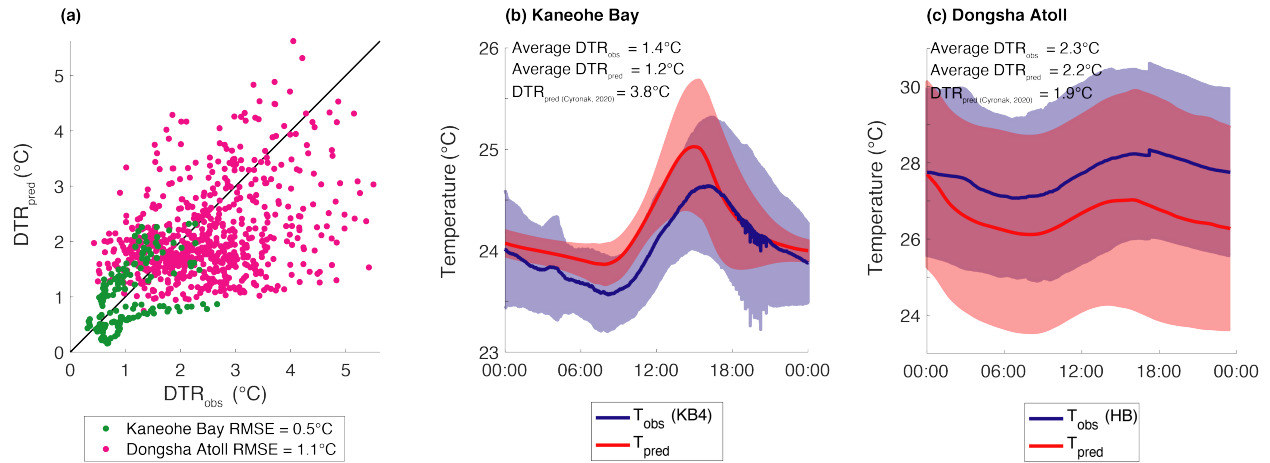
Figure 5.7: Heat Budget prediction of temperature.
(a) Observed DTR and predicted DTR from the heat budget analysis at Kaneohe Bay and Dongsha Atoll. **(b)** Composite day average of observed (blue) and predicted (red) temperature at KB4 (Kaneohe Bay). **(c)** Composite day average of observed (blue) and predicted (red) temperature at HB (Dongsha Atoll). Shaded area on **(b)** and **(c)** represents one standard deviation of the data in the composite average.

edges that the relationship breaks down when internal waves are present. Internal waves are leading to much higher values of DTR than the depth-DTR relationship would predict, especially on the forereef slope. When only data on the reef flat 500 m back from (west of) the reef crest, is included, to remove the influence of internal waves, the average RMSE is 2.1°C.

5.4.2 Including advection in the prediction of DTR

A simple heat budget which includes advection of heat across the reef flat due to flow driven by tides, winds, and waves, can improve the estimate of DTR. Furthermore, we are able to estimate seasonally-variable DTR, instead of a static DTR estimate using only time-averaged water depth. Using the heat budget (described in Section 5.2.9), temperature on the reef flat was estimated for each day at Kaneohe Bay during the deployment in January 2017.

Table 5.5: Daily Temperature Range at Kaneohe Bay and Dongsha Atoll.

Site, depth, average DTR observed, predicted from the heat budget and predicted from Cyronak et al. (2020). Overbars indicate averages for that location.

Site	Location	Depth (m)	$\overline{DTR_{obs}}(°C)$	$\overline{DTR_{pred}}(°C)$	$DTR_{Cyronak\ et\ al.\ (2020)}(°C)$
	KB1	1.5	0.7	0.7	2.3
	KB1.1	1.3	0.7	0.7	2.7
	KB1.2	1.4	0.7	0.8	2.5
	KB2	1.5	0.7	0.9	2.4
	KB2.1	1.4	0.8	0.9	2.6
	KB2.2	1.3	1.0	1.0	2.8
Kaneohe	KB3	1.3	1.1	1.0	2.6
Bay	KB3.1	1.2	1.2	1.1	2.8
	KB3.2	1.2	1.3	1.2	3.0
	KB4	0.9	1.4	1.2	3.8
	KB4.1	0.9	1.4	1.3	3.7
	KB4.2	0.6	1.5	1.3	5.9
	KB5	0.5	1.6	1.3	7.7
Dongsha	HA	1.4	2.8	2.1	2.5
Atoll	HB	1.8	2.3	2.2	1.9

The inputs to the model are described in Section 5.2.8 and 5.2.9. Water temperature was predicted (T_{pred}) in the cross section (grey dashed line, Figure 5.1f), using Equation 5.14. Results of the DTR predicted from the heat budget (DTR_{pred}) compared to the observed DTR at each location on the reef flat (DTR_{obs}) produced a RMSE of 0.5°C (Figure 5.7a). This RMSE is improved from the static predicted DTR from the depth-DTR relationship (RMSE = 2.6°C, Cyronak et al., 2020). Results at each location are available in Table 5.5. For example, at KB4 (Figure 5.1f), the average DTR_{obs} was 1.4°C, the average DTR_{pred} was 1.2°C (Figure 5.7b). Using the relationship from Cyronak et al. (2020), the average DTR_{pred} would be 3.8°C.

At Dongsha Atoll, the heat budget was estimated for the reef flat for each day of the longer-term data (from June 2013 to June 2014). Temperature was predicted from the heat budget (T_{pred}) across the reef flat from reef crest to the lagoon, and compared to the the temperature at the long-term loggers (HA and HB, Figure 5.1e). Results of the DTR predicted

from the heat budget (DTR_{pred}) compared to the observed DTR at the long-term loggers (DTR_{obs}) produced a RMSE of 1.1°C (Figure 5.7a), which is improved from the RMSE using the depth-DTR estimate (RMSE = 2.0°C at HA and HB, Cyronak et al., 2020). All results are available in Table 5.5. At HB (Figure 5.1e), the average DTR_{obs} was 2.3°C, the average DTR_{pred} was 2.2°C (Figure 5.7b). Using the relationship from Cyronak et al. (2020), the DTR_{pred} would be 1.9°C. At Dongsha, the average DTR_{pred} from the heat budget is not as close to the observed values, likely due to the influence of internal waves and overestimates of flow on the reef flat, discussed below. We are able to predict a time and spatially-variable DTR using the heat budget, instead of a static value, and the overall RMSE in the DTR estimates is improved.

Including atmospheric and advective fluxes in the estimate of DTR does improve predictions, however, the heat budget estimate does have some complications. First, the advective heat flux could be over or underestimated, due to overestimates of significant wave height and not including pressure gradients due to surface gravity waves. As discussed in Section 5.2.9, if overestimates of the advective flux leads to a change in temperature greater than two times the maximum DTR at each reef, those results are not included in the estimates of DTR. For Dongsha, where there was 342 days of longer term data at HA and HB, we were able to estimate DTR on the reef for 336 days using our heat budget. Estimates of DTR could be greatly improved if *in-situ* observations of flow at at least one location on the reef flat are available.

The simple heat budget used here is one-dimensional, and flow on all reefs is not. At Dongsha Atoll, flow is primarily in the cross-shore direction, which simplifies heat budget estimates. However, at Kaneohe Bay, there is significant flow in the cross-shore and along-shore direction. The advective flux term in the simple heat budget used here would be improved if the along-shore component was also included, and might account for the difference between the

observed and predicted DTR from the heat budget at Kaneohe Bay.

The values of significant wave height (H_S) from the ERA5 dataset, included in the model estimate of flow, could lead to errors in the estimates of flow on the reef flat, as discussed in Section 5.2.8. Significant wave height values were decreased at each site by a factor of $c = 0.82$ at Dongsha Atoll and $c = 0.65$ at Kaneohe Bay. Although the decreased significant wave height is used in the model, there could still be times when flow on the reef is likely overestimated, leading to unrealistic advective heat fluxes. The wave direction from the ERA5 dataset could also be a factor leading to poor estimates of flow on the reef, if the location where the ERA5 data is gathered has a different wave field. The heat budget model could be greatly improved if observations of wave statistics near the reef crest were available.

The magnitude of the pressure gradient term is dependent on the reef morphology. The pressure gradient term is larger at Dongsha Atoll than it is at Kaneohe Bay. For the period where observations are available, values of $\Delta\eta$ range from -0.20 to 0.22 m at Dongsha Atoll. At Kaneohe Bay, values of $\Delta\eta$ range from -0.08 to -0.02 m. At Kaneohe Bay, there are channels north and south of the barrier reef (length $\sim 5km$ which allow for exchange, and decrease the pressure gradient between the lagoon and offshore. At Dongsha Atoll, the large lagoon (approximately 17 km in diameter) and the two channels on the opposite side of the atoll, leads to a greater pressure gradient between the offshore and lagoon on the east reef flat. Furthermore, flow on the reef flat could be under or overestimated because we are unable to estimate $\Delta\eta_r$. In Reid et al. (2020), $\Delta\eta$ was estimated over small distances on the reef flat, and the residual sea level pressure gradient was significant and attributed to the pressure driven flow from sea level setup by surface gravity waves breaking on the reef crest. Here, we are using pressure estimates from offshore to the lagoon, and this residual pressure gradient would likely be small and caused by wind events causing setup between the lagoon and offshore. For the period where observations are available, $\Delta\eta_{tide}$ captures

most of the variability in $\Delta\eta$ ($R^2 = 0.71, p < 0.001$) at Dongsha Atoll. In this case, only including the tidal term is a good estimate of the flow due to pressure gradients at Dongsha Atoll. At Kaneohe Bay, the tidal pressure gradient ($\Delta\eta_{tide}$) captures less of the variability in $\Delta\eta$ ($R^2 = 0.28, p < 0.001$), however, since the magnitude of $\Delta\eta$ is much smaller here, not including this term would not significantly impact estimates of flow on the reef.

Another physical mechanism that is not included in the heat budget estimates of temperature on the reef flat is internal waves. At Dongsha Atoll, this mechanism is contributing to the high DTR near the reef crest, as internal wave cooled water is transported onshore by tide, wave and wind driven flow (Reid et al., 2019, 2020). In Reid et al. (2019), the influence of internal waves is evident in SST data. Internal wave cooled water mixes to the surface as internal waves shoal on the reef slope at Dongsha Atoll. The offshore boundary condition that is being used in the heat budget estimates would not include the influence of internal waves because of the temporal (1 hour), and the spatial (0.25°) resolution of the ERA5 data. The SST data from the ERA5 dataset being used for the boundary condition is the closest location to the reef crest, however it is approximately 8 km from the reef crest, and likely does not include the influence of internal waves (see Figure 5a from Reid et al., 2019, for the region of influence of internal waves on SST). Consequently, the heat budget would not capture the influence of internal waves on the reef flat. This could explain why DTR was under predicted at HA (see Table 5.5), which is closer to the reef crest, where we would expect higher values of DTR due to the influence of internal waves. *In-situ* observations of temperature at the reef crest to use as a boundary condition, instead of offshore SST, would likely improve the heat budget model estimates of temperature on the reef flat at Dongsha.

Table 5.6: Summary of Results

	Dongsha Atoll	Kaneohe Bay	Ofu-Olosega
Reef Morphology	Atoll reef	Barrier reef	Fringing reef
Study month	June	January	March
Latitude	20.66°N	21.46°N	14.17°S
Mean Temperature (°C)	22.9 to 30.3	24.0 to 24.1	30.0 to 30.3
DTR (°C)	3.0 to 10.0	0.5 to 1.6	0.2 to 2.5
Total variance (°C2)	0.7 to 4.9	0 to 0.3	0 to 0.3
Residence times (hrs) Only data 500m back from the reef crest, and depths <3 m included	0.7 to 22.1 (DTS data: 8 days and C1, C2, C3, V1 V2 data: 16 days)	1.3 to 29.7	*n/a
DTR Prediction RMSE (°C) Depth-DTR (Cyronak et al., 2020) Heat Budget	2.0 1.1 (Longer term data: 342 days)	2.6 0.5 (January 2017: 13 days)	*n/a *n/a

*n/a: not available because bathymetry data unavailable

5.4.3 Comparing results across reef morphologies

The three sites included in this study have very different morphologies and patterns of flow and environmental variability (see Table 5.6 for a summary of results). The three major types of coral reefs are represented by these sites: Dongsha Atoll, a coral atoll, Kaneohe Bay, a barrier reef system, and Ofu-Olosega, a fringing reef system. There are significant differences in the patterns in mean temperature and DTR across the three sites. First, the east reef flat and reef slope at Dongsha Atoll, experiences strong gradients in mean water temperature and diurnal temperature range. The range of mean temperatures is the largest at Dongsha Atoll, and are warmest near the lagoon, and colder offshore on the reef slope (Figure 5.2a). The range of mean DTR values from the lagoon to the reef slope (3.1°C to 10.0°C) was also the largest at Dongsha, compared to the other sites (Figure 5.2d). Both of these results are likely driven by the large internal waves arriving at Dongsha Atoll, which are setting the offshore boundary condition and driving significant temperature changes across the reef flat (Reid et al., 2019), and are not evident at the other sites.

The barrier reef at Kaneohe Bay experiences very different patterns of water temperature. The mean water temperature is opposite the pattern at Dongsha Atoll, with colder water near the lagoon, and warmer temperatures towards the reef crest and offshore (Figure 5.2b). The gradient in DTR is also opposite Dongsha Atoll, with largest DTRs near the lagoon, decreasing offshore (Figure 5.2e). This reverse trend could be driven by the opposite slopes in water depth at the two reefs (Figure 5.5a,b), and the influence of internal waves at Dongsha Atoll. Both reefs have higher DTR in the shallowest regions of the reef flat, however the range of mean DTR values at Kaneohe Bay ($0.5°C$ to $1.6°C$) is much smaller than those observed at Dongsha Atoll. This is likely because the deployment occurred in the winter season, and surface heat fluxes at Kaneohe Bay were much smaller than those observed at Dongsha Atoll, and because there was no internal wave influence at Kaneohe Bay.

The patterns of variability in temperature at Ofu-Olosega are very different from those seen at Dongsha Atoll and Kaneohe Bay. Flow in the back reef pools at Ofu is primarily in the along-shore direction, as are the strong gradients in mean temperature and DTR, although there are also gradients in the cross-shore direction. (Figure 5.2c,f). Lowest mean temperatures ($30.1°C$) in the back reef pools occur towards the south-west, where residence time is likely shorter (see drifter experiments in Rogers et al., 2018). Mean temperature increases towards the north-east ($30.3°C$) where residence times would be longer. Patterns in mean DTR are more complicated at Ofu, with the highest mean DTR ($2.5°C$) observed in the shallow regions of the lagoon close to shore. There is a sharp gradient in the DTR on either side of the ava outflow, with highest values to the south ($2.5°C$), and a sharp decrease to the north.

At Dongsha Atoll, total variance in temperature is lowest near the lagoon, and increases in the offshore (eastward direction), as does the percentage of variance in the high frequency

133

(1 to 3 hours) band (Figure 5.3d). This is likely due to the influence of internal waves on the reef; Reid et al. (2019) found that the influence of internal waves was greatest near the reef crest, and decreased towards the lagoon. At Kaneohe Bay, the total variance is highest near the lagoon, and decreases in the offshore (north-eastward) direction, which is opposite the trend seen at Dongsha Atoll, likely due to the reversed bathymetry cross section and lack of internal wave influence. Here, increased residence times and shallow depths near the lagoon likely contribute to the high variance there, unlike Dongsha Atoll, where the pattern in total variance is driven by the internal wave influence. The total variance in temperature at Ofu increases in the along-shore direction, as residence time increases (see Figure 1b in Rogers et al., 2018, for drifter experiments in the back reef pools). This is similar to the cross-shore trend seen at Kaneohe Bay, where total variance is largest where residence times are longest. Also, increased total variance is observed in the near shore shallow region at Ofu, similar to Kaneohe Bay.

From the gradient EOF at Dongsha Atoll (Figure 5.4a,d), we see a significant gradient between the reef flat and the reef slope, which is largest in the afternoon, when the shallow reef flat is significantly warmer than the cold reef slope. The gradient EOF at Kaneohe Bay reveals a gradient from the lagoon to offshore, which changes sign over a diurnal cycle, with the shallow reef flat towards the lagoon colder than offshore in the early morning, and warmer than offshore in the afternoon (Figure 5.4b,e). This differs from the gradients seen at Dongsha Atoll, where the shallow reef flat is always warmer than offshore, and the magnitude of the cross-reef gradient is much greater. The gradient EOF for Ofu reveals similar patterns of variability in the cross-shore direction to Kaneohe Bay, with the shallow near-shore region being warmer than offshore in the offshore reef crest in the afternoon, and cooler in the morning (Figure 5.4c,f). There is also a significant gradient in the along-shore direction, which is the largest in the early morning and afternoon. The region south of the ava is warmer than the region north of the ava in the afternoon, and colder in the morning.

134

The correlation between atmospheric heat flux and the temporal amplitude of the mode 1 gradient EOF was found for each deployment site. A lag between the atmospheric heat flux, and the subsequent heating response of the water is expected, so the the correlation is found for $\pm$ 6 hours at each site to determine when the maximum correlation occurs. At Dongsha Atoll, the maximum correlation ($R^2 = 0.48, p <$0.001) between the atmospheric heat flux and the temporal amplitude of the gradient EOF had a lag of 3.3 hours (with the atmospheric heat flux leading the temporal amplitude). The maximum correlation between atmospheric heat flux and the temporal amplitude of the gradient EOF at Kaneohe Bay was weak ($R^2 = 0.16, p <$0.001) and had a lag of 0.5 hours. The correlation between the atmospheric heat flux and the temporal amplitude of the gradient EOF was moderate ($R^2 = 0.52, p <$0.001), and had a lag of 1.6 hours (with atmospheric heat flux leading the temporal amplitude).

The patterns of residence time are different at Dongsha Atoll and Kaneohe Bay. At Kaneohe Bay, the positive relationship between DTR and residence time (Figure 5.5) is driven by the the bathymetry on the reef flat. Deeper regions near the reef crest have shorter residence times and lower values of DTR due to decreased atmospheric heating and cooling . Residence time increases towards the back of the reef, where DTR is greater in the shallower region. A different relationship is seen at Dongsha, due to the opposite bathymetry, and the influence of internal waves. Shallow regions close to the reef crest have short residence times, and a large range of DTR due to increased atmospheric heating and cooling, and influence of internal wave cooled water. Further back on the reef, towards the lagoon, residence times are longer and DTR is smaller, due to decreased atmospheric heating and cooling in deeper waters. The influence of internal waves also decreases towards the lagoon, as seen in Reid et al. (2019), which leads to lower values of DTR. Furthermore, these two sites experience similar ranges of daily average residence time (from approximately 1 hr to 1 day). This is a unexpected result, because the reef at Dongsha Atoll is much wider ($\sim$ 3 km) compared

to Kaneohe Bay ($\sim$ 1.5 km). At Dongsha Atoll, the wide reef flat leads to longer residence times for water that travels from the reef crest to the lagoon. At Kaneohe Bay there is more along-shore flow, and water particles spend more than one tidal cycle on the reef flat when travelling from the reef crest to the lagoon.

Tide, wind and surface waves are all significant processes driving flow on the east reef flat at Dongsha Atoll (Reid et al., 2020). The significant physical processes driving DTR at Dongsha were surface waves (from the longer-term data), wind and atmospheric flux and the offshore boundary condition (from the longer-term data) (Figure 5.6b,c,d,e). Tides were not significantly correlated with DTR at Dongsha. Surface waves are the dominant process driving flow at Kaneohe Bay (Lowe et al., 2009a), however, tides, surface waves and wind were all significantly correlated with DTR (Figure 5.6a,b,c). Atmospheric flux was not significantly correlated with DTR, although if longer-term data from Kaneohe Bay (especially data from the summer season) was available we might observe a correlation between atmospheric flux and DTR. Tidal modulation of breaking waves on the reef crest were found to be the primary process driving flow in the back-reef pools at Ofu (Koweek et al., 2015). From the analysis of the physical mechanisms at Ofu, tides and waves have a relationship with DTR, but only the relationship with tides was significant (Figure 5.6a). Unlike the other two sites, there was not significant correlation between wind and DTR at Ofu. Atmospheric forcing had a significant relationship with DTR in the longer-term Ofu data. Here we explore dynamical hypothesis related to various physical mechanisms which are contributing to changes in DTR on these coral reefs. Future research could include site specific multiple regression models using these forcing mechanisms to better understand what is driving diurnal variability at each site.

We see distinctive spatial gradients in temperature and residence time at these three coral reefs. These patterns are largely driven by the physical mechanisms which govern flow at these sites. We expect this to be true for other reefs with similar morphologies and atmo-

spheric forcing conditions.

5.5 Conclusion

The high spatial and temporal resolution of temperature gathered at Dongsha Atoll, Ka-
neohe Bay and Ofu-Olosega reveals spatial gradients in water temperature at reef scales.
Each site has distinct thermal environments which are governed by atmospheric forcing and
the physical mechanisms driving circulation, and consequently residence time on the reefs.
Previously, daily temperature range has been predicted by time-averaged water depth on a
coral reef (Cyronak et al., 2020), which has been shown to be a good zeroth order estimate.
However, by including physical mechanisms driving flow on the reef and atmospheric flux,
we are able to improve predictions of DTR at Dongsha Atoll and Kaneohe Bay. Using the
heat budget model to predict DTR not only improves predictions on a reef scale, but also
allows for seasonal variability to assessed. Until reliable satellite measurements of water
temperature at reef scales (<1 km) and diurnal variability are available, *in-situ* observations
and models will need to be used obtain these statistics.

Temperature is a conservative tracer, and has significant ecological implications on coral
reefs; however, pH, oxygen and nutrient concentration, and salinity are also important pa-
rameters for understanding reef health. Cyronak et al. (2020) also provided a relationship
between depth and daily pH range. Flow across the reef will also influence these biogeo-
chemical parameters.

In order to apply this simple analytical heat budget model for predicting water temper-
ature on other reefs, the minimum observations that are required are bathymetry in the
cross-section where the heat budget model is being estimated, the temperature gradient

(ΔT_{avg}) that is used to estimate an initial temperature across the reef, and pressure gradients across the reef flat. All other inputs to the heat budget model are taken from remotely sensed and/or modelled data. If high resolution remotely sensed SST is available, this could be used as the initial condition of temperature on the reef. Additionally, previous *in-situ* pressure measurements are necessary to estimate the tidally driven sea level change $(\Delta \eta_{tide})$; however, it is possible these could be estimated from a tidal model. If gradients in water temperature can be gathered from high resolution remotely sensed SST, and pressure gradients could be gathered from a tidal model, then estimates of reef scale variability in DTR could be made without *in-situ* inputs.

The ability to predict spatial gradients in thermal environments on coral reefs where we do not have *in-situ* temperature measurements will be critical for understanding and predicting bleaching variability in a changing climate. Incorporating physical mechanisms which drive advection and atmospheric fluxes of heat improves predictions of DTR on the coral reefs studied here, and this model can be applied to reefs globally with minimal previous *in-situ* observations, and remotely sensed and model data as inputs. Incorporating this simple analytical model of how water temperature is shaped by physical forcing on a reef scale into models currently being used to predict coral bleaching and resilience could improve those models and our understanding of coral resilience on a global scale.

Chapter 6

Conclusion

The purpose of this work was to understand the physical processes which are driving spatial and temporal variability on coral reefs. In Section 1.2, three questions were posed, from understanding the physical processes driving flow and variability at Dongsha Atoll, and the influence of internal waves here, to a broader question about the physical processes that shape reef-scale gradients in temperature and if temperature variability can be predicted from globally available data sources. In the following section, these questions and a summary of the results are presented.

6.1   Summary

1. What are the physical processes controlling the residence time of water, and creating reef-scale (<1km) environmental gradients on coral reef ecosystems?

Chapter 3 describes the temperature environment and physical processes which drive flow

on the east reef flat at Dongsha Atoll. Determining the processes that drive flow at Dongsha Atoll is vital to our understanding of the mechanisms that shape the coral community there. Many studies of the processes that drive flow on reefs have been completed, however this study looks at a reef with a unique morphology and remote location, with distinctive results.

There are temperature microclimates across the east reef flat at Dongsha Atoll (Figure 3.3), which exhibit variability in mean temperature and daily temperature range. Near the reef crest, in shallow water, mean temperature was the lowest and daily temperature range was the highest. Offshore, internal wave cooled water coming onshore likely contributes to the low mean temperatures here. Closer to the lagoon, where water was deeper, mean temperatures were higher, and daily temperature range was lower. Diurnal variability was significant across the reef flat, due to solar heating and cooling on the shallow reef, and temperature varied at higher frequencies near the reef crest.

The physical processes which drive these thermal microclimates vary temporally and spatially across the reef flat. Tides, wind and waves are all contributing to flow across the reef flat, and a simple analytical model for flow was used to attribute the flow at two locations on the reef flat (Figure 3.4). Closer to the reef crest (E3), tides and surface waves accounted for approximately half of the flow across the reef flat, and wind contributed minimally. Closer to the lagoon in deeper water (E5), wind contributed to approximately 18% of the flow, and surface waves and tides accounted for approximately 40% of the flow. The contribution of wind driven flow was found to be significant across the reef under certain forcing conditions, unlike previous studies which have shown wind is almost never a dominant force.

Residence time of water was estimated across the reef flat through particle tracking simulations (Figure 3.5). These simulations revealed that residence times were shorter near the reef crest (average 3.6 h), and longer near the lagoon (average 8.6 h). The source of water

140

(originating offshore vs. from the lagoon) across the reef flat varied spatially and temporally. Futhermore, it was shown that if flow across the reef was unidirectional, the patterns in residence time would be very different from the observed tidally varying flow on the reef flat. The wide reef flat here leads to complex patterns of tidal excursion of water on the reef flat which was also determined using particle tracking simulations (Figure 3.7). The excursion of offshore water varies temporally due to changes in oceanographic forcing on the reef, and could have significant impacts on the temperature and biogeochemistry across the reef flat. Under some forcing conditions, offshore, internal wave cooled water travels across the reef flat to the lagoon; however, under some forcing conditions, the water does not make it across the reef flat (Figure 3.6).

The anomalously wide reef flat at Dongsha Atoll leads to the observed thermal microclimates here, and the observed variability in flow across the reef flat. The physical processes which drive flow across the reef flat govern the residence time and source of water on the reef flat, which can significantly impact the biogeochemistry. This can help us to understand the variations in benthic cover and bleaching across the reef. The high thermal variability seen on the reef flat at Dongsha can contribute to the thermal tolerance of corals, and an understanding of what is driving the gradients in temperature seen here is important for understanding resilience in a changing climate.

2. How do internal waves shape the physical and chemical environment on coral reefs?

Chapter 4 outlines the influence of internal waves on the temperature and nutrient environment on the east reef flat at Dongsha Atoll. Quantifying the influence of internal waves on the shallow reef flat can help us to understand resilience of corals, and why some corals thrive under different conditions. The magnitude of the influence of internal waves on the shallow reef will be important in a changing climate.

Using Distributed Temperature Sensing (DTS) technology, we are able to observe the influence of internal waves on the shallow reef flat. Deep, cold water is mixed to the surface when internal waves shoal on the east reef slope at Dongsha Atoll (Figure 4.2). This internal wave cooled water is subsequently brought onto the shallow reef flat by tides, wind and surface waves. By creating a heat budget, we can see that atmospheric heating and advection of heat adequately predict observed heating rates on the reef flat (Figure 4.2, 4.4 and A.1).

The heat budget was modified to remove the influence of internal waves on the reef flat, and we found that instantaneously, temperatures could $2.0°C \pm 0.2°C$ higher on the reef flat. The cummulative effect of internal waves was largest near the reef crest, and decreased towards the reef flat (Figure 4.6). Furthermore, the influence of internal waves changes in time under different forcing conditions. When currents on the reef flat are smaller in magnitude, and tidally reversing, the influence of internal waves is smaller near the lagoon. When currents are larger in magnitude and unidirectional, due to high wind and waves, the influence of internal waves across the entire reef is greater (Figure 4.6).

The cumulative influence of internal waves was compared to the Degree Heating Week (DHW) metric, and we found that without internal waves, an change in DHW of $0.7°C$ would occur, which would result in approximately four times the probability of a bleaching occuring. The cooling effect that internal waves have at Dongsha could be important for the coral communities on the shallow reef, by buffering them from thermal stress and bleaching.

The influence of internal waves on the nutrient budget on the reef flat was also determined. Using a temperature-nutrient relationship from offshore measurements of nutrients, we are able to estimate the flux of nutrients onto the reef flat at Dongsha (Figure 4.7). We found that internal waves increase episodic nutrient fluxes by approximately four-fold (Figure 4.8).

142

The influence of internal waves on the shallow coral reef at Dongsha Atoll is significant, and could be a mechanism contributing to the high net ecosystem calcification rates here. Regions of the reef that receive internal wave cooled water have been observed to have lower mortality rates than regions which are not exposed to the internal wave influence. This influence would not be uncommon on other reefs which experience internal wave cooling (Appendix B), and could help to identify which reefs may provide thermal refuge in a changing climate.

3. What are the physical processes which are shaping reef-scale (<1km) gradients in temperature, and can important temperature metrics, such as daily temperature range, be predicted from larger scale, globally available data sources, paired with a dynamical understanding of reef-scale circulation and heat fluxes?

Chapter 5 examines the physical processes that are driving spatial and temporal variability in temperature across three reef ecosystems. The observations presented here are from Dongsha Atoll, a coral atoll in the northern South China Sea, Kaneohe Bay, a barrier reef system on Oahu, Hawaii, and the fringing reef at Ofu-Olosega, in American Samoa. Here, I use *in-situ* observations to examine the thermal environments at the three sites and the physical processes contributing to daily temperature range (DTR). Also, I create a heat budget model to improve predictions of DTR across the reef flat at Dongsha Atoll and Kaneohe Bay.

Thermal microclimates were observed at the three sites, with each site exhibiting gradients in the mean temperature and daily temperature range across the reef (Figure 5.2), distinguishing the shallow reefs from the open ocean. These gradients in mean temperature and DTR were largest at Dongsha Atoll, due to the internal wave influence there, and smaller at Kaneoehe Bay and Ofu-Olosega. Spectral analysis also revealed gradients in the variance

and the frequencies that are contributing to the variance across each study site (Figure 5.3). A gradient empirical orthogonal analysis was completed to see where the largest gradients exist on each reef, and how they change in time (Figure 5.4). Particle tracking was completed at Dongsha Atoll and Kaneohe Bay, and compared to DTR at locations across the reef flats (Figure 5.5). The two sites exhibited different relationships between DTR and residence time, which can be attributed to the influence of internal waves at Dongsha Atoll, and the reverse cross-reef bathymetric slopes at the two sites.

These analyses reveal distinctive patterns of variability at each site, which can be attributed to the physical processes which are driving flow at each site, the atmospheric forcing, and influence of internal waves. Five physical processes, tides, including wind, waves, atmospheric forcing, and the offshore temperature boundary condition, which are likely driving changes in temperature at the three sites were compared to DTR across the three sites (Figure 5.6) to determine what processes are significant at each location.

Previous studies have shown that a static value for DTR can be predicted from depth. Here, I use a heat budget model to determine spatially and temporally variable DTR at Dongsha Atoll and Kaneohe Bay, using minimal previous *in-situ* measurements, and remotely sensed and model data. The basic input data needed to estimate the heat budget is bathymetry of the reef, an average gradient in temperature across the reef, and previous pressure measurements. The model can be greatly improved with *in-situ* flow measurements, and one temperature measurement for the offshore boundary condition. Improving predictions of DTR, which has been shown to be an influential metric on coral reefs, by including atmospheric forcing and advection in the model, can develop our global understanding of bleaching variability and resilience on a reef-scale.

6.2 Future research

The studies completed at Dongsha Atoll describe the processes that drive flow there, and quantify the influence of internal waves may help inform what is shaping the coral ecosystem on the east reef flat, and also other areas of the reef flat and the lagoon. I hope that this study will inform future modelling efforts of Dongsha Atoll, and be useful for ecologists and biologists studying the unique environment here.

An understanding of internal wave activity can help to explain coral diversity and reef development in different regions of the world. With climate change, increased stratification of the world's oceans is expected due to higher sea surface temperature (SST), and with that there is an expected increase in internal wave generation (DeCarlo et al., 2015). Internal waves are expected to be one mechanism of buffering the corals from bleaching events and providing nutrients for growth, and future studies should explore the influence of internal waves on other coral reefs. These reefs may prove to be communities of corals with increased resilience, and should be prioritized for protection, and potential regeneration capacity.

Future research should look at the processes driving flow and residence time in the lagoon. There has been observed hypoxia in the lagoon, and understanding the physical processes which drive those episodes is critical. As internal waves travel around Dongsha, there has been satellite observations of the internal waves refracting around the atoll. Future research could focus on what happens when the internal waves reach the two channels on the west side of Dongsha, and how the internal waves continue to travel westward after encountering the atoll. Understanding how internal waves refract around the atoll and influence the lagoon at Dongsha will be crucial for understanding the coral community within the lagoon.

The development of tools to gather high spatial and temporal resolution temperature data,

and other environmental data is crucial to the study of environmental variability on coral reefs. Improving the spatial and temporal resolution of remote sensing products will be vital to oceanographic research. Using geostationary satellites may help with improving temporal resolution of data. Developing algorithms to remove the influence of clouds and improving the spatial resolution of data will also be integral.

With the increased availability of smaller spatial and temporal resolution of remote sensing products, estimating reef-scale variability will be easier; however, the continued development of *in-situ* tools is also important. DTS is a new and innovative tool for making high spatial resolution measurements of temperatures. It can be useful for measuring small scale physical processes over a large distance. In our case, DTS was used at Dongsha Atoll to track cold water intrusions onto the reef flat and quantify the influence of IWs. It was also used to identify different thermal microclimates across the reef, at Dongsha and Ofu. Deploying DTS in an oceanographic setting is not an easy task, and there have been some studies to test deployment and calibration techniques (for example Sinnett et al., 2020). Some challenges include the unwieldy and delicate nature of the fiber optic cables, powering the instrument and ensuring the calibration baths can be maintained in a remote environment. Further development of the tool for oceanographic deployment, by improving power sources and integrity, making the instrument and fiber optic cables more rugged and easier to deploy, and furthering calibration techniques, will be vital for future research.

Finally, continued evaluation of environmental variability on a reef-scale is integral because it will inform coral community structure, and spatial gradients in bleaching response. Further studies that look at reef-scale variability of other parameters such as pH, oxygen, nutrients, and salinity would help to understand community structure and bleaching response.

A model of reef scale environmental variability that could be applied to reefs globally would

be critical to understanding this spatial variability in bleaching, and could inform which areas need to be prioritized for protection, and what regions may be more resilient to a changing climate. Quantifying gradients in environmental variability on a global scale, and incorporating this into models of adaptability and acclimatization to improve predictions of responses to a changing environment would be a significant contribution. For example, Logan et al. (2014) looked at how different adaptive processes could affect coral bleaching. This study used data from the Millennium Coral Reef Mapping Project, which classifies reefs by type and location, morphology of the reef, and depth. By incorporating a model of how environmental variability responds to physical forcing on a reef-scale, it could be possible to improve predictability of the model.

Bibliography

Alford, M. H., and Coauthors, 2015: The formation and fate of internal waves in the south china sea. *Nature*, **521 (7550)**, 65–9.

Alpers, W., and V. Vlasenko, 2002: Study of secondary internal wave generation by the interaction of an internal solitary wave with an underwater bank by using ers sar imagery and a numerical model. *Proceeding of Pan Ocean Remote Sensing Conference(PORSEC)*, 162–166.

Alpers, W., H. Wang-Chen, and L. Hock, 1997: Observation of internal waves in the andaman sea by ers sar. *Geoscience and Remote Sensing, 1997. IGARSS'97. Remote Sensing-A Scientific Vision for Sustainable Development., 1997 IEEE International*, IEEE, Vol. 4, 1518–1520.

Apel, J. R., 1999: Are strongly sheared baroclinic currents sources for internal solitons? *The 1998 WHOI/IOS/ONR Internal Solitary Wave Workshop: Contributed Papers*, 172.

Apel, J. R., and F. I. Gonzalez, 1983: Nonlinear features of internal waves off baja california as observed from the seasat imaging radar. *Journal of Geophysical Research: Oceans*, **88 (C7)**, 4459–4466.

Apel, J. R., J. R. Holbrook, A. K. Liu, and J. J. Tsai, 1985: The sulu sea internal soliton experiment. *Journal of Physical Oceanography*, **15 (12)**, 1625–1651.

Barkley, H. C., A. L. Cohen, Y. Golbuu, V. R. Starczak, T. M. DeCarlo, and K. E. Shamberger, 2015: Changes in coral reef communities across a natural gradient in seawater ph. *Science Advances*, **1 (5)**, e1500 328.

Barshis, D. J., J. T. Ladner, T. A. Oliver, F. O. Seneca, N. Traylor-Knowles, and S. R. Palumbi, 2013: Genomic basis for coral resilience to climate change. *Proc Natl Acad Sci U S A*, **110 (4)**, 1387–92.

Barshis, D. J., J. H. Stillman, R. D. Gates, R. J. Toonen, L. W. Smith, and C. Birkeland, 2010: Protein expression and genetic structure of the coral porites lobata in an environmentally extreme samoan back reef: does host genotype limit phenotypic plasticity? *Mol Ecol*, **19 (8)**, 1705–20.

Bay, R. A., and S. R. Palumbi, 2014: Multilocus adaptation associated with heat resistance in reef-building corals. *Curr Biol*, **24 (24)**, 2952–6.

Beardsley, R. C., and Coauthors, 2004: Barotropic tide in the northeast south china sea. *IEEE Journal of Oceanic Engineering*, **29 (4)**, 1075–1086.

Becker, B., M. Merrifield, and M. Ford, 2014: Water level effects on breaking wave setup for pacific island fringing reefs. *Journal of Geophysical Research: Oceans*, **119 (2)**, 914–932.

Budyko, M. I., 1974: *Climate and life.* Academic Press, New York.

Cantin, N. E., and J. M. Lough, 2014: Surviving coral bleaching events: Porites growth anomalies on the great barrier reef. *PloS one*, **9 (2)**, e88 720.

Castillo, K. D., J. B. Ries, J. M. Weiss, and F. P. Lima, 2012: Decline of forereef corals in response to recent warming linked to history of thermal exposure. *Nature Climate Change*, **2 (10)**, 756–760.

Chiu, C.-S., S. R. Ramp, C. W. Miller, J. F. Lynch, T. F. Duda, and T. Y. Tang, 2004: Acoustic intensity fluctuations induced by south china sea internal tides and solitons. *IEEE Journal of Oceanic Engineering*, **29 (4)**, 1249–1263.

Chow, C., J. Hu, L. R. Centurioni, and P. P. Niiler, 2008: Mesoscale dongsha cyclonic eddy in the northern south china sea by drifter and satellite observations. *Journal of Geophysical Research: Oceans*, **113 (C4)**.

Codiga, D. L., 2011: Unified tidal analysis and prediction using the utide matlab functions. Graduate School of Oceanography, University of Rhode Island.

Cohen, A. L., and M. Holcomb, 2009: Why corals care about ocean acidification: uncovering the mechanism. *Oceanography*, **22 (4)**, 118–127.

Coles, S. L., and P. L. Jokiel, 1992: Effects of salinity on coral reefs. *Pollution in tropical aquatic systems*, 147–166.

Coutis, P., and J. Middleton, 2002: The physical and biological impact of a small island wake in the deep ocean. *Deep Sea Research Part I: Oceanographic Research Papers*, **49 (8)**, 1341–1361.

Craig, P., C. Birkeland, and S. Belliveau, 2001: High temperatures tolerated by a diverse assemblage of shallow-water corals in american samoa. *Coral Reefs*, **20 (2)**, 185–189.

Cuet, P., C. Pierret, E. Cordier, and M. Atkinson, 2011: Water velocity dependence of phosphate uptake on a coral-dominated fringing reef flat, la réunion island, indian ocean. *Coral Reefs*, **30 (1)**, 37–43.

Cyronak, T., and Coauthors, 2020: Diel temperature and ph variability scale with depth across diverse coral reef habitats. *Limnology and Oceanography Letters*, **5 (2)**, 193–203.

Dai, C., 2004: Dong-sha atoll in the south china sea: Past, present and future. *Islands of the World VIII International Conference, Kinmen Island, Taiwan.*

Davis, K. A., R. S. Arthur, E. C. Reid, J. S. Rogers, O. B. Fringer, T. M. DeCarlo, and A. L. Cohen, 2020: Fate of internal waves on a shallow shelf. *Journal of Geophysical Research: Oceans.*

Davis, K. A., J. J. Leichter, J. L. Hench, and S. G. Monismith, 2008: Effects of western boundary current dynamics on the internal wave field of the southeast florida shelf. *Journal of Geophysical Research: Oceans*, **113 (C9)**.

Davis, K. A., S. J. Lentz, J. Pineda, J. T. Farrar, V. R. Starczak, and J. H. Churchill, 2011: Observations of the thermal environment on red sea platform reefs: a heat budget analysis. *Coral Reefs*, **30 (S1)**, 25–36.

DeCarlo, T. M., A. L. Cohen, G. T. F. Wong, K. A. Davis, P. Lohmann, and K. Soong, 2017a: Mass coral mortality under local amplification of 2 degrees c ocean warming. *Sci Rep*, **7**, 44586.

DeCarlo, T. M., A. L. Cohen, G. T. F. Wong, F. Shiah, S. J. Lentz, K. A. Davis, K. E. Shamberger, and P. Lohmann, 2017b: Community production modulates coral reef ph and the sensitivity of ecosystem calcification to ocean acidification. *Journal of Geophysical Research: Oceans*, **122 (1)**, 745–761.

DeCarlo, T. M., K. B. Karnauskas, K. A. Davis, and G. T. F. Wong, 2015: Climate modulates internal wave activity in the northern south china sea. *Geophysical Research Letters*, **42 (3)**, 831–838.

Defant, A., 1961: Tides in the mediterranean and adjacent seas. observations and discussion. *Physical Oceanography*, **1**, 364–456.

Dong, C., J. C. McWilliams, and A. F. Shchepetkin, 2007: Island wakes in deep water. *Journal of Physical Oceanography*, **37 (4)**, 962–981.

Donner, S. D., 2009: Coping with commitment: projected thermal stress on coral reefs under different future scenarios. *PLoS One*, **4 (6)**, e5712.

Duda, T. F., J. F. Lynch, J. D. Irish, R. C. Beardsley, S. R. Ramp, C.-S. Chiu, T. Y. Tang, and Y.-J. Yang, 2004: Internal tide and nonlinear internal wave behavior at the continental slope in the northern south china sea. *IEEE Journal of Oceanic Engineering*, **29 (4)**, 1105–1130.

Eakin, C., and Coauthors, 2018: Unprecedented three years of global coral bleaching 2014-17 [in "State of the Climate in 2017"]. *Bulletin of American Meteorological Society*, **99 (8)**, S74–S75, doi:10.1175/2018BAMSStateoftheClimate.1.

Egbert, G. D., and S. Y. Erofeeva, 2002: Efficient inverse modeling of barotropic ocean tides. *Journal of Atmospheric and Oceanic Technology*, **19 (2)**, 183–204.

Eich, M. L., M. A. Merrifield, and M. H. Alford, 2004: Structure and variability of semidiurnal internal tides in mamala bay, hawaii. *Journal of Geophysical Research: Oceans*, **109 (C5)**.

Elachi, C., and J. Cimino, 1982: Shuttle imaging radar-a (sir-a) experiment. *NASA STI/Recon Technical Report N*, **83**.

Fairall, C., E. F. Bradley, J. Hare, A. Grachev, and J. Edson, 2003: Bulk parameterization of air–sea fluxes: Updates and verification for the coare algorithm. *Journal of climate*, **16 (4)**, 571–591.

Fairall, C. W., E. F. Bradley, D. P. Rogers, J. B. Edson, and G. S. Young, 1996: Bulk parameterization of air-sea fluxes for tropical ocean-global atmosphere coupled-ocean atmosphere response experiment. *Journal of Geophysical Research: Oceans*, **101 (C2)**, 3747–3764.

Falter, J. L., R. J. Lowe, Z. Zhang, and M. McCulloch, 2013: Physical and biological controls on the carbonate chemistry of coral reef waters: effects of metabolism, wave forcing, sea level, and geomorphology. *PLoS One*, **8 (1)**, e53 303.

Fu, K.-H., Y.-H. Wang, L. S. Laurent, H. Simmons, and D.-P. Wang, 2012: Shoaling of large-amplitude nonlinear internal waves at dongsha atoll in the northern south china sea. *Continental Shelf Research*, **37**, 1–7.

Fu, L., and B. Holt, 1984: Internal waves in the gulf of california: Observations from a spaceborne radar. *Journal of Geophysical Research: Oceans*, **89 (C2)**, 2053–2060.

Fu, L.-L., and B. Holt, 1982: *Seasat views oceans and sea ice with synthetic-aperture radar*, Vol. 81. California Institute of Technology, Jet Propulsion Laboratory.

Garrett, C., and W. Munk, 1979: Internal waves in the ocean. *Annual Review of Fluid Mechanics*, **11 (1)**, 339–369.

Glynn, P., 1993: Coral reef bleaching: ecological perspectives. *Coral reefs*, **12 (1)**, 1–17.

Glynn, P., and L. D'croz, 1990: Experimental evidence for high temperature stress as the cause of el nino-coincident coral mortality. *Coral reefs*, **8 (4)**, 181–191.

Glynn, P. W., 1991: Coral reef bleaching in the 1980s and possible connections with global warming. *Trends in Ecology & Evolution*, **6 (6)**, 175–179.

Goldberg, W. M., 2016: Atolls of the world: Revisiting the original checklist. *Atoll Research Bulletin*, **610**.

Goreau, T. F., 1964: Mass expulsion of zooxanthellae from jamaican reef communities after hurricane flora. *Science*, **145 (3630)**, 383–386.

Goreau, T. J., and R. L. Hayes, 1994: Coral bleaching and ocean" hot spots". *Ambio-Journal of Human Environment Research and Management*, **23 (3)**, 176–180.

Gourlay, M. R., and G. Colleter, 2005: Wave-generated flow on coral reefs—an analysis for two-dimensional horizontal reef-tops with steep faces. *Coastal Engineering*, **52 (4)**, 353–387.

Green, R. H., N. L. Jones, M. D. Rayson, R. J. Lowe, C. E. Bluteau, and G. N. Ivey, 2018: Nutrient fluxes into an isolated coral reef atoll by tidally driven internal bores. *Limnology and Oceanography.*

Guadayol, O., N. J. Silbiger, M. J. Donahue, and F. I. Thomas, 2014: Patterns in temporal variability of temperature, oxygen and ph along an environmental gradient in a coral reef. *PloS one*, **9 (1)**, e85 213.

Hausner, M. B., F. Suarez, K. E. Glander, N. van de Giesen, J. S. Selker, and S. W. Tyler, 2011: Calibrating single-ended fiber-optic raman spectra distributed temperature sensing data. *Sensors (Basel)*, **11 (11)**, 10 859–79.

Hearn, C. J., 1999: Wave-breaking hydrodynamics within coral reef systems and the effect of changing relative sea level. *Journal of Geophysical Research: Oceans*, **104 (C12)**, 30 007–30 019.

Hearn, C. J., 2011: Perspectives in coral reef hydrodynamics. *Coral Reefs*, **30 (S1)**, 1–9.

Hefner, B. B., J. S. Rogers, S. A. Maticka, S. G. Monismith, and C. B. Woodson, 2019: Instrumentation for direct measurements of wave-driven flow over a fringing reef crest. *Limnology and Oceanography: Methods.*

Helfrich, K. R., 1992: Internal solitary wave breaking and run-up on a uniform slope. *Journal of Fluid Mechanics*, **243**, 133–154.

Helfrich, K. R., and W. K. Melville, 2006: Long nonlinear internal waves. *Annu. Rev. Fluid Mech.*, **38**, 395–425.

Hench, J. L., J. J. Leichter, and S. G. Monismith, 2008: Episodic circulation and exchange in a wave-driven coral reef and lagoon system. *Limnology and Oceanography*, **53 (6)**, 2681–2694.

Heywood, K. J., D. P. Stevens, and G. R. Bigg, 1996: Eddy formation behind the tropical island of aldabra. *Deep Sea Research Part I: Oceanographic Research Papers*, **43 (4)**, 555–578.

Hoegh-Guldberg, O., 1999: Climate change, coral bleaching and the future of the world's coral reefs. *Marine and freshwater research*, **50 (8)**, 839–866.

Hoegh-Guldberg, O., and G. J. Smith, 1989: The effect of sudden changes in temperature, light and salinity on the population density and export of zooxanthellae from the reef corals stylophora pistillata esper and seriatopora hystrix dana. *Journal of experimental marine biology and ecology*, **129 (3)**, 279–303.

Hoegh-Guldberg, O., and Coauthors, 2007: Coral reefs under rapid climate change and ocean acidification. *Science*, **318 (5857)**, 1737–42.

Hofmann, G. E., and Coauthors, 2011: High-frequency dynamics of ocean ph: a multi-ecosystem comparison. *PloS one*, **6 (12)**, e28 983.

Holcomb, M., D. C. McCorkle, and A. L. Cohen, 2010: Long-term effects of nutrient and co 2 enrichment on the temperate coral astrangia poculata (ellis and solander, 1786). *Journal of Experimental Marine Biology and Ecology*, **386 (1)**, 27–33.

Holloway, P., E. Pelinovsky, and T. Talipova, 2003: Internal tide transformation and oceanic internal solitary waves. *Environmental stratified flows*, Springer, 29–60.

Howell, T. L., and W. S. Brown, 1985: Nonlinear internal waves on the california continental shelf. *Journal of Geophysical Research: Oceans*, **90 (C4)**, 7256–7264.

Hsu, M.-K., and A. K. Liu, 2000: Nonlinear internal waves in the south china sea. *Canadian Journal of Remote Sensing*, **26 (2)**, 72–81.

Hsu, M.-K., A. K. Liu, and C. Liu, 2000: A study of internal waves in the china seas and yellow sea using sar. *Continental Shelf Research*, **20 (4)**, 389–410.

Hu, J., H. Kawamura, H. Hong, and Y. Qi, 2000: A review on the currents in the south china sea: seasonal circulation, south china sea warm current and kuroshio intrusion. *Journal of Oceanography*, **56 (6)**, 607–624.

Hughes, T. P., and Coauthors, 2003: Climate change, human impacts, and the resilience of coral reefs. *science*, **301 (5635)**, 929–933.

Hughes, T. P., and Coauthors, 2017: Global warming and recurrent mass bleaching of corals. *Nature*, **543 (7645)**, 373–377.

Inall, M., D. Aleynik, T. Boyd, M. Palmer, and J. Sharples, 2011: Internal tide coherence and decay over a wide shelf sea. *Geophysical Research Letters*, **38 (23)**.

Jackson, C., 2007: Internal wave detection using the moderate resolution imaging spectro-radiometer (modis). *Journal of Geophysical Research: Oceans*, **112 (C11)**.

Jackson, C. R., and J. Apel, 2004: An atlas of internal solitary-like waves and their properties. *Contract*, **14 (03-C)**, 0176.

Jantzen, C., G. M. Schmidt, C. Wild, C. Roder, S. Khokiattiwong, and C. Richter, 2013: Benthic reef primary production in response to large amplitude internal waves at the similan islands (andaman sea, thailand). *PLoS One*, **8 (11)**, e81 834.

Jones, N. L., R. J. Lowe, G. Pawlak, D. A. Fong, and S. G. Monismith, 2008: Plume dispersion on a fringing coral reef system. *Limnology and Oceanography*, **53 (5part2)**, 2273–2286.

Kealoha, A. K., and Coauthors, 2019: Heterotrophy of oceanic particulate organic matter elevates net ecosystem calcification. *Geophysical Research Letters*, **46 (16)**, 9851–9860.

Keiner, L. E., and X.-H. Yan, 1997: Empirical orthogonal function analysis of sea surface temperature patterns in delaware bay. *IEEE Transactions on Geoscience and remote sensing*, **35 (5)**, 1299–1306.

Kim, H. R., S. Ahn, and K. Kim, 2001: Observations of highly nonlinear internal solitons generated by near-inertial internal waves off the east coast of korea. *Geophysical Research Letters*, **28 (16)**, 3191–3194.

Kobs, S., D. M. Holland, V. Zagorodnov, A. Stern, and S. W. Tyler, 2014: Novel monitoring of antarctic ice shelf basal melting using a fiber-optic distributed temperature sensing mooring. *Geophysical Research Letters*, **41 (19)**, 6779–6786.

Koweek, D. A., R. B. Dunbar, S. G. Monismith, D. A. Mucciarone, C. B. Woodson, and L. Samuel, 2015: High-resolution physical and biogeochemical variability from a shallow back reef on ofu, american samoa: An end-member perspective. *Coral Reefs*, **34 (3)**, 979–991.

Kraines, S., T. Yanagi, M. Isobe, and H. Komiyama, 1998: Wind-wave driven circulation on the coral reef at bora bay, miyako island. *Coral Reefs*, **17 (2)**, 133–143.

Leichter, J. J., and S. J. Genovese, 2006: Intermittent upwelling and subsidized growth of the scleractinian coral madracis mirabilis on the deep fore-reef slope of discovery bay, jamaica. *Marine Ecology Progress Series*, **316**, 95–103.

Leichter, J. J., B. Helmuth, and A. M. Fischer, 2006: Variation beneath the surface: quantifying complex thermal environments on coral reefs in the caribbean, bahamas and florida. *Journal of Marine Research*, **64 (4)**, 563–588.

Leichter, J. J., G. Shellenbarger, S. J. Genovese, and S. R. Wing, 1998: Breaking internal waves on a florida (usa) coral reef: a plankton pump at work? *Marine Ecology Progress Series*, 83–97.

Leichter, J. J., H. L. Stewart, and S. L. Miller, 2003: Episodic nutrient transport to florida coral reefs. *Limnology and Oceanography*, **48 (4)**, 1394–1407.

Leichter, J. J., M. D. Stokes, J. L. Hench, J. Witting, and L. Washburn, 2012: The island-scale internal wave climate of moorea, french polynesia. *Journal of Geophysical Research: Oceans*, **117 (C6)**, n/a–n/a.

Leichter, J. J., S. R. Wing, S. L. Miller, and M. W. Denny, 1996: Pulsed delivery of sub-thermocline water to conch reef (florida keys) by internal tidal bores. *Limnology and Oceanography*, **41 (7)**, 1490–1501.

Lentz, S. J., J. H. Churchill, K. A. Davis, J. T. Farrar, J. Pineda, and V. Starczak, 2016: The characteristics and dynamics of wave-driven flow across a platform coral reef in the red sea. *Journal of Geophysical Research: Oceans*, **121 (2)**, 1360–1376.

Lentz, S. J., K. A. Davis, J. H. Churchill, and T. M. DeCarlo, 2017: Coral reef drag coefficients–water depth dependence. *Journal of Physical Oceanography*, **47 (5)**, 1061–1075.

Lerczak, J. A., M. Hendershott, and C. Winant, 2001: Observations and modeling of coastal internal waves driven by a diurnal sea breeze. *Journal of Geophysical Research: Oceans*, **106 (C9)**, 19 715–19 729.

Lerczak, J. A., M. C. Hendershott, and C. D. Winant, 1999: Observations of the internal tide on the southern california shelf. *Dynamics of Oceanic Internal Gravity Waves II: Proc. of the Aha Hulikoa Hawaiian Winter Workshop*, 9–20.

Lesser, M., W. Stochaj, D. Tapley, and J. Shick, 1990: Bleaching in coral reef anthozoans: effects of irradiance, ultraviolet radiation, and temperature on the activities of protective enzymes against active oxygen. *Coral reefs*, **8 (4)**, 225–232.

Lesser, M. P., and J. H. Farrell, 2004: Exposure to solar radiation increases damage to both host tissues and algal symbionts of corals during thermal stress. *Coral reefs*, **23 (3)**, 367–377.

Lilly, J., 2019: jlab: A data analysis package for matlab, v. 1.6.6. Jonathan M. Lilly, URL http://www.jmlilly.net/software.

Liu, A., Y.-H. Zhao, T. Tang, and R. Ramp, Steven, 2003: Model-data assimilation of internal waves during asiaex-2001. Calhoun, URL https://calhoun.nps.edu/handle/10945/60087.

Liu, A. K., Y. S. Chang, M.-K. Hsu, and N. K. Liang, 1998: Evolution of nonlinear internal waves in the east and south china seas. *Journal of Geophysical Research: Oceans*, **103 (C4)**, 7995–8008.

Liu, A. K., J. R. Holbrook, and J. R. Apel, 1985: Nonlinear internal wave evolution in the sulu sea. *Journal of Physical Oceanography*, **15 (12)**, 1613–1624.

Liu, A. K., and M. K. Hsu, 2004: Internal wave study in the south china sea using synthetic aperture radar (sar). *International Journal of Remote Sensing*, **25 (7-8)**, 1261–1264.

Liu, G., and Coauthors, 2018: Predicting heat stress to inform reef management: Noaa coral reef watch's 4-month coral bleaching outlook. *Frontiers in Marine Science*, **5**, 57.

Logan, C. A., J. P. Dunne, C. M. Eakin, and S. D. Donner, 2014: Incorporating adaptive responses into future projections of coral bleaching. *Global Change Biology*, **20 (1)**, 125–139.

Longuet-Higgins, M. S., and R. Stewart, 1962: Radiation stress and mass transport in gravity waves, with application to 'surf beats'. *Journal of Fluid Mechanics*, **13 (4)**, 481–504.

Longuet-Higgins, M. S., and R. Stewart, 1964: Radiation stresses in water waves; a physical discussion, with applications. *Deep Sea Research and Oceanographic Abstracts*, Elsevier, Vol. 11, 529–562.

Lowe, R. J., and J. L. Falter, 2015: Oceanic forcing of coral reefs. *Ann Rev Mar Sci*, **7**, 43–66.

Lowe, R. J., J. L. Falter, M. D. Bandet, G. Pawlak, M. J. Atkinson, S. G. Monismith, and J. R. Koseff, 2005: Spectral wave dissipation over a barrier reef. *Journal of Geophysical Research: Oceans*, **110 (C4)**.

Lowe, R. J., J. L. Falter, S. G. Monismith, and M. J. Atkinson, 2009a: A numerical study of circulation in a coastal reef-lagoon system. *Journal of Geophysical Research*, **114 (C6)**.

Lowe, R. J., J. L. Falter, S. G. Monismith, and M. J. Atkinson, 2009b: Wave-driven circulation of a coastal reef–lagoon system. *Journal of Physical Oceanography*, **39 (4)**, 873–893.

Lucas, A. J., P. J. Franks, and C. L. Dupont, 2011: Horizontal internal-tide fluxes support elevated phytoplankton productivity over the inner continental shelf. *Limnology and Oceanography: Fluids and Environments*, **1 (1)**, 56–74.

Maritorena, S., A. Morel, and B. Gentili, 1994: Diffuse reflectance of oceanic shallow waters: Influence of water depth and bottom albedo. *Limnology and oceanography*, **39 (7)**, 1689–1703.

McClanahan, T., J. Maina, R. Moothien-Pillay, and A. Baker, 2005: Effects of geography, taxa, water flow, and temperature variation on coral bleaching intensity in mauritius. *Marine Ecology Progress Series*, **298**, 131–142.

McPhee-Shaw, E. E., D. A. Siegel, L. Washburn, M. A. Brzezinski, J. L. Jones, A. Leydecker, and J. Melack, 2007: Mechanisms for nutrient delivery to the inner shelf: Observations from the santa barbara channel. *Limnology and Oceanography*, **52 (5)**, 1748–1766.

Mei, C. C., 1989: *The applied dynamics of ocean surface waves*, Vol. 1. World scientific.

Monismith, S. G., 2007: Hydrodynamics of coral reefs. *Annual Review of Fluid Mechanics*, **39 (1)**, 37–55.

Monismith, S. G., 2014: Flow through a rough, shallow reef. *Coral Reefs*, **33 (1)**, 99–104.

Monismith, S. G., and Coauthors, 2010: Flow effects on benthic grazing on phytoplankton by a caribbean reef. *Limnology and Oceanography*, **55 (5)**, 1881–1892.

Monsen, N. E., J. E. Cloern, L. V. Lucas, and S. G. Monismith, 2002: A comment on the use of flushing time, residence time, and age as transport time scales. *Limnology and Oceanography*, **47 (5)**, 1545–1553.

Moore, C. D., J. R. Koseff, and E. L. Hult, 2016: Characteristics of bolus formation and propagation from breaking internal waves on shelf slopes. *Journal of Fluid Mechanics*, **791**, 260–283.

Morton, B., and G. Blackmore, 2001: South china sea. *Marine Pollution Bulletin*, **42 (12)**, 1236–1263.

Munk, W. H., 1940: Internal waves in the gulf of california. Ph.D. thesis, California Institute of Technology.

Nash, J. D., E. L. Shroyer, S. M. Kelly, M. E. Inall, T. F. Duda, M. D. Levine, N. L. Jones, and R. C. Musgrave, 2012: Are any coastal internal tides predictable? *Oceanography*, **25 (2)**, 80–95.

NOAA Pacific Islands Fisheries Science Center, Coral Reef Ecosystem Division, Pacific Islands Benthic Habitat Mapping Center, 2010: Gridded bathymetry of the banktop and slope environments of Ofu and Olosega Islands of the Manu'a Island group, American Samoa. Available at http://www.soest.hawaii.edu/pibhmc (2020/11/24).

NOAA Pacific Islands Fisheries Science Center, Coral Reef Ecosystem Division, Pacific Islands Benthic Habitat Mapping Center, 2011: Gridded bathymetry of Kaneohe Bay, Windward Side Oahu, Main Hawaiian Islands, USA. Available at http://www.soest.hawaii.edu/pibhmc (2020/11/24).

Noble, M., B. Jones, P. Hamilton, J. Xu, G. Robertson, L. Rosenfeld, and J. Largier, 2009: Cross-shelf transport into nearshore waters due to shoaling internal tides in san pedro bay, ca. *Continental Shelf Research*, **29 (15)**, 1768–1785.

Ogura, S., 1933: The tides in the seas adjacent to japan. *Bull. Hydrogr. Office*, **7**, 189p.

Oliver, T. A., and S. R. Palumbi, 2011: Do fluctuating temperature environments elevate coral thermal tolerance? *Coral Reefs*, **30 (2)**, 429–440.

Oppen, M. J., and Coauthors, 2017: Shifting paradigms in restoration of the world's coral reefs. *Global Change Biology*.

Orr, M. H., and P. C. Mignerey, 2003: Nonlinear internal waves in the south china sea: Observation of the conversion of depression internal waves to elevation internal waves. *Journal of Geophysical Research: Oceans*, **108 (C3)**.

Osborne, A., and T. Burch, 1980: Internal solitons in the andaman sea. *Science*, **208 (4443)**, 451–460.

Osborne, A., T. Burch, and R. Scarlet, 1978: The influence of internal waves on deep-water drilling. *Journal of Petroleum Technology*, **30 (10)**, 1,497–1,504.

Padman, L., and S. Erofeeva, 2004: A barotropic inverse tidal model for the arctic ocean. *Geophysical Research Letters*, **31 (2)**.

Palumbi, S. R., D. J. Barshis, N. Traylor-Knowles, and R. A. Bay, 2014: Mechanisms of reef coral resistance to future climate change. *Science*, **344 (6186)**, 895–898.

Pan, X., G. T. F. Wong, T. M. DeCarlo, J.-H. Tai, and A. L. Cohen, 2017: Validation of the remotely sensed nighttime sea surface temperature in the shallow waters at the dongsha atoll. *Terrestrial, Atmospheric and Oceanic Sciences*, **28 (3)**, 517.

Pandolfi, J. M., S. R. Connolly, D. J. Marshall, and A. L. Cohen, 2011: Projecting coral reef futures under global warming and ocean acidification. *science*, **333 (6041)**, 418–422.

Pelinovsky, E., P. Holloway, and T. Talipova, 1995: A statistical analysis of extreme events in current variations due to internal waves from the australian north west shelf. *Journal of Geophysical Research: Oceans*, **100 (C12)**, 24 831–24 839.

Perry, R. B., and G. R. Schimke, 1965: Large-amplitude internal waves observed off the northwest coast of sumatra. *Journal of Geophysical Research*, **70 (10)**, 2319–2324.

Pineda, J., V. Starczak, A. Tarrant, J. Blythe, K. Davis, T. Farrar, M. Berumen, and J. C. da Silva, 2013: Two spatial scales in a bleaching event: Corals from the mildest and the most extreme thermal environments escape mortality. *Limnology and Oceanography*, **58 (5)**, 1531–1545.

Pinkel, R., 2000: Internal solitary waves in the warm pool of the western equatorial pacific. *Journal of physical oceanography*, **30 (11)**, 2906–2926.

Pinkel, R., M. Merrifield, M. McPhaden, J. Picaut, S. Rutledge, D. Siegel, and L. Washburn, 1997: Solitary waves in the western equatorial pacific ocean. *Geophysical research letters*, **24 (13)**, 1603–1606.

Ramp, S., Y. Yang, and F. Bahr, 2010: Characterizing the nonlinear internal wave climate in the northeastern south china sea. *Nonlinear Processes in Geophysics*, **17 (5)**, 481.

Ramp, S. R., and Coauthors, 2004: Internal solitons in the northeastern south china sea. part i: Sources and deep water propagation. *IEEE Journal of Oceanic Engineering*, **29 (4)**, 1157–1181.

Raven, J., and Coauthors, 2005: *Ocean acidification due to increasing atmospheric carbon dioxide.* The Royal Society.

Reed, R. K., 1976: On estimation of net long-wave radiation from the oceans. *Journal of Geophysical Research*, **81 (33)**, 5793–5794.

Reid, E. C., T. M. DeCarlo, A. L. Cohen, G. T. Wong, S. J. Lentz, A. Safaie, A. Hall, and K. A. Davis, 2019: Internal waves influence the thermal and nutrient environment on a shallow coral reef. *Limnology and Oceanography.*

Reid, E. C., S. J. Lentz, T. M. DeCarlo, A. L. Cohen, and K. A. Davis, 2020: Physical processes determine spatial structure in water temperature and residence time on a wide reef flat. *Journal of Geophysical Research: Oceans.*

Riegl, B., and W. E. Piller, 2003: Possible refugia for reefs in times of environmental stress. *International Journal of Earth Sciences*, **92 (4)**, 520–531.

Rogers, J. S., S. A. Maticka, V. Chirayath, C. B. Woodson, J. J. Alonso, and S. G. Monismith, 2018: Connecting flow over complex terrain to hydrodynamic roughness on a coral reef. *Journal of Physical Oceanography*, **48 (7)**, 1567–1587.

Rogers, J. S., S. G. Monismith, D. A. Koweek, W. I. Torres, and R. B. Dunbar, 2016: Thermodynamics and hydrodynamics in an atoll reef system and their influence on coral cover. *Limnology and Oceanography*, **61 (6)**, 2191–2206.

Rosenfeld, L. K., F. B. Schwing, N. Garfield, and D. E. Tracy, 1994: Bifurcated flow from an upwelling center: a cold water source for monterey bay. *Continental Shelf Research*, **14 (9)**, 931–964.

Rosman, J. H., and J. L. Hench, 2011: A framework for understanding drag parameterizations for coral reefs. *Journal of Geophysical Research*, **116 (C8)**.

Rubenstein, D., 1999: Observations of cnoidal internal waves and their effect on acoustic propagation in shallow water. *IEEE journal of oceanic engineering*, **24 (3)**, 346–357.

Safaie, A., and Coauthors, 2018: High frequency temperature variability reduces the risk of coral bleaching. *Nature communications*, **9**.

Schoepf, V., M. U. Jung, M. T. McCulloch, N. E. White, M. Stat, and L. Thomas, 2020: Thermally variable, macrotidal reef habitats promote rapid recovery from mass coral bleaching. *Frontiers in Marine Science*, **7**, 245.

Schoepf, V., M. Stat, J. L. Falter, and M. T. McCulloch, 2015: Limits to the thermal tolerance of corals adapted to a highly fluctuating, naturally extreme temperature environment. *Sci Rep*, **5**, 17 639.

Schramek, T., P. Colin, M. Merrifield, and E. Terrill, 2018: Depth-dependent thermal stress around corals in the tropical pacific ocean. *Geophysical Research Letters*, **45 (18)**, 9739–9747.

Selker, J. S., and Coauthors, 2006: Distributed fiber-optic temperature sensing for hydrologic systems. *Water Resources Research*, **42 (12)**.

Shamberger, K. E., A. L. Cohen, Y. Golbuu, D. C. McCorkle, S. J. Lentz, and H. C. Barkley, 2014: Diverse coral communities in naturally acidified waters of a western pacific reef. *Geophysical Research Letters*, **41 (2)**, 499–504.

Sharples, J., C. M. Moore, and E. R. Abraham, 2001: Internal tide dissipation, mixing, and vertical nitrate flux at the shelf edge of ne new zealand. *Journal of Geophysical Research: Oceans*, **106 (C7)**, 14 069–14 081.

Shih, P. T.-Y., D. Arumugam, and S.-W. Shyue, 2011: Bathymetric lidar survey of penghu islands and dongsha atoll using an ellipsoidal height system for bathymetric mapping in shallow waters and difficult-to-navigate environments. *Sea Technology*, **52 (11)**, 42–45.

Shroyer, E., J. Moum, and J. Nash, 2010: Energy transformations and dissipation of nonlinear internal waves over new jersey's continental shelf. *Nonlinear processes in Geophysics*, **17 (4)**, 345.

Sinnett, G., K. A. Davis, A. J. Lucas, S. N. Giddings, E. C. Reid, M. Harvey, and I. Stokes, 2020: Distributed temperature sensing for oceanographic applications. *Journal of Atmospheric and Oceanic Technology*.

Sinnett, G., and F. Feddersen, 2014: The surf zone heat budget: The effect of wave heating. *Geophysical Research Letters*, **41 (20)**, 7217–7226.

Small, J., and J. Martin, 2002: The generation of non-linear internal waves in the gulf of oman. *Continental Shelf Research*, **22 (8)**, 1153–1182.

Smith, L. W., H. H. Wirshing, A. C. Baker, and C. Birkeland, 2008: Environmental versus genetic influences on growth rates of the corals pocillopora eydouxi and porites lobata (anthozoa: Scleractinia)1. *Pacific Science*, **62 (1)**, 57–69.

Smith, W. H., and D. T. Sandwell, 1997: Global sea floor topography from satellite altimetry and ship depth soundings. *Science*, **277 (5334)**, 1956–1962.

Smyth, N., and P. Holloway, 1988: Hydraulic jump and undular bore formation on a shelf break. *Journal of Physical Oceanography*, **18 (7)**, 947–962.

Spalding, M. D., and B. E. Brown, 2015: Warm-water coral reefs and climate change. *Science*, **350 (6262)**, 769–771.

St Laurent, L., H. Simmons, T. Y. Tang, and Y. Wang, 2011: Turbulent properties of internal waves in the south china sea. *Oceanography*, **24 (4)**, 78–87.

Suárez, F., M. B. Hausner, J. Dozier, J. S. Selker, and S. W. Tyler, 2011: Heat transfer in the environment: Development and use of fiber-optic distributed temperature sensing. *Developments in Heat Transfer*, InTech.

Symonds, G., K. P. Black, and I. R. Young, 1995: Wave-driven flow over shallow reefs. *Journal of Geophysical Research*, **100 (C2)**.

Taebi, S., R. J. Lowe, C. B. Pattiaratchi, G. N. Ivey, G. Symonds, and R. Brinkman, 2011: Nearshore circulation in a tropical fringing reef system. *Journal of Geophysical Research*, **116 (C2)**.

Thompson, R. O. R. Y., and T. J. Golding, 1981: Tidally induced 'upwelling' by the great barrier reef. *Journal of Geophysical Research*, **86 (C7)**, 6517.

Thomson, D. J., 1982: Spectrum estimation and harmonic analysis. *Proceedings of the IEEE*, **70 (9)**, 1055–1096.

Tkachenko, K. S., and K. Soong, 2017: Dongsha atoll: A potential thermal refuge for reef-building corals in the south china sea. *Marine environmental research*, **127**, 112–125.

Tyler, S. W., J. S. Selker, M. B. Hausner, C. E. Hatch, T. Torgersen, C. E. Thodal, and S. G. Schladow, 2009: Environmental temperature sensing using raman spectra dts fiber-optic methods. *Water Resources Research*, **45 (4)**.

Van Emmerik, T., A. Rimmer, Y. Lechinsky, K. Wenker, S. Nussboim, and N. Van de Giesen, 2013: Measuring heat balance residual at lake surface using distributed temperature sensing. *Limnology and Oceanography: Methods*, **11 (2)**, 79–90.

Van Hooidonk, R., and Coauthors, 2016: Local-scale projections of coral reef futures and implications of the paris agreement. *Scientific reports*, **6 (1)**, 1–8.

van Woesik, R., P. Houk, A. L. Isechal, J. W. Idechong, S. Victor, and Y. Golbuu, 2012: Climate-change refugia in the sheltered bays of palau: analogs of future reefs. *Ecology Evolution*, **2 (10)**, 2474–84.

van Woesik, R., K. Sakai, A. Ganase, and Y. Loya, 2011: Revisiting the winners and the losers a decade after coral bleaching. *Marine Ecology Progress Series*, **434**, 67–76.

Vercauteren, N., H. Huwald, E. Bou-Zeid, J. S. Selker, U. Lemmin, M. B. Parlange, and I. Lunati, 2011: Evolution of superficial lake water temperature profile under diurnal radiative forcing. *Water resources research*, **47 (9)**.

Vlasenko, V., 2005: Generation of secondary internal waves by the interaction of an internal solitary wave with an underwater bank. *Journal of Geophysical Research*, **110 (C2)**.

Wall, M., L. Putchim, G. Schmidt, C. Jantzen, S. Khokiattiwong, and C. Richter, 2015: Large-amplitude internal waves benefit corals during thermal stress. *Proceedings of the Royal Society of London B: Biological Sciences*, **282 (1799)**, 20140 650.

Walter, R. K., C. B. Woodson, R. S. Arthur, O. B. Fringer, and S. G. Monismith, 2012: Nearshore internal bores and turbulent mixing in southern monterey bay. *Journal of Geophysical Research: Oceans*, **117 (C7)**, n/a–n/a.

Walter, R. K., C. B. Woodson, P. R. Leary, and S. G. Monismith, 2014: Connecting wind-driven upwelling and offshore stratification to nearshore internal bores and oxygen variability. *Journal of Geophysical Research: Oceans*, **119 (6)**, 3517–3534.

Wang, Y.-H., C.-F. Dai, and Y.-Y. Chen, 2007: Physical and ecological processes of internal waves on an isolated reef ecosystem in the south china sea. *Geophysical Research Letters*, **34 (18)**.

Wang, Z., 1997: A study of ocean internal waves using space shuttle data. Ph.D. thesis, University of Delaware.

Webster, P. J., and R. Lukas, 1992: Toga coare: The coupled ocean—atmosphere response experiment. *Bulletin of the American Meteorological Society*, **73 (9)**, 1377–1416.

Willmott, C. J., 1982: Some comments on the evaluation of model performance. *Bulletin of the American Meteorological Society*, **63 (11)**, 1309–1313.

Wolanski, E., P. Colin, J. Naithani, E. Deleersnijder, and Y. Golbuu, 2004: Large amplitude, leaky, island-generated, internal waves around palau, micronesia. *Estuarine, Coastal and Shelf Science*, **60 (4)**, 705–716.

Wolanski, E., and B. Delesalle, 1995: Upwelling by internal waves, tahiti, french polynesia. *Continental Shelf Research*, **15 (2-3)**, 357–368.

Wolanski, E., and G. Pickard, 1983: Upwelling by internal tides and kelvin waves at the continental shelf break on the great barrier reef. *Marine and Freshwater Research*, **34 (1)**, 65–80.

Wong, G. T., L. Li-Tzu Hou, and K. Li, 2017: Preservation of seawater samples for soluble reactive phosphate, nitrite, and nitrate plus nitrite analyses by the addition of sodium hydroxide. *Limnology and Oceanography: Methods*, **15 (3)**, 320–327.

Wong, G. T. F., T.-L. Ku, H. Liu, and M. Mulholland, 2015a: The oceanography of the northern south china sea shelf-sea (nosocs) and its adjacent waters—overview and highlights1. Elsevier.

Wong, G. T. F., X. Pan, K.-Y. Li, F.-K. Shiah, T.-Y. Ho, and X. Guo, 2015b: Hydrography and nutrient dynamics in the northern south china sea shelf-sea (nosocs). *Deep Sea Research Part II: Topical Studies in Oceanography*, **117**, 23–40.

Woodson, C., 2018: The fate and impact of internal waves in nearshore ecosystems. *Annual review of marine science*, **10**, 421–441.

Wyatt, A. S., J. J. Leichter, L. T. Toth, T. Miyajima, R. B. Aronson, and T. Nagata, 2020: Heat accumulation on coral reefs mitigated by internal waves. *Nature Geoscience*, **13 (1)**, 28–34.

Zeeman, M. J., J. S. Selker, and C. K. Thomas, 2014: Near-surface motion in the nocturnal, stable boundary layer observed with fibre-optic distributed temperature sensing. *Boundary-Layer Meteorology*, **154 (2)**, 189–205.

Zeng, K., and W. Alpers, 2004: Generation of internal solitary waves in the sulu sea and their refraction by bottom topography studied by ers sar imagery and a numerical model. *International Journal of Remote Sensing*, **25 (7-8)**, 1277–1281.

Zeng, X., S. Peng, Z. Li, Y. Qi, and R. Chen, 2014: A reanalysis dataset of the south china sea. *Scientific data*, **1**, 140 052.

Zhou, J., X. Zhang, and P. H. Rogers, 1991: Resonant interaction of sound wave with internal solitons in the coastal zone. *The Journal of the Acoustical Society of America*, **90 (4)**, 2042–2054.

Zimmerman, R. C., and J. N. Kremer, 1984: Episodic nutrient supply to a kelp forest ecosystem in southern california. *Journal of Marine Research*, **42 (3)**, 591–604.

Appendix A

Heat Budget for Dongsha Atoll

A.1 Heat Budget at E3 and E5

The heat budget was constructed for E3 and E5 using the near bed DTS temperature and velocity and water depth measurements. A simple balance of the atmospheric and advective heat flux can adequately predict the observed heating rate on the reef flat at these locations (Figure A.1), and the two components of the heat budget are similar in magnitude throughout the experiment. The atmospheric heat flux is driven by solar heating on the reef flat, and is large on 4-6 June and 9-11 June, and smaller on 7-8 June due to high cloud cover. The advective heat flux at both locations varies over a short time scale, and is much higher at E3, due to larger gradients in temperature. The advective heat flux increases on 9-11 June due to increased tidal currents, wind and waves. There is some disagreement between the observed and the simple model, when there are strong temperature fronts in the control volume over which the heat budget is being averaged, for example at E3 from 00:00 to 03:00 on June 5, and to a lesser extent 00:00 to 03:00 on June 4, 2014.
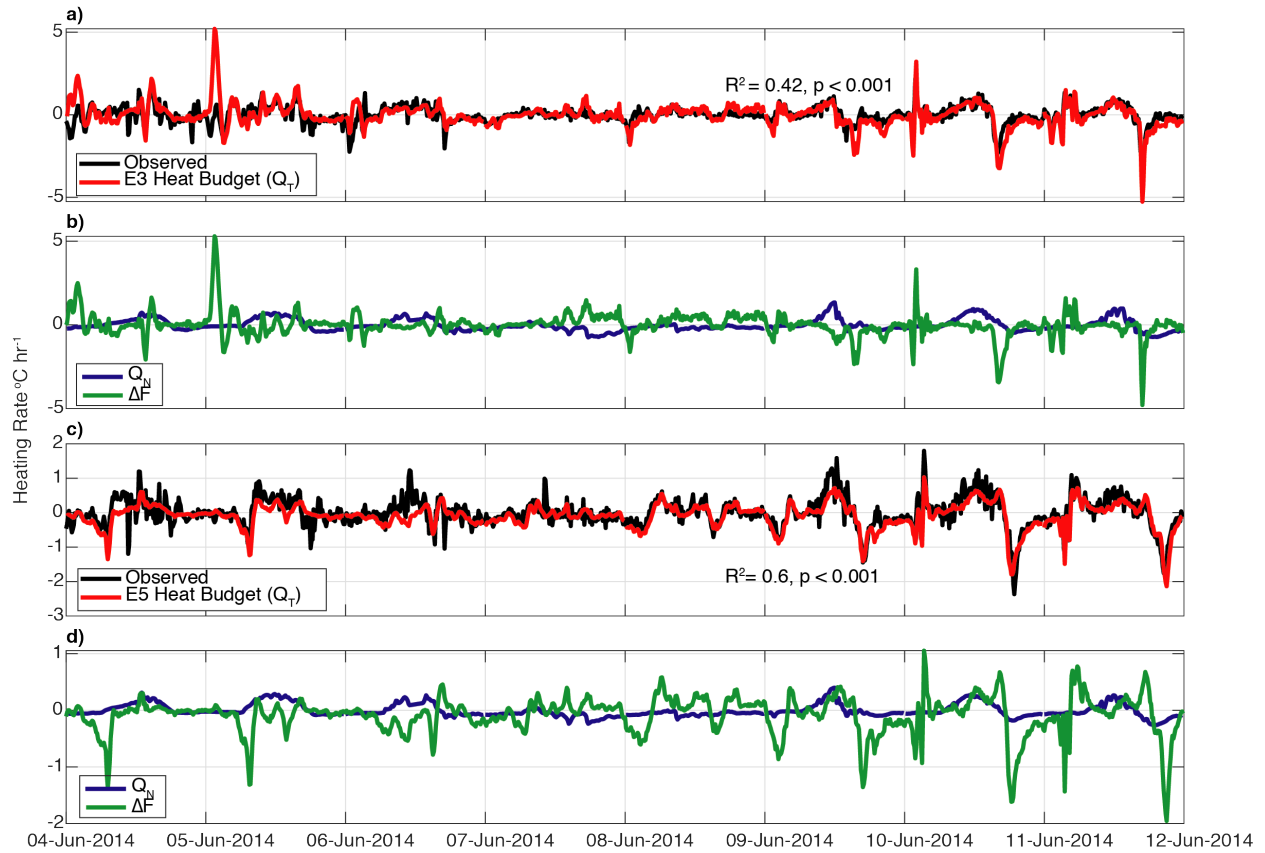
Figure A.1: **Heat Budget for E3 and E5.** Panel **a** shows the simple heat budget for E3. The red line is the predicted net heat flux, and the black line is the observed heat flux for the control volume for E3. Panel **b** shows the atmospheric heat flux (blue line) and advective heat flux (green line) at E3. Panel **c** shows the simple heat budget for E5. The red line is the predicted net heat flux, and the black line is the observed heat flux for the control volume at E5. Panel **d** shows the atmospheric heat flux (blue line) and advective heat flux (green line) for E5.

Appendix B

Internal Wave Locations Literature Review

Table B.1: Internal Wave Locations

Location	*Observations*	*References*
Gulf of Mexico	In Situ Observations, Satellite Imagery	Smith and Sandwell (1997); Rubenstein (1999); Jackson and Apel (2004)
North Brazil Shelf	Satellite Imagery	Smith and Sandwell (1997); Jackson and Apel (2004)
South Brazil Shelf	Satellite Imagery	Smith and Sandwell (1997); Jackson and Apel (2004)
Central American Pacific Coast	Satellite Imagery	Smith and Sandwell (1997); Jackson and Apel (2004)

Continued on next page

Location	*Observations*	*References*
East China Sea	Satellite Imagery	Smith and Sandwell (1997); Liu et al. (1998); Hsu et al. (2000); Jackson and Apel (2004)
Eastern Equatorial Pacific	Satellite Imagery	Smith and Sandwell (1997); Jackson and Apel (2004)
Gulf of California and Baja Pacific Coast	In Situ Observations, Satellite Imagery	Munk (1940); Fu and Holt (1982); Apel and Gonzalez (1983); Fu and Holt (1984); Smith and Sandwell (1997); Jackson and Apel (2004)
Northeast Japan	Satellite Imagery	Smith and Sandwell (1997); Jackson and Apel (2004)
Sea of Japan and Korean Strait	In Situ Observations, Satellite Imagery	Smith and Sandwell (1997); Kim et al. (2001); Jackson and Apel (2004)
California Coast	In Situ Observations, Satellite Imagery	Howell and Brown (1985); Smith and Sandwell (1997); Lerczak et al. (1999, 2001); Jackson and Apel (2004)
Yellow Sea	In Situ Observations, Satellite Imagery	Ogura (1933); Defant (1961); Zhou et al. (1991); Smith and Sandwell (1997); Hsu et al. (2000); Jackson and Apel (2004)
Galapagos	Satellite Imagery	Smith and Sandwell (1997); Jackson and Apel (2004)

166

Location	*Observations*	*References*
New Guinea	In Situ Observations, Satellite Imagery	Webster and Lukas (1992); Pinkel et al. (1997); Smith and Sandwell (1997); Pinkel (2000); Jackson and Apel (2004)
New Zealand	In Situ Observations, Satellite Imagery	Smith and Sandwell (1997); Sharples et al. (2001); Jackson and Apel (2004)
Arabian Sea	Satellite Imagery	Smith and Sandwell (1997); Small and Martin (2002); Jackson and Apel (2004)
Bay of Bengal	Satellite Imagery	Smith and Sandwell (1997); Jackson and Apel (2004)
North East Africa	Satellite Imagery	Smith and Sandwell (1997); Wang (1997); Jackson and Apel (2004)
South East Africa	Satellite Imagery	Smith and Sandwell (1997); Jackson and Apel (2004)
Bali Sea	Satellite Imagery	Jackson (2007)
Banda Sea	Satellite Imagery	Jackson (2007)
Flores Sea	Satellite Imagery	Jackson (2007)
Halmahera Sea	Satellite Imagery	Jackson (2007)
Mulucca Sea	Satellite Imagery	Jackson (2007)
Savu Sea	Satellite Imagery	Jackson (2007)
Sumba Sea	Satellite Imagery	Jackson (2007)
Celebes Sea	Satellite Imagery	Jackson (2007)

Location	*Observations*	*References*
Andaman Sea	In Situ Observations, Satellite Imagery	Perry and Schimke (1965); Osborne et al. (1978); Osborne and Burch (1980); Elachi and Cimino (1982); Alpers et al. (1997); Smith and Sandwell (1997); Jackson and Apel (2004); Vlasenko (2005); Jackson (2007); Wall et al. (2015)
Palau	In Situ Observations	Wolanski et al. (2004)
North West Australia	In Situ Observations, Satellite Imagery	Smyth and Holloway (1988); Pelinovsky et al. (1995); Smith and Sandwell (1997); Holloway et al. (2003); Jackson and Apel (2004); Nash et al. (2012)
Mamala Bay, Hawaii	In Situ Observations	Eich et al. (2004); Jones et al. (2008)
Moorea	In Situ Observations	Leichter et al. (2012)
Tahiti	In Situ Observations	Wolanski and Delesalle (1995)

Location	*Observations*	*References*
South China Sea	In Situ Observations, Satellite Imagery	Smith and Sandwell (1997); Liu et al. (1998); Apel (1999); Hsu and Liu (2000); Liu et al. (2003); Orr and Mignerey (2003); Beardsley et al. (2004); Chiu et al. (2004); Duda et al. (2004); Jackson and Apel (2004); Liu and Hsu (2004); Ramp et al. (2004); St Laurent et al. (2011); Fu et al. (2012); Alford et al. (2015)
Florida	In Situ Observations, Satellite Imagery	Fu and Holt (1982); Leichter et al. (1996); Smith and Sandwell (1997); Leichter et al. (1998); Apel (1999); Leichter et al. (2003); Jackson and Apel (2004); Davis et al. (2008)
Sulu Sea	In Situ Observations, Satellite Imagery	Apel and Gonzalez (1983); Apel et al. (1985); Liu et al. (1985); Smith and Sandwell (1997); Alpers and Vlasenko (2002); Jackson and Apel (2004); Zeng and Alpers (2004)
Great Barrier Reef	In Situ Observations, Satellite Imagery	Thompson and Golding (1981); Wolanski and Pickard (1983); Smith and Sandwell (1997); Jackson and Apel (2004)